Organogels for Intratumoural Delivery

Masar Basim Mohsin Mohamed (MSc)

Submitted to the University of Nottingham for the degree of Doctor of Philosophy

March 2017

Declaration

The work in this thesis in chapters 1, 2, 3 and 4 has been carried out by myself and no part has been submitted for any degree at the University of Nottingham or any other institutions except for the synthesis of *N*4-myristoyl gemcitabine by Kathryn Skilling, when she was a PhD student and this material was part of her thesis.

Masar Basim Mohsin Mohamed

March 2017

Abstract

The importance of localised delivery of chemotherapeutic drugs for cancer treatment and specifically solid tumours has been widely reported. In this study, the anticancer drug *N*4-myristoyl gemcitabine (a lipophilic form of gemcitabine) was formulated as organogel to achieve a localised depot delivery. Thus, the first goal of this study was to evaluate the suitability of the oragnogel for intartumoural injection and this attained by investigating the thermostability and elasticity of the organogel. Further to this, the second goal was to slow the release of *N*4-myristoyl gemcitabine from the organogel. Accomplishment of these two goals will guarantee a better efficacy of cancer treatment by obtaining direct contact of the organogel containing the *N*4-myristoyl gemcitabine with the cancerous cells. The studies herein selected the 12-hydroxystearic acid (12-HSA) as the gelator and using 2 types of solvents the liquid part of the organogel. The first type of solvent was a series of oils which were soybean oil (SO), medium chain triglyceride (MCT), glyceryl tributyrate (TGB) and glyceryl triacetate (GTA) whilst, the second type of solvent was propylene glycol (PG).

Initially thermal stability was screened using table top rheology and DSC from 0.5% to 5% w/w 12-HSA in different oils. Also to test the mechanical strength of the organogels, amplitude sweep, frequency sweep, time dependant recovery and creep and recovery tests were executed to differentiate between the organogels. The best organogels were the 5% w/w 12-HSA in SO and MCT due to their highest thermal stability, denser scaffolds, thixotropic behaviour and were the least compliant. The same experiments were utilised to evaluate the selected range of 0.5% to 14% w/w 12-HSA in PG. 14% w/w 12-HSA in PG was selected again due to its higher thermal stability, thixotropic

behaviour and was less compliant compared to other concentrations of 12-HSA in PG.

Drug release from the selected organogels was then carried out. The cumulative percentage released from 0.5% and 0.3% w/w *N*4-myristoyl gemcitabine in 5% w/w 12-HSA/MCT organogels as a solid organogel was 18.95% and 26.62% after 30 days whilst for the organogel liquefied with N-methyl pyrrolidone (NMP), the cumulative percentage released was 35.02% and 34.37% within the same frame time. Further to this, a sample and separate release method was used to study the liquefied form of the 5% w/w 12-HSA/MCT. Also, this method revealed that the 5% w/w 12-HSA/MCT organogels gave a slow release of *N*4-myristoyl gemcitabine and 56.18% and 70.07% was released from the 0.5% and 0.3% w/w selected organogels respectively within 30 days.

For the 14% w/w 12-HSA in PG organogel, the cumulative percentage released for 0.5% and 0.3% w/w *N*4-myristoyl gemcitabine in 14% w/w 12-HSA/PG organogels was 26% and 40% respectively after 30 days.

To conclude, our selected organogels (5% w/w 12-HSA/MCT and 14% w/w 12-HSA/PG) met the goal of our work firstly, by showing the strength and the elasticity to be injected. Secondly, they were able to slow down the release of *N*4-myristoyl gemcitabine.

Acknowledgment

I would like to thank my supervisors Dr Maria Marlow and Prof. Stephanie Allen for their help, guidance, support and patience throughout my studies. Also, I am very grateful to Dr Vincenzo Taresco for his unconditional help. Furthermore, I appreciate the help and the advice that I received from Dr Giovanna Sicilia and Dr Timothy Easun. I am thankful to my parents and my cousin Amani Raad Al-Hasoon who are always supporting and encouraging. Lastly, I want to extend my thanks to my country the republic of Iraq and ministry of high education and scientific research to let me have this opportunity to study at the University of Nottingham.

List of abbreviation

1,1´-dioctadecyl-3,3,3´,3´-tetramethylindodicarbocyanine perchlorate (DiD) oil; $DiIC_{18}(5)$ oil)	DiD
12-Hydroxysteraic acid	12-HSA
3D	Three dimensional
4-*N*-myristoyl gemcitabine	gemcitabine C14
5 fluorouracil	5-FU
Attenuated total reflectance- Fourier transform infrared spectroscopy	ATR-FTIR
deoxycytidine triphosphate	dCTP
Differential scanning calorimeter	DSC
difluorodeoxycytidine triphosphate	dFdCTP
difluorodeoxycytidine diphosphate	dFdCDP
difluorodeoxycytidine monophosphate	dFdCMP
Disodium hydrogen phosphate	Na_2HPO_4
Dodecyl sulphate sodium salt	SDS
Gemcitabine	GEM
Glyceryl triacetate	GTA
Glyceryl tributyrate	TGB
Linear viscoelastic region	LVER
Loss modulus	G″
Medium chain triglyceride	MCT
Minimum gelation concentration	MGC
N-methyl pyrrolidone	NMP
Pascal	Pa

Propylene glycol	PG
Scanning electron microscopy	SEM
Soybean oil	SO
Storage modulus	G′
Transmission electron microscopy	TEM
X- ray diffraction	XRD

Table of contents

List of Figures

List of Tables

Chapter one

Introduction

Abstract

There is a considerable interest and research in localised targeted delivery for treating cancer, particularly solid tumours that have a poor prognosis. The following section presents a brief overview of the solid tumours and then focuses on Gemcitabine (GEM) and GEM prodrugs. Indeed the overall goal of our research is to deliver a fatty acid derivative of GEM to treat solid tumours. Hence we have also reviewed localised targeted delivery in cancer therapy and cover in depth the approach we are developing in this project of an intra-tumoural injection of an organogel.

1. Introduction

Cancer is a lethal disease which led to 9 million deaths in 2015 and further increases in deaths arising from cancer are predicted [1]. These statistics showed that most of cancer deaths were due to solid tumours [2]. The first option in the treatment of a solid tumour is surgical removal of tumour; however, many cases of solid tumours cannot be treated by surgery. The reason behind this as mentioned by Giacchetti *et al* is metastases or the spread that has occurred through the organ. For instance, in the case of liver cancer, the invasion is to both liver lobes and through the blood vessels [3]. Moreover, solid tumours develop many structural abnormalities due to the growth of the cancerous cells and this needs nourishing by blood vessels within the tumour. These blood vessels are leaky and chaotic in nature. Further to this, these blood vessels have few smooth muscles and are deficient of both cells lining of the endothelial and the basement membrane. These defects lead to irregular blood flow. Sequentially, all these irregularities increase the hydrostatic pressure outside the blood vessels, hypoxia and acidosis [4, 5]. Altogether, these abnormalities in solid tumours not

only led to having complications in removing the tumours by surgery but also the administration of chemotherapeutic drugs. The penetration of drugs into the tumour can be poor. As an example, for cells of human colorectal cancer treated with gemcitabine that were near blood vessels, cell proliferation completely stopped whereas cells that were distal to the blood vessels re-proliferated quickly, due to poor chemotherapeutic penetration into the solid tumour [6].

For these reasons, there is a great interest in localising chemotherapeutics in the tumour where Wolinsky *et al* stated that the localised therapy increases the bioavailability of the chemotherapeutics which in turn decreases the chemotherapeutic systemic side effects [7]. This will be described in section **1.2** comprehensively**.**

1.1 Gemcitabine

We are focusing our research on a gemcitabine (GEM) prodrug and this is due to the importance of GEM in the treatment of many cancers. The efficacy of GEM was promising in the cell line laboratory experiments but this was not shown in the clinical treatment of patients with GEM. This is due to many factors that decrease the GEM availability in the tumours such as the hydrophilicity of GEM, rapid metabolism and some patients showed low levels of transporters of GEM. Thus we will describe GEM in detail. GEM as shown in Figure 1-1 is classified as an antimetabolites and a pyrimidine analogue (2,2-difluorodeoxycytidine) [8].

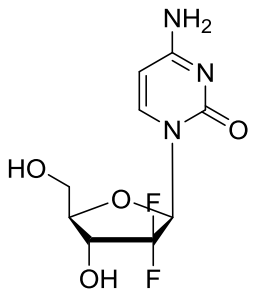

Figure 1-1: Chemical structure of gemcitabine.

1.1.1 Mechanism of GEM action

Efficient entry of gemcitabine (GEM) to the cell membrane requires a plasma membrane nucleoside transporter which means gemcitabine is actively transported [9]. Spratlin *et al* found that patients with pancreatic adenocarcinoma who have human equilibrative nucleoside transporter 1 (hENT1) had significantly longer median survival times than those patients with no hENT1 (4 months versus 13 months) [10].

Intracellularly, GEM is phosphorylated by deoxycytidine kinase to give difluorodeoxycytidine monophosphate (dFdCMP) and then converted to difluorodeoxycytidine diphosphate(dFdCDP) and difluorodeoxycytidine triphosphate (dFdCTP). Cytotoxicity of GEM is associated with both the S phase and the growth phase and this toxicity is as a result of the competition of dFdCTP with deoxycytidine triphosphate (dCTP) where the latter is a weak inhibitor of DNA polymerase. The incorporation of dFdCTP into DNA and the incorporation of more than one nucleotide result in DNA strand termination. The more the cells are able to incorporate dFdCTP into DNA, the more the GEM is capable of inducing apoptosis. The toxicity of GEM also leads to depletion of deoxyribonucleotide pools which is important for the synthesis of the DNA [11].

1.1.2 GEM pharmacokinetics

GEM can be metabolised to the less active metabolite by cytidine deaminase which removes the NH2 group from the cytidine ring allowing the uracil metabolite to be exported from the cell [12].
Deamination is the main process to metabolise the GEM in the blood, liver and kidneys which gives an inactive metabolite of uracil derivative. This process is very rapid leading to having a very short half –life [13]. GEM's short half-life is 15 minutes when it is administered intravenously and excreted in urine [14, 15].

1.1.3 Treatment of pancreatic cancer by GEM

Since our organogel gel depot approach has been designed for gastric, oesophagael or pancreatic cancer, we have focused our review on the use of GEM in these cancers.

The surgery is the first choice to treat from pancreatic cancer, but the disappointing survival rates advocate adjuvant treatments. The main cause of the low rate of survival after the operation is due to the metastasis or locoregional recurrence. Paulson *et al* reported that the median survival time of patients who have undergone surgery and received chemotherapy was higher in comparison with those who had just surgery alone. The administration of GEM gave a higher surviving rate but with significant side effects [16]. In another pancreatic cancer study, GEM improved the clinical response of patients such as pain reduction and increased in body weight [17].

In addition, the local recurrence is the main reason for using chemotherapy in combination with the application of external beam radiations in pancreatic cancer. This was proved in the studies that involved radiation after giving chemotherapy with drugs such as GEM and 5 fluorouracil (5-FU) which gave higher survival rates [16].

Since 1997, GEM has been considered the better treatment for pancreatic cancer as compared to 5-FU [18]. However, the metastasis has led clinicians to evaluate the combination of GEM with other drugs such as irinotecan, 5-FU, cisplatin, oxaliplatin and capcitabine and gave a positive significant effect on response rate and reduction in disease progression over monotherapy [19]. This was due to the synergetic impact of the two anticancer drugs that showed strong antiproliferative effect [20]. For example, the combination therapy was tried by Kawakami by combining gemcitabine and cisplatin in treating advanced biliary tract cancer and the result revealed that the median survival time was 11.7 months versus 8.1 months in the case of treatment with GEM alone [21].

1.1.4 The resistance to GEM treatment

The GEM treatment showed a decrease in its efficiency; where for example Narunsky *et al* stated that clinically pancreatic cancers resist cytotoxic drugs, despite the fact that these cancer cells in the culture experiments are very sensitive to this drug. Most likely, this is due to the changing in matrix and density of the stroma in the pancreatic ductal adenocarcinoma which leads to the blockage of blood vessels. This blockage prevents the chemotherapeutic drugs including GEM from entering the tumour [22, 23]. Also, the hydrophilic properties of GEM plays a role in increasing the resistance to GEM by its inability to permeate the cancerous cells [24].

1.1.5 Prodrugs of GEM

As mentioned before, the efficacy of GEM as a chemotherapeutic medicine is hampered by two factors. Firstly, GEM is rapidly metabolised and secondly due to its hydrophilicity, it requires an active transport mechanism to enter into cells. Both of these factors decrease the drug availability in cancerous tissue. Due to GEM's importance in treating many cancer and its drawbacks as just described, lipophilic prodrugs of GEM have been proposed.

The goal in the synthesis of many derivatives of GEM was to protect the 4-amino group of GEM from the metabolic pathway where GEM is metabolised to 2, 2-difluorodeoxyuridine [25]. Thus, many researchers have worked on the synthesis of many amide prodrugs such as valeroyl, lauroyl, and stearoyl linear acyl derivatives as shown in Figure 1-2 which gave more stable and lipophilic prodrugs. These prodrugs ensured passive diffusion into cells and as a result, the cytotoxic activity was higher than gemcitabine [26-28].

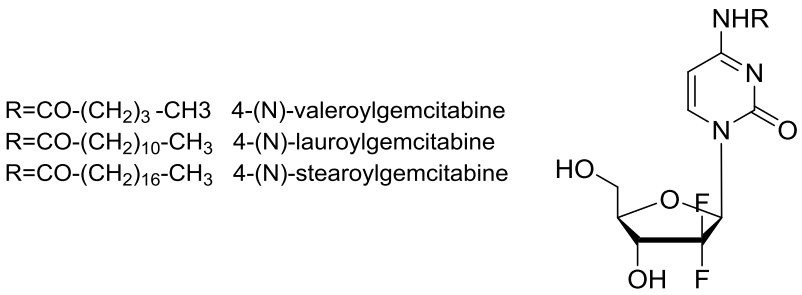

Figure 1-2: Chemical structure of acyl gemcitabine prodrugs.

Another study by Pili *et al*, they synthesised a prodrug of gemcitabine by conjugating a squaline molecule as shown in Figure 1-3. This addition was encouraging which helped to protect the GEM from rapid deamination and prevented it from conversion to an inactive metabolite and as a consequence, the cytotoxic activity was improved [29].

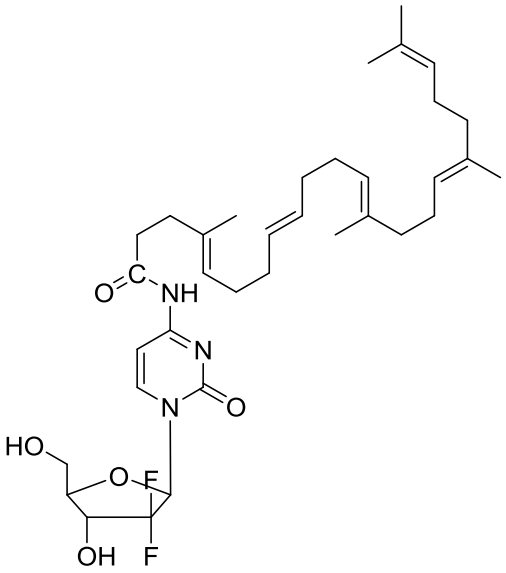

Figure 1-3: Chemical structure of squaline gemcitabine prodrug.

Additionally, Wickremsinhe *et al* studied extensively the LY2334737 (2′-deoxy-2′, 2′-difluoro-N-(1-oxo-2-propylpentyl)-cytidine) as shown in Figure 1-4 which is an amide prodrug of GEM, where this prodrug was designed for oral administration and resulted firstly in a reduction

of gastrointestinal toxicity and secondly the prodrug was absorbed through gastrointestinal tract [30].

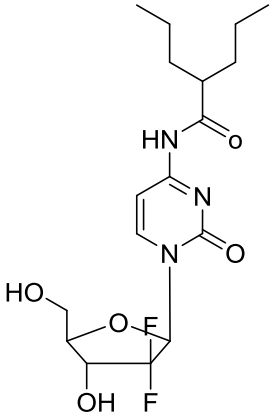

Figure 1-4: Chemical structure of LY2334737.

Also, Wickremsinhe *et al* in another *in vitro* study showed that less than 14% of LY2334737 degraded after 6 hours. This led to giving LY2334737 in metronomic low doses and this delivery was effective [31]. The metronomic dose is a programme of chemotherapeutic therapy where low doses of anticancer drugs are given to avoid any extension of the usual rest period [32].

Furthermore, Pasut *et al* synthesised amide prodrugs of GEM by conjugating GEM to poly ethylene glycol (PEG) polymers of 5 or 20 kDa polymer and folic acid. These prodrugs plasma profiles showed a longer half-life, higher bioavailability and lower clearance compared to the GEM. Also, this prodrug's antiproliferative activity was tested against many cell lines such as promyelocytic leukaemia, cervix epithelial adenocarcinoma colon adenocarcinoma, breast cancer and nasopharyngeal epidermal carcinoma. These tests showed the GEM had a better cytotoxicity than the prodrugs but these prdrugs still had an acceptable cytotoxicity especially the targeted prodrugs with folic acid [33].

1.2 Drug delivery systems for cancer therapy

Many drug delivery systems have been studied and developed with aim of achieving high localised concentrations of chemotherapeutic drugs within the tumour. These systems could be divided into 2 categories according to the method of administration [7].

1.2.1 Nano-materials administered intravenously

The first category which is delivered intravenously is nano- materials such as polymer nanoparticles, liposomes and dendrimers. These nano-materials circulate in the blood stream for a long period and since the tumour has its unique structure with leaky blood vessels, there is uptake of these nanoparticles into the tumour and not into healthy tissue. This is known as passive targeting. To enable these nano- materials to remain circulating in blood stream they need to avoid elimination by the kidney and uptake by phagocytic cells, mainly in the liver. Firstly, the kidney can eliminate the particles less than 10 nm [34]. Secondly, Kupffer cells in the liver can phagocytose particles larger than 100 nm [35]. Thus, these nano- materials should be between 10 nm and 100 nm in size and either neutral or negatively charged. In general nanoparticle phagocytosis by cells of the reticular endothelial system including Kupffer cells can be prevented by adding a hydrophilic steric barrier e.g. polyethylene glycol chains to the particles. This addition helps to decrease the interactions of the surfaces of these particles with the proteins due to the hydrophilicity of polyethylene glycol which attracts water and repels proteins. However, the uptake of PEGylated particles by tumour is a challenging issue as these polyethylene glycol chains decrease the interaction with tumour surfaces. Another approach to localising chemotherapeutic drugs as opposed to passive targeting is active targeting [36].

This concept came from the fact that the tumours overexpress many receptors, antigens and enzymes. This has been taken advantage of by conjugating chemotherapeutic drugs to molecules known as ligands. These ligands have an affinity to the overexpressed molecules in the tumour such as Herceptin which binds HER-2 expressing cells in breast cancer. Also, the epidermal growth factor receptor was targeted by the cetuximab [37]. Moreover, folic acid was used to target folate receptors that are overexpressed by tumour cell membranes. The main drawbacks of this active transport is the ability of the ligand–chemotherapeutic complex to target healthy organs that express a great level of the same receptor such as folate receptors expressed highly in placenta [38, 39].

Polymer nano-particles such as the silica and the organically modified silica nano-particles which are their diameter is less than 20 nm and easily synthesised [40]. Also, hydrophobic modified glycol chitosan was used to be loaded with the anticancer drug docetaxel [41]. The localisation can be achieved by conjugating the chemotherapeutic agent to a polymer that has an affinity to the tumour and initiating the release of chemotherapeutic from their polymer carrier by applying external stimuli such as the temperature. Qin *et al* developed nano materials to deliver doxorubicin. This system was obtained via covalently conjugating folic acid to the nanographene oxide-polyvinylpyrrolidone, where nanographene oxide-polyvinylpyrrolidone was already connected by π-π stacking. As mentioned above, the folic acid molecules target the chemotherapeutic drugs to the cancerous cells. Thus the folic acid-polyvinylpyrrolidone-nanographene oxide system has a synergetic effect, by firstly folic acid targeting to the cancerous cell plasma membrane and then secondly, the nanographene oxide providing photothermal therapy. This synergetic effect helped to decrease the tumour resistance to chemotherapeutic drugs [42].

Liposomes are another method of delivering cytotoxic drugs where these liposomes are comprised of a non-toxic phospholipid bilayer. Such as distearoylphosphatidylcholine and cholesterol liposomes diameter is 100nm [43]. The first clinically approved anticancer as liposomes injection is Doxorubicin HCl [44]. When the phospholipid bilayer of liposome was modified with polyethylene glycol, this led to increasing in circulation times. The main drawback is poor drug transfer by non-targeting liposomes [45]. The transfer of anticancer drugs into the tumour depends on the leaky tumour vasculature and this is not a constant and could be different from one tumour to another. This leads to a negative effect on drug availability and low accumulation in the tumour. Therefore there was a development in liposome targeting by applying mild hyperthermia to the tumour tissue i.e. 43 °C and this helped in increasing the drug accumulation in the tumour [46].

1.2.2 Intratumoral therapy

Actually, only a few percentage of the systemic dose of nano-materials are found in the tumours while the remainder of the anticancer dose goes to healthy organs [47]. Thus, intratumoural therapy has the potential to increase the concentration of drug in the tumour, not only by the injection directly into the tumour but also by placing the drug delivery system adjacent to the cancerous tissue using for example films, gels, wafers and rods. These dosage forms are intended as a controlled release drug delivery system to treat cancerous tissues over extended periods of times from days to weeks. Also, the poor penetration of chemotherapeutic drugs into the tumour is one of the main obstacles in cancer treatment. Thus, it was sensible to consider the intratumoural or local therapy as a good alternative route of the nano-materials to overcome this resistance and to ensure the presence of

chemotherapeutics in the tumour. Also, this route helps to decrease the systemic side effects of chemotherapeutic drugs. Nonetheless, the main negative effect of intratumoural implants is the hydrophobic nature of the polymers leading to local inflammation [48]. The following paragraphs will describe different examples of formulations such as wafer, films, rods, hydrogel and organogels for intratumoural delivery.

Starting with the Gliadel® **wafer**, this is the most advanced technology as this commercially available implant is used in the treatment of glioblastoma. It is used after removing the tumour by arranging several wafers at the site of the surgery and is a polyanhydride biodegradable wafer containing carmustine [49, 50].

Polymers **films** have also been developed by Liu *et al* where 10% w/w of paclitaxel was incorporated in poly (glycerol monostearate co-e-caprolactone) polymer films. The film was sutured to the superficial fascia at the resection site. The results revealed that the paclitaxel film inhibited any new growth of non-small-cell lung tumour. The paclitaxel concentration in the local area of the tumour at day 10 was 3000 fold higher in comparison with paclitaxel when administered systemically. Also, it was found that for intravenous administration of paclitaxel half of the systemic dose was eliminated in the first day and less than 0.5% was found locally in the lung to treat the tumour [51].

A chitosan film was also used to deliver ellagic acid in different concentrations and this film stopped the growth and induced apoptosis in melanoma cells [52].

In 1990 cisplatin was formulated as **rods** using starch and polyether hydrogel where rods of starch gave 100% release of the cisplatin after 2 hours whilst hydrogel rods gave 100% release of the cisplatin after 1 day [53].

Rods with a bromodeoxyuridine incorporated improved the radio sensitisation of cancerous cells when bombarded with radiation as will be described. Bromodeoxyuridine competes with thymidine incorporation into DNA. The rods for cell sensitisation were prepared using the copolymer bis(p-carboxyphenoxy)propane-sebacic acid (20:80) mixed and milled with bromodeoxyuridine and then melted to 80 °C followed by ejecting the melted mixture using an eppendorf combitip. This step was followed by cooling down the rods to room temperature. The rods were 8 x1 mm and divided into 3 pieces which were inserted into 3 different positions in the tumour. After 3 days of implantation, the response was good for the first dose of radiation compared with an acute radiation dose to the tumour [54].

The main advantage of hydrogels and organogels is their ability to be injected and form a gel in situ avoiding the need for surgery to localise them in the tissue as needed for the wafers and films as just described above [55].

Hydrogels have been extensively studied as dosage form for intratumoural delivery [56-59]. For example Kim *et al* formulated paclitaxel by using poly(organophosphazene) to prepare a thermosensitive hydrogel an intratumoural delivery therapy. The paclitaxel hydrogel (0.6% w/w drug loading) was injected into human xenograft tumours in mice and followed for 4 weeks. This study showed a decrease in tumour size, but after 14 days there was tumour growth again and indicates that the duration of treatment was 14 days only [60]. Also, Ta *et al* emphasized the importance of injection of hydrogel into tumours over the microspheres and nanoparticles due to the lack of achieving better results in solid cancer treatment [61].

Organogel: In situ forming organogels have also been used where the 10 % w/w of N-stearoyl L-alanine (m) ethyl esters in safflower oil was

solubilised by N-methyl pyrrolidone (NMP) and injected as a liquid. These organogels were loaded with leuprolid to treat prostate cancer and injected subcutaneously [62]. Also, rivastigmine organogels to treat Alzheimer's disease have also been developed where this organogel was composed of N-behenoyl L-tyrosine methyl ester in safflower oil and was also injected subcutaneously as a liquid using NMP [63].

Several studies have focused on studying organogel injection into the tumours such as Wu *et al* who prepared organogels using the system of phospholipids, medium chain triglycerides and ethanol to incorporate doxorubicin. This system showed after giving a single dose a size reduction of the S180 sarcoma tumour [64]. Also, Gao *et al* studied another organogel system which is phenylboronic acid gelator in 4:1 PEG 200 / water to deliver doxorubicin [65].

The distinctive thing in this organogel is the liquid phase which is either an organic solvent or oil that helps to host lipophilic drugs and to create a platform for the depot formulation. Table summarizes the intravenous and intratumoural administration for cancer therapy.

Table 1-1: Summary of localised intravenous and intratumoural administration

Methods of anticancer administration	Examples of administration	Advantage	Disadvantage
Intravenous Administration	Liposomes, polymer nano-particles	leaky nature of blood vessels of tumour led to liposomes and polymer nano-particles be taken by tumour rather than other normal tissues in the body [35].	1-Liposomes and polymer nano-particles should be modified by PEG to increase circulation time [36]. 2-particle size of liposomes and nano-particles should be larger than 10 nm to avoid elimination by kidney and smaller than 100 nm to avoid eliminated by liver [34, 35]. 3- penetration is not selective to the tumour and can enter any organ in the body [47] .
Intratumoural Administration	Wafers	The distribution of wafer in the site of surgery after removal of the tumour to increase the bioavailability of anticancer drug into the tumour and decrease the systemic side effect [66].	Wafer needs surgery to be localised.
	Films	Films need to be put onto the surface of the resection site to localise the anticancer drug and decrease the systemic side effect.	Films need to be sutured to fix them to the surfaces [51].
	Rods	Inserted inside the tumour to localise and decrease the systemic side effects of the anticancer drug.	Rods do not last for long period [53].
	Hydrogel	Injected to form gel in situ to localise and decrease the systemic side effects of anticancer.	The drug is captured within a cross linked network and does not last for long periods [67].
	Organogel	1-Injected to form gel in situ to localise and decrease the systemic side effects of anticancer drug. 2-The oils or the organic solvent guarantee including lipophilic drug to create a depot formulation.	Local inflammation [68].

1.3 Organogels

Organogels have been selected in our work to create a depot for sustained drug release and injection intra-tumourally. As the organgel is the selected dosage form in this current study, we need to know in detail what an organogel is as will be described.

Organogels have a wide application in the pharmaceutical industry and are defined as a soft, solid or solid-like material which contains both a solid and solvent. The gelator forms a 3D fibre network structure which holds the solvent in non-flowing microdomains. The flow of solvent is prevented by surface tension and capillary forces. The gelator concentration is generally not more than 15 % w/w [69]. Also, organogels have viscoelastic properties that means those gels show a solid behaviour at low shear and a fluid behaviour at a high shear. Moreover, organogels are either opaque or are transparent and this is due to the component of organogels. Chirality is another property of low molecular weight gelators to form stable solid organogels for instance; crown ether phthalocyanine organogel was composed of super coils helical fibres. These fibres were due to π-stacking between aromatic substituent rings which helped in growing of molecules to single fibres. Sequentially, these fibres twisted around each other and formed a helical, stable and strong superstructure. This is in contrast to flat aggregation with the lack of the chiral centre, where the contact area between molecules was less which led to uncontrolled aggregation and a weak gel [70, 71].

1.3.1 Limitations of organogels

These gels need to be stored at a specific temperature to prevent syneresis i.e. the leakage of oil from the three-dimensional network

[72]. Rogers *et al* investigated the 12-hydroxystearic acid at different temperatures over a period of a month. The results showed that the organogels stored at 5 °C had the maximum amount of immobilised oils in comparison with organogels stored at 30 °C [73].

1.3.2 Benefits of organogels

The huge interest in organogels has started due to their unique advantages and characteristics, for example, ease of preparation, microbial growth resistance, low cost (i.e. low concentrations of gelator are required) and the capability of incorporation of both hydrophilic and hydrophobic drugs. All these benefits have driven the industrial interest in organogels in many research areas besides the drug delivery area. Firstly, the petrochemical industry uses gelators to control flammable solvents by immobilising them and also uses them in the prevention of oil spillages [74]. Interestingly, Basak *et al* found the simple aromatic amino acid phenylglycine with long fatty acyl chain was selectively holding the fuel oil at low concentrations (from 1.07 % w/v to 2.06 % w/v) from a mixture of oil and water at room temperature [75]. Secondly, due to the ability of organogelators to assemble themselves in many oils including edible oils, there is a considerable interest in the food industry. Due to health risks associated with cardiovascular disease for trans fatty acids and saturated fats in processed food these organogels from edible oils are being considered. For this reason, self-assembled gelators were a part of the science solution where for example, 12-hydroxystearic acid can immobilize canola oil [76, 77]. Thirdly, organogels have been utilised in cosmetics where Morales *et al* formulated Aloe Vera and hydrocotyle asiatica in pluronic lecithin organogel to treat cellulites. These organogels gave 100% release of the active constituents after 2 hours [78]. Raut emphasised the importance of organogels in the cosmetic treatment of

skin ageing and specifically lecithin organogels which gave good skin permeation of many hydrophilic and lipophilic antiaging agents [79].

1.3.3 Classification of organogels

Gels can be classified according to the solvent, gelator and intermolecular interactions. According to the solvent, the gels divided into either hydrogels if the continuous phase is water or organogels when the solvent is organic [80].

Also the nature of gelators could be a low molecular weight gelator or a polymeric gelator. The low molecular weight gelators (LMWG) are small molecules with a molecular weight less than 3000 Da for example, *n*-alkanes, substituted fatty acids, sorbitan monostearate, steroids and others. Chemical gels are held together by strong covalent bonds, and hence the gel cannot be re-dissolved and are thermally irreversible. While the physical gels are held together by non-covalent bonds such as hydrogen bonding, π-π stacking, van der Waals interactions and are thermally reversible [81, 82]. Chemical structure can predict the type of bond for example the amide and carbonyl groups in amino acids and urea leads to hydrogen bonding which is responsible for gelation. The aromatic rings can form π-π stacking in compounds like cholesterol. Indeed, some compounds can form more than one type of bond such as the assemble of the gelator N-Carbobenzoxy-L-Valine-Hexadecane Hydrazide where FTIR studies revealed the intermolecular hydrogen bonding between these C=O and N-H group and where the hydrophobic interactions were between alkyl groups [83] .

1.3.4 3D structure of Gelators

Low molecular weight gelators assemble themselves by physical interaction to form either a solid or a fluid fibre matrix. Since these matrixes are thermoreversible, they can transition to a solution by heating. Rheology is the main technique to differentiate between the fluid and solid fibre matrix. The comparison between the two types can be described by three main points which are the strength, the junction points between fibres and the presence of chirality in the structure.

A solid fibre matrix is strong and this is due to the junction points between fibres which are mainly constant. In the contrary to the solid fibre matrix, the fluid fibre matrix is weak because the junction points that in the gel are transient. Furthermore, there is a continual process of breaking and rejoining of these junctions as shown in Figure 1-5 A and B. Chirality has no effect on the fluid fibre matrix [70].

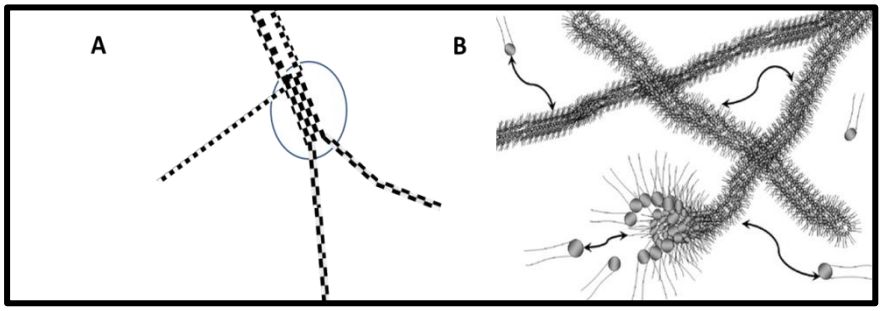

Figure 1-5: Adapted from the reference no [70] and shows the junctions between fibers where A is a solid matrix and B is a fluid filled matrix.

The transient junction is due to the fibres crossing over each other, while permanent junction is due to the growth of fibres either in a tip or side branch position as shown in Figure 1-6. This is highly affected by the degree of saturation or cooling and it was noticeable that the tip branching usually occurs at a high supersaturating concentration which leads to wide angles of crystallographic mismatch branching. Tip branching was observed in 4.1% of N-lauroyl-L-glutamic acid di-*n*-butylamide / iso-stearyl alcohol organogel by utilising scanning electron microscopic images (SEM). This technique has been done using CO_2 to extract fluid and to have a non-disturbed scaffold [84]. When the mixture is at a lower supersaturation concentration, the side branching is the dominant one and leads to small angle crystallographic mismatch branching [85]. This side branching has been observed in 2% agarose water gel and this gel was examined by using field emission scanning electronic microscopy coupled with a flash-freeze-drying technique to extract solvent and obtain an unbroken scaffold [85, 86].

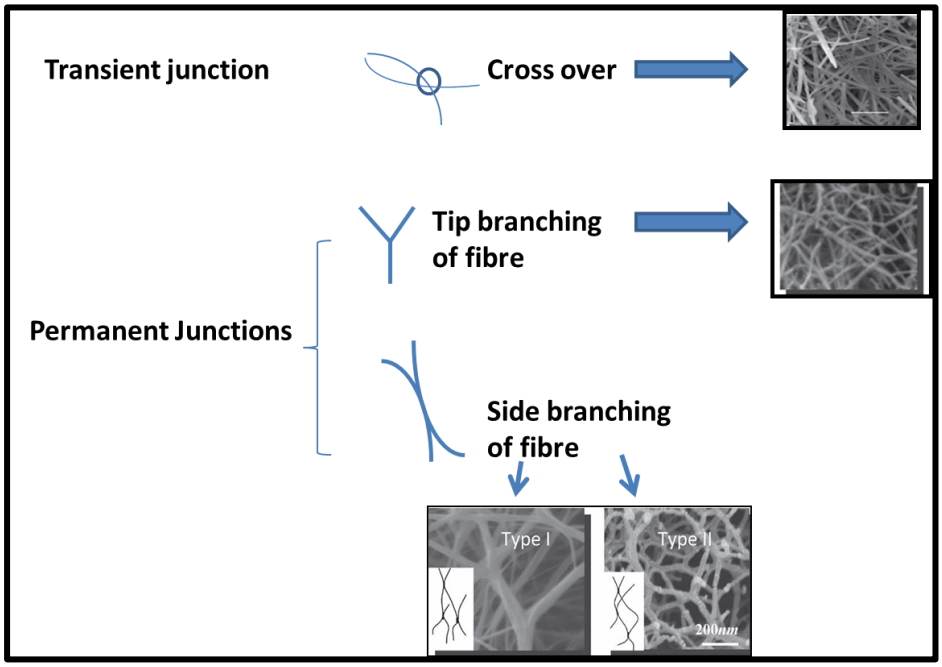

Figure 1-6: Differences between junctions and different types of branching where this figure is adapted from reference no. [85] .

Also, supersaturation can affect the scaffold structure by changing the temperature while keeping the concentration constant. This was demonstrated when investigating 2 % w/w of 12-HSA/ canola oil organogel by polarised microscope with applying different cooling rates 10, 5 and 1 °C/min. Cooling rates above 5 °C/min showed great effect on the formation of scaffold where the nucleation onset happened at lower temperature leading to formation of smaller crystals and large number of nuclei [87].

Furthermore, it was found out that the addition of a surfactant Tween 80 helped in creating a more branched network of 2.5 mol% of N-lauroyl-L-glutamic acid-di-*n*-butulamide/ isosterayl alcohol organogel. As the concentration of Tween 80 increased from 0.33 x 10^4 to 1.4 x 10^4 mol % the branching distance between 2 neighbouring branching points in the scaffold decreased from 2.5 µm to 0.5 µm. These Tween

80 additions helped in increasing the storage modulus from $9x10^5$ Pa to 1.2 $x10^6$ Pa and this meant an improvement in the 3D structure of the scaffold. It is thought the surfactant molecules were adsorbed on the surface of the tip of the developing fibres leading to mismatch branching [88].

Additionally, it was found that the addition of a suitable polymer enhanced the 3D scaffold structure of the 10% w/w of L-DHL (lanosta-8,24-dien-3β-ol:24,25-dihydrolanosterol/ di-isooctylphthalate organogel. This organogel showed short needle-like fibres but the addition of 0.01 % w/w of ethylene/vinyl acetate copolymer helped in decreasing the mesh size of the scaffold. A further decrease in the mesh size of the network was then observed upon increasing ethylene/vinyl acetate copolyme to 0.1 % w/w. This improvement in the scaffold formation was due to the strong adsorption of the polymer on the tip of the growing fibre. This led to mismatch branching that helped in creating a branching scaffold and retarding the growth of fibres [89].

1.3.5 Gelators

The solid part responsible for the gelation of organogels is the gelator and this gelator can aggregate in different solvents to form organogels. Generally, this aggregation depends on the chemical structure of the gelator, and the balance of gelator-gelator and gelator-solvent interactions occurred via the hydrophobic and hydrophilic groups in the same molecule of the gelator. For hydrogels, the interactions amongst the hydrophobic groups stimulate the assembly of gelator in water, while the hydrophilic groups promote the solubility of gelator in water. The opposite is true for hydrophilic groups of gelators in organic solvents in that they promote self-assembly particularly hydrogen

bonding. Organogelation occurs when the interactions of gelator-gelator are greater than the interactions of gelator-solvent [90]. In the next paragraphs we will present several low molecular gelators in different categories according to the parent molecules.

1.3.5.1 Fatty acid and sorbitan derivatives

Furthermore, the **Sorbitan monopalmitate** which is a non-ionic surfactant composed of natural fatty acid (palmitic acid) and the sugar alcohol (sorbitol) as shown in Figure 1-7, where this gelator was able to form an organogel with castor oil at 25% w/w. This combination gave a homogenous smooth and slightly yellowish organogel where the optical images showed a fibre network [69].

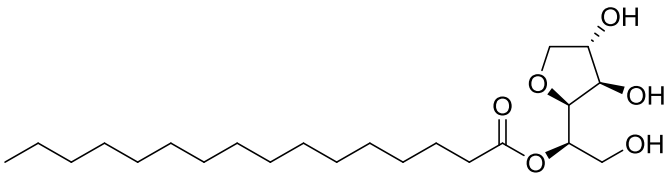

Figure 1-7: Chemical structure of sorbitan monopalmitate

Sorbitan monostearate: it is a hydrophobic, non-ionic surfactant and it is an ester of sorbitan and stearic acid as shown in Figure 1-8. This gelator at 10% w/v formed white opaque organogel with hexadecane and the optical images of the organogel showed a tubular scaffold [91]. Also, sorbitan monostearate gelled sesame oil where the lowest concentration was 15% w/w and optical images showed a needle like network [92], where the difference between sorbitan monostearate and sorbitan monpalmitate is the chain length of fatty acids.

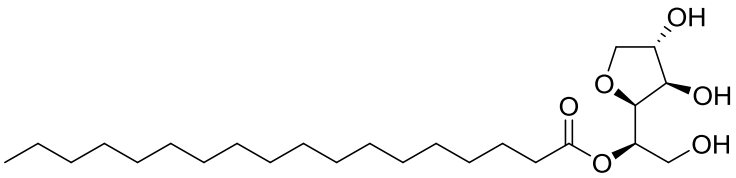

Figure 1-8: Chemical structure of sorbitan monostearate.

Sorbitan tri-stearate: this gelator as shown in Figure 1-9 and lecithin were evaluated by Pernetti *et al* using from 6% to 20% w/w in sunflower oil and individually they did not gel the oil. However, when sorbitan tri-stearate and lecithin were added in these proportions 40: 60 and 60: 40; they gave a synergetic effect and gelled the sunflower oil, where the polarised images of 50:50 of the combination of sorbitan tri-stearate and lecithin gave a needle like scaffold [93].

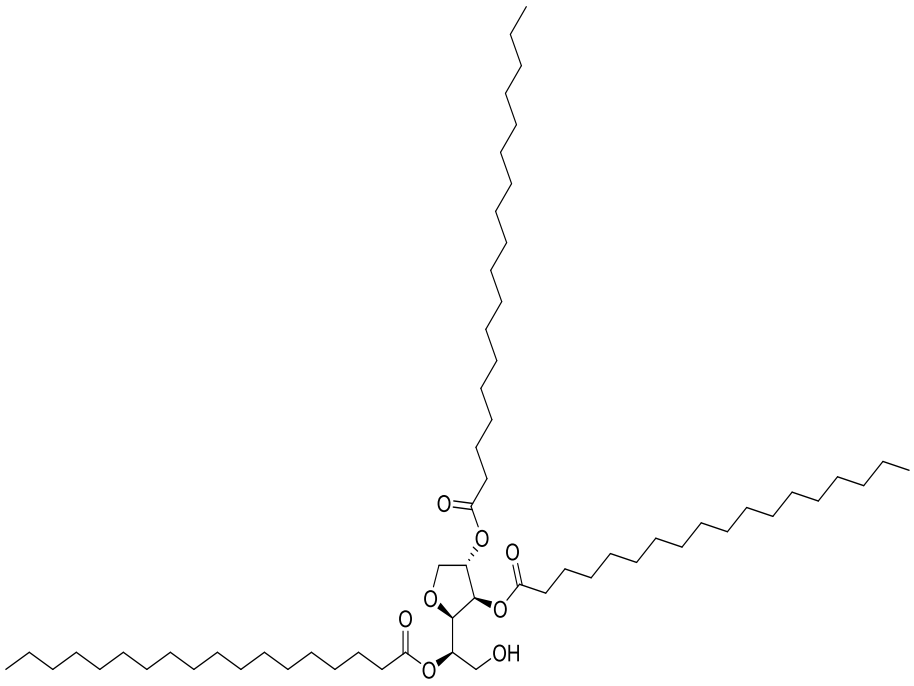

Figure 1-9: Chemical structure of Sorbitan tri-stearate.

1.3.52 Alkanes

Abdallah and Weiss prepared organogels by using long alkanes as a gelator as shown in Figure 1-10 and short alkane as a liquid part of organogels, where 0.12 % w/w of teracosane was capable of forming a scaffold in heptane, decane and dodecane. Also, these solvents were gelled by 0.04% w/w of octacosane and *n*-hexatriacontane. The optical images of the *n*-hexatriacontane organogel showed crystalline strands and the only forces responsible for gelation were the London dispersion forces [94].

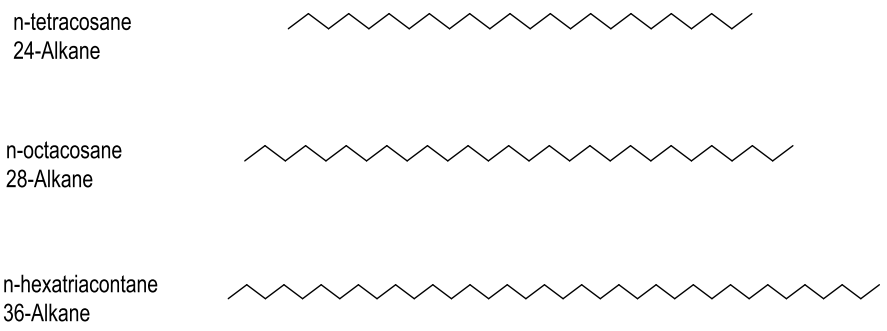

Figure 1-10: Chemical structure of different alkane as gelators.

The same research group produced acyclic alkanes with one hetero atom as shown in Figure 1-11. They found that dioctadecylamine solidified many solvents at 3% w/w such as alkanes, aromatic liquids, alkanols, methylene chloride, and silicone oil; where the other gelators: trioctadecylamine and ditetradecylsulfide gelled only the silicone oil and alkanol and octadecylamine and methyldioctadecylamine just gelled the silicone oil. Dioctadecylamine's ability to gell many solvents was attributed to it being both a hydrogen bond donor and acceptor [95].

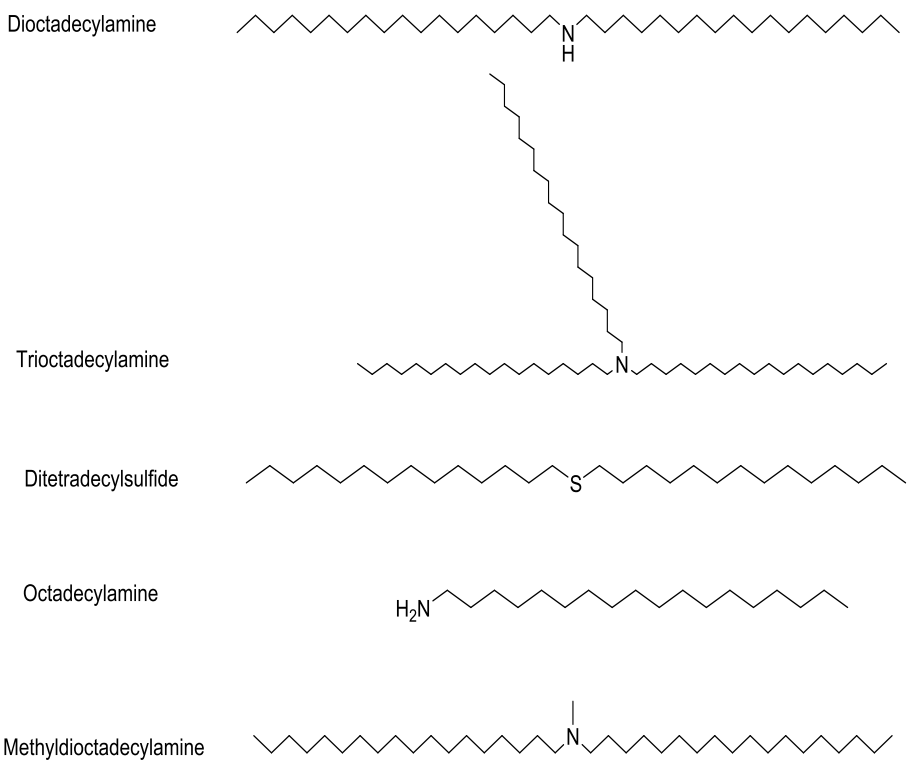

Figure 1-11: Chemical structure of different alkanes with one hetero atom.

1.3.5.3 Steroids

Steroids can act as gelator such as the the paramagnetic D-homosteroidal nitroxide free radical as shown in Figure 1-12 gelled cyclohexane at a 2% w/w concentration and where it's TEM showed a fibre network [96].

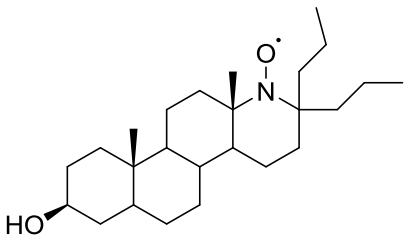

Figure 1-12: Chemical structure of paramagnetic D-homosteroidal nitroxide free radical.

Gelators **A** and **B** as shown Figure 1-13 include cholesterol in the R group, at 5% w/w were capable of gelation of different solvents such as 1-hexanol, 1- octanol, 1-nananol and 1-decanol. The scanning electron micrograph (SEM) of gelator **A** showed two different spherulites diameters of 200 nm and 2500 nm. While gelator **B** SEM images gave a rolled film like morphology [97].

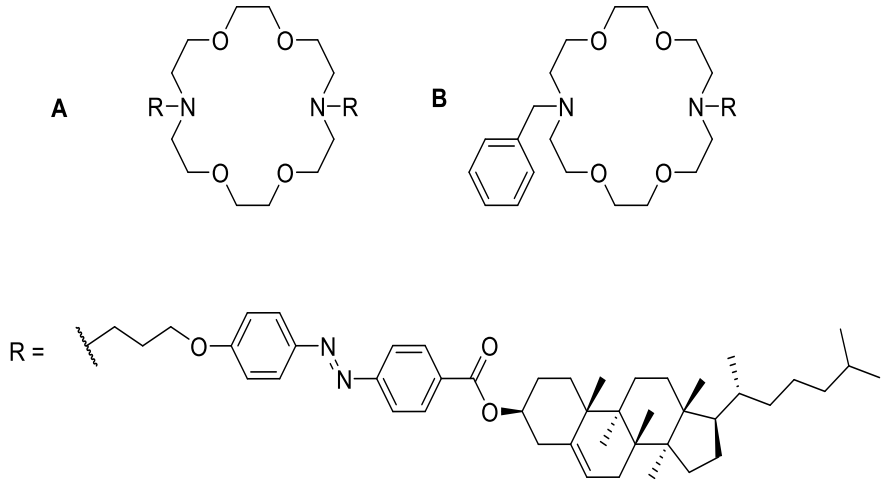

Figure 1-13: Chemical structure of cholesterol derivative gelators.

Moreover, β-Sitosterol and Ɣ-Oryzanol as shown in Figure 1-14 gelled sunflower oil at a concentration of 8% when mixed in the following proportions 20:80, 40:60, 60:40, 80:20 [98].

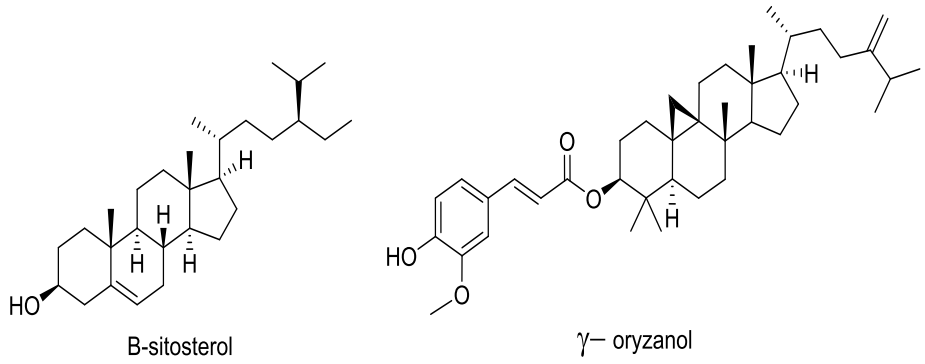

Figure 1-14: Chemical structure of β-Sitosterol and ϒ-Oryzanol.

1.3.5.4 Amino acid derivatives of steroids

Li *et al* conjugated different amino acids such as glycine, L-alanine, D-alanine, L-phenyl alanine, and D-phenyl alanine with cholesterol as shown in Figure 1-15 to have in addition to the hydrophobic nature of cholesterol the potential for the hydrogen bonding. The 2.5 % w/w of these gelators have been mixed with different solvents and the L-alanine and D-alanine cholesterol gelators formed organogels with a wide range of solvents. The L-alanine cholesterol in ethanol gave a turbid gel and it's SEM images showed stacked and hollow rod like structure while the same gelator in 1-octanol showed a transparent gel and it's SEM images showed rods [99]. Suzuki and Hanabusu reviewed all L-lysine derivatives gelators and commented that they were biocompatible biodegradable and were cheap to produce [100].

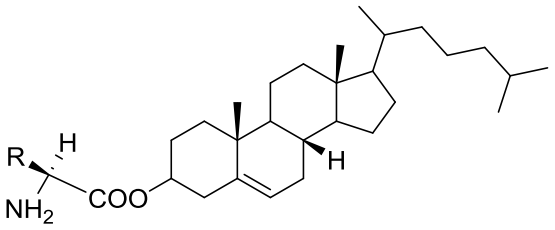

derivative of L-amino acd

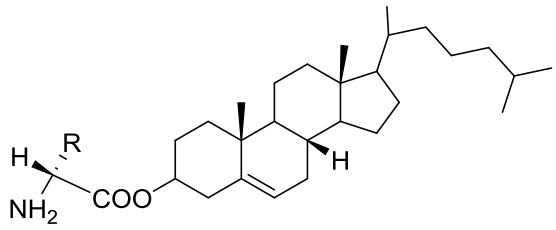

derivative of D-amino acid

Figure 1-15: Chemical structure of L-amino acid and D-amino acid cholesterol gelators.

1.3.5.5 Peptide gelators

Maji *et al* found the synthetic tri peptide which is [Boc-Ala(alanine)-Aib(amino-isobutyric acid) -Ala(3)-OMe] at low concentration (0.5% w/v) formed transparent gels in benzene and its scanning electron microscopy photo showed entangled long fibres [101]. Also, Banerjee *et al* synthesised a gelator by Boc protecting the terminal of a five amino acid chain, Boc-Leu(1)-Val(2)-Phe(3)-Phe(4)-Ala(5)-OMe as shown in Figure 1-16. This amino acid sequence and specifically diphenyl alanine helped to create a gelator and the minimum amounts of solvent required were 1.1 %, 1.4 %, 1.7% and 1.9% w/v in 1,2 dichlorobenzene, *m*-xylene, toluene and benzene respectively. The TEM images showed that scaffolds created by this gelator were networks of entangled fibres [102].

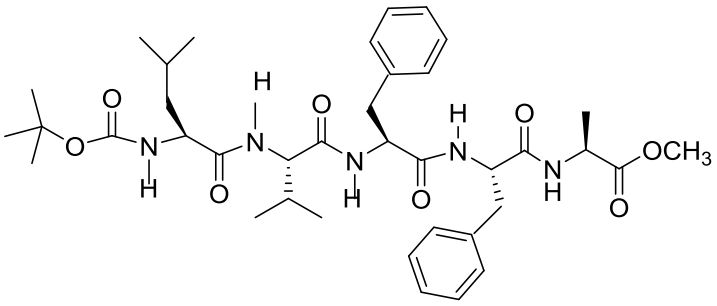

Figure 1-16: Chemical structure of Boc-Leu(1)-Val(2)-Phe(3)-Phe(4)-Ala(5)-OMe.

1.3.5.6 Urea derivatives

Brinksma synthesised a bis urea cyclohexane gelator as shown in Figure 1-17 which was able to form oragnogels with: 1-propanol, 1-butanol, 1-hexanol, and 1-octanol and formed organogels. This gelator at low concentration 0.5% w/v showed transparent organogels, while at high concentration of 5% w/v exhibited turbid organogels. This gelator in different study exhibited fibre networks by electron microscope and its FTIR showed a shift in peaks associated with the amide I and amide II regions where the gelator changed from liquid to solid due to hydrogen bonding [103, 104].

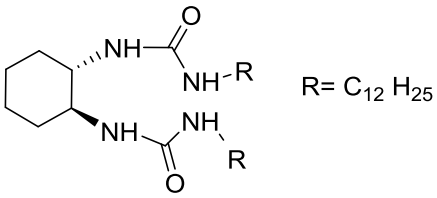

Figure 1-17: Chemical structure of bis urea cyclohexane gelator.

1.3.6 Formation of organogels

To form the organogel, the first step is heating the LMWG in a suitable solvent. This step is followed by a cooling step. This transition from heating to cooling leads to either crystallisation of the low molecular weight gelator *i.e.* molecules start to organise themselves in crystals or, molecules disorganise themselves in aggregates to form amorphous precipitates, or a gel can be formed as shown in Figure 1-18.

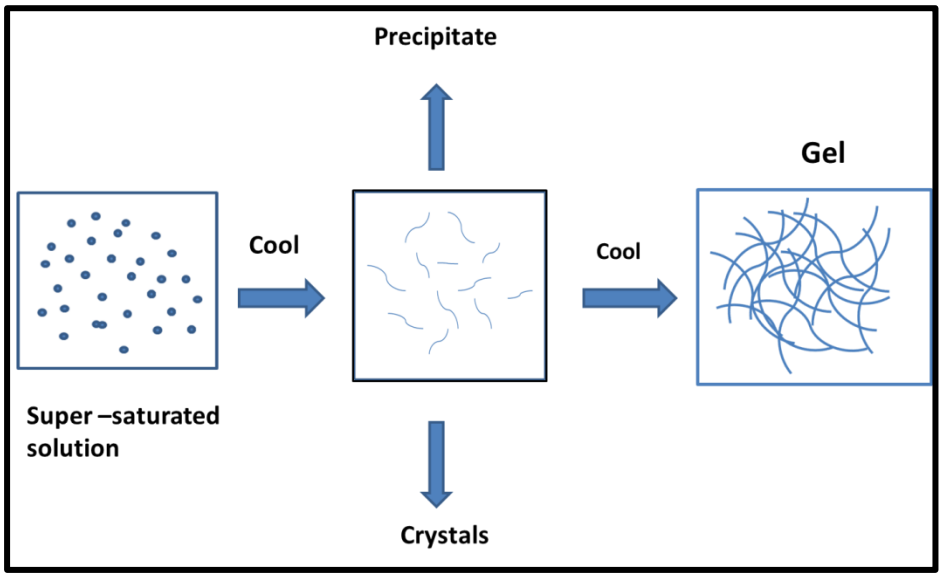

Figure 1-18: Aggregation process of low molecular weight gelator and is adapted from reference no. [81] .

Generally, the entangled fibre like structure is formed by a spontaneous self-assembly of individual molecules of gelator. Gelators aggregate in different structures such as platelets, tubules, rods and others. Optical microscopy studies show that the start of the fibrous network is nucleation of these gelator molecules which stimulates the growth and the branching as shown in Figure 1-19 [85]. These aggregates have a

uniform diameter. Hence, the growth or the self-assembling process largely depends on the nature of the gelator. For instance, sorbitan monostearate (Span 40) molecules assemble themselves into two layers facing each other. This is due to the molecules consisting of a hydrophilic group (sorbitol) which aggregate head to head whilst the hydrophobic tail (fatty acid chain) arrange themselves tail to tail. In turn, these aggregations form the nuclei of tubule structures as shown in Figure 1-20 [82].

Another example is N-stearoyl-L-alanine methyl ester which self assembles through both hydrogen bonding and van der Waals forces as shown in Figure 1-21. These two examples represent one-dimensional growth to form fibres [105]. In addition, the gelator hexatriacontane forms thin microplatelets which grow in equal rates along two axes to give a different form of growth which is two-dimensional as shown in Figure 1-22 [105, 106].

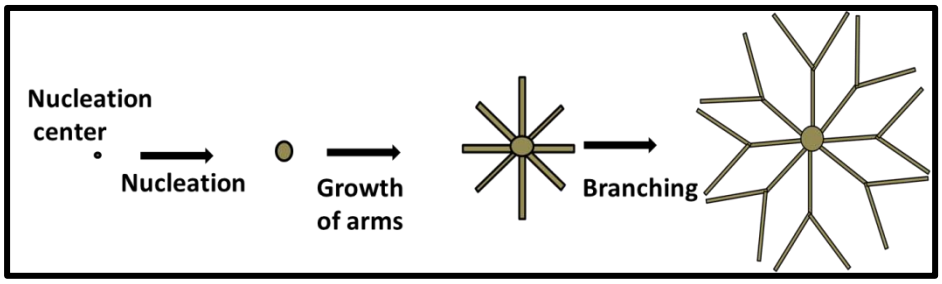

Figure 1-19: Nucleation and fiber formation adapted from reference no. [85].

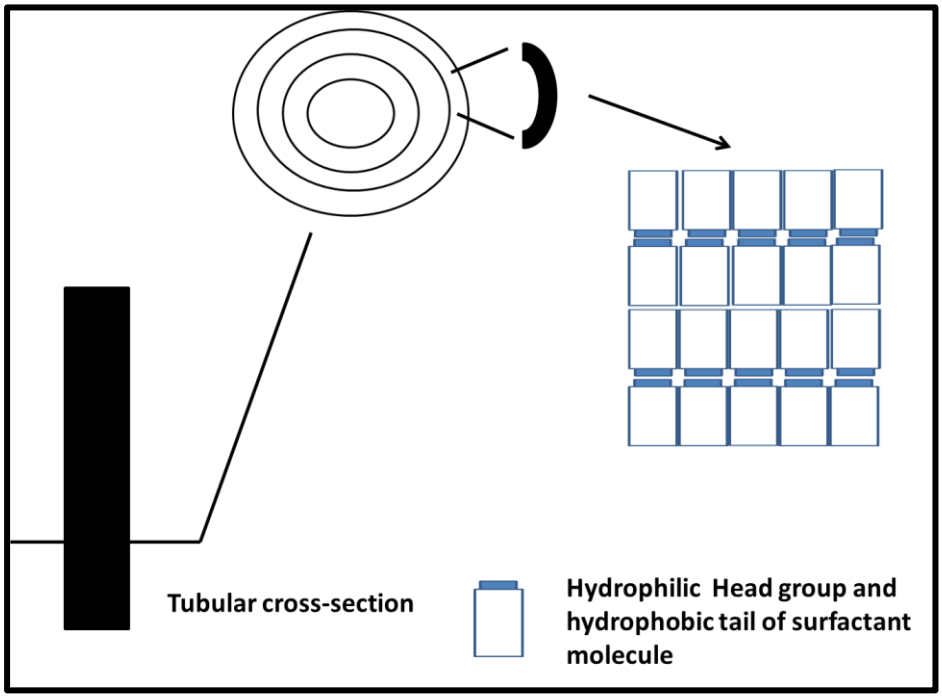

Figure 1-20: Aggregation of span 40 adapted from reference no. [82].

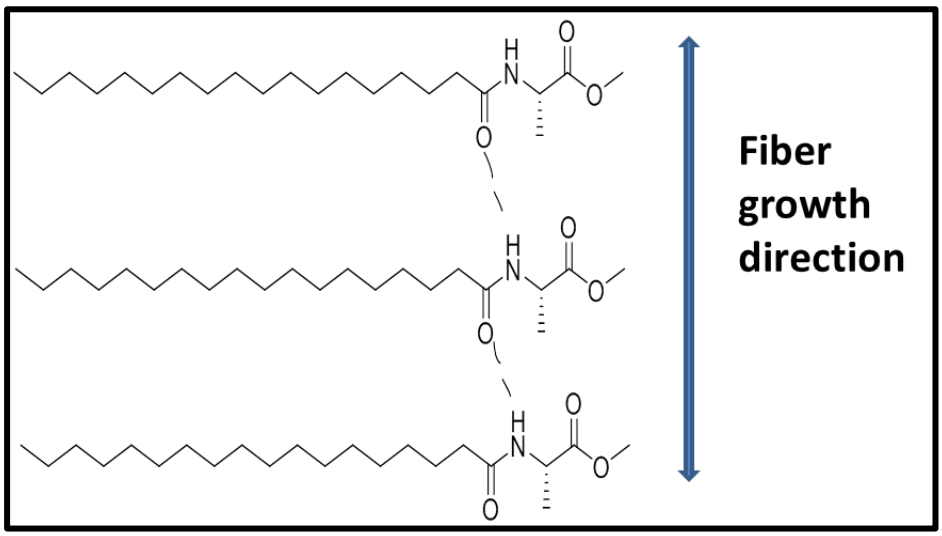

Figure 1-21: Aggregation of N-stearoyl-L alanine methyl ester adapted from reference no. [105].

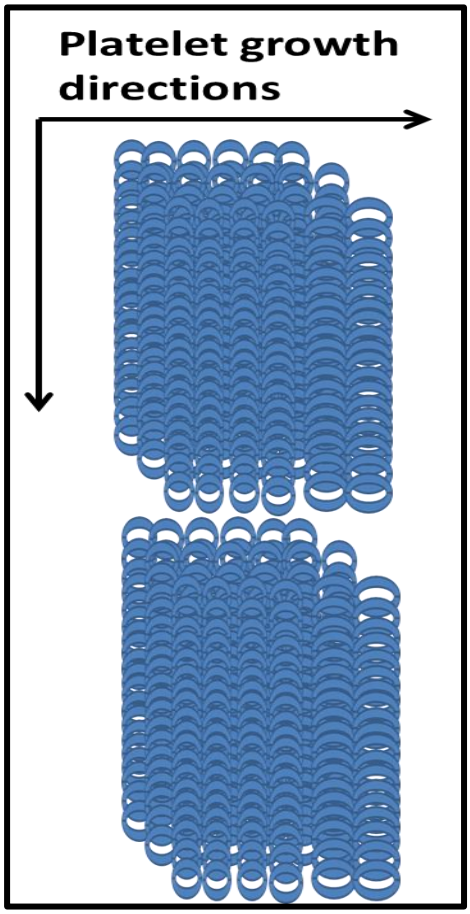

Figure 1-22: Two dimensional growth of hexatriacontane gelator adapted from reference no. [105].

1.4 12-hydroxystearic acid properties

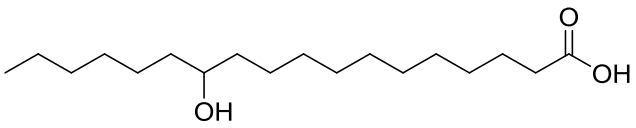

Figure 1-23: Chemical structure of 12-HSA.

The main gelator that was used in this research is the 12-hydroxystearic acid as shown in Figure 1-23 where the 12-hydroxystearic acid (12-Hydroxyoctadecanoic acid) has empirical formula $C_{18}H_{36}O_3$ with a melting point range 71-74 °C. Commercially, this material contains

15% of stearic acid and 85% of D-12-hydroxystearic acid while Burkhardt *et al* referenced that the commercial 12-HSA contains 20 to 30% impurities of ricinoleic, ricinelaidic, stearic, or oleic acid. This gelator is derived from castor oil by hydrogenation of ricinoleic acid. 12-HSA has been used to gel edible oils such as canola oil [76, 107, 108].

1.4.1 Impact of 12-HSA chemical structure on gelation.

Stearic acid self-assembles due to both London dispersion forces and hydrogen bonding. Stearic acid shows a lower ability as a gelator in comparison with D-12-HSA. This is because of the presence of a hydroxyl group in the skeleton of stearic acid. Hydroxyl groups provide the structure of the stearic acid the ability to hydrogen bond and to gel a wide variety of solvents [109, 110]. The position of the hydroxyl on the skeleton of stearic acid has an effect on the gelation as demonstrated by Abraham *et al* who studied the position of hydroxyl group at C2 and C3 and organogels were not formed by these compounds with mineral oil. This is because with these positions of the hydroxyl group, the molecules were unable to form hydrogen bonds which in turn retarded the growth of fibres. Whilst, the compounds prepared with hydroxyl groups at C6, C8, C10, C12 and C14 using the same solid content, were able to form organogels and their FTIR and X-ray diffraction results showed the same pattern for all organogels. These results suggested that these molecules assembled themselves in the same manner [111].

Also, Wu *et al* studied the gelation of 12-HSA using different solvents and this gelation was explored by FTIR, X- ray diffraction (XRD) and optical microscope. Figure 1-24A shows the gelation of organogels of 12-HSA in hexane and dodecane. The12-HSA molecules aggregate in a way to form cyclic dimers. This kind of dimerisation led to form fibres, which were observed by optical images. The FTIR study revealed the

presence of a peak associated with the carbonyl group of 12-HSA at 1690 cm^{-1} and the crystal arrangement of 12-HSA was hexagonal polymorph as determined by XRD. Whilst, the organogels of 12-HSA in acetonitrile showed 12-HSA aggregations as an acyclic dimer as presented in Figure 1-24B. The optical images of these organogels showed spherulites and the carbonyl peak in FTIR spectrum appeared at 1720 cm^{-1}. Also, the XRD showed the 12-HSA arrangement gave a triclinic polymorph [112].

Moreover, Rogers *et al* has probed the gelation of 12-HSA in mineral oil by synchrotron infrared spectromicroscopy and they found that the hydrogen bonds between hydroxyl-hydroxyl groups were responsible for both the transient junctions and the growth of the fibres longitudinally as shown in Figure 1-25. The carbonyl-carbonyl hydrogen bonds were responsible for the dimerization of 12-HSA molecules [113].

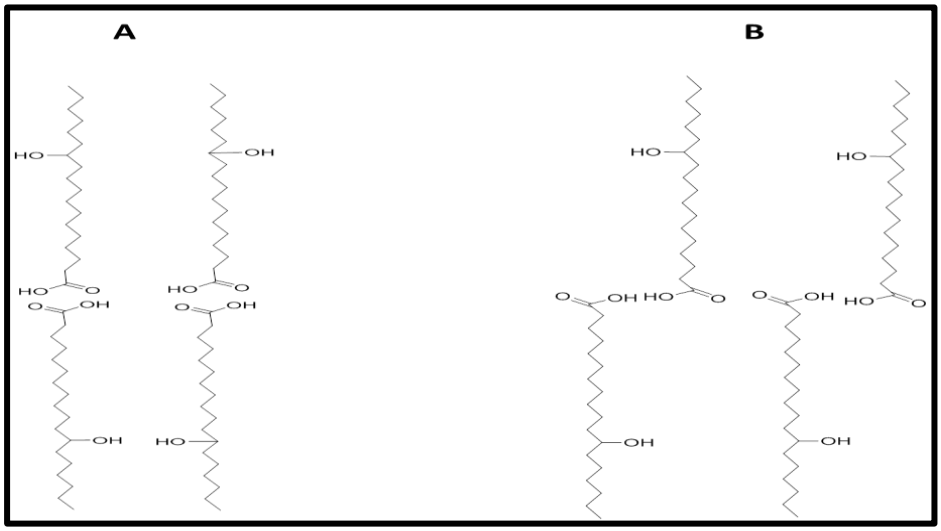

Figure 1-24: Schematic diagram of the 2 possible dimerization of 12-HSA where A represents the cyclic dimerization and B represents acyclic dimerization, this figure is adapted from reference no. [112].

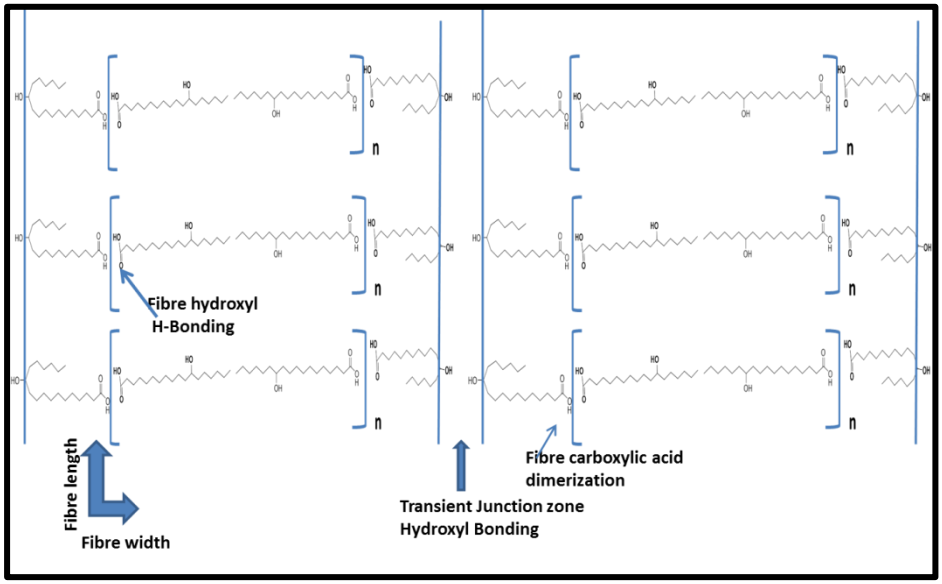

Figure 1-25: Depiction of the development of the fibre scaffold by 12-HSA molecules and this figure was adapted from reference no. [113].

1.5 Characterisation of organogels

Different characterisations studies can be carried out to evaluate the specific properties of organogels as listed below.

1-Hydrogen bonding: the major non-covalent interactions to form organogels are hydrogen bonding which can be detected by Fourier - transform infra-red spectroscopy. For example, the 2-aminobenzothiazole and 1,3,5-benzenetricarboxylic gelators have a carbonyl group (ester and amide groups respectively) which have specific absorption bands in the IR spectra and hence can be used to detect changes in hydrogen bonding [114].

2-Morphological properties: the nano scale structure of the organogels can be visualised using, TEM and atomic force microscopy (AFM) [115]. Moreover, optical microscope or the polarised light microscope can show how the aggregates form the scaffolds.

3-Rheological properties: Oscillatory measurements are used to determine the viscoelastic properties of organogels. Parameters such as the elastic modulus or storage modulus (G′) and viscous or loss modulus (G″) can be measured to identify if the organogel is solid like or not. There are several tests used to determine G′ and G″ of the organogel and the first test is the amplitude sweep where the % strain is increased at a constant low frequency. Also, this test specifies the point of % strain that the gel structure breaks down (i.e. the flow point) where the G′ is equal to G″. Moreover, it shows the linear viscoelastic region which reflects the following: stability of the organogel , the strength of the organogel and the range of the % strain where G′ is constant [116]. Secondly, the frequency sweep test where this test is run at a constant strain but with different frequencies where G′ should be independent of frequency for a solid branched fibre network. This was noticed in the 1.5% w/w of dibenzylidene / liquid paraffin organogel where the G′ was frequency independent [117].

4-Phase transition temperatures: the transfer between the phases of organogel which are the solid phase and the liquid phase can be determined using different techniques as follows:

a- Vial inversion method where the phase transition to a solid is when on inversion of the vial there is no flow [118].

b- Differential scanning calorimetry can determine the melting and crystallisation temperatures and the enthalpy of crystallisation and melting.

c- Rheology, where at low % strain and low frequencies the gel is heated on the rheometer plate and when G′ is equivalent to G″, this represents the phase transition temperature.

1.6 Aims and objectives

The goal of this research is to prepare organogels for intratumoural delivery specifically for unresectable tumours. The organogel can release the lipophilic prodrug of GEM slowly inside the tumour. The prodrug can also overcome the problems of GEM as described in **section 1.1.5** which are the rapid metabolism, the hydrophilicity and the transport of Gem into the cells by active transport. Organgels were selected where the oils and propylene glycol are good solvents for the prodrug of GEM. The selection of the gelator for this research was 12-HSA because of its availability and it's widely used within other industries but not for intratumoural delivery.

The main aim of this study is a preparation of organogels that are suitable for intatumoural injection using 12-HSA with firstly, the range of oils where they are soybean oils (SO), medium chain triglyceride (MCT) glyceryl tributyrate (TGB) and glyceryl triacetate (GTA) and secondly preparation of organogels with propylene glycol (PG). These oragnogels were investigated according to our aim by studying the

thermal stability and the robustness of the oragnogel to guarantee the presence of organogel in the tumour for long period and this was assessed in chapter 2 and 3. These characteristics help to reach to the second main aim in our work which is the depot that aids in slowing down the release of *N*4- myristoyl gemcitabine.

Objectives of Chapter 2 and 3

- Formulation of 12-HSA in oils and in PG at different concentrations.
- Determine the transition temperatures from solution to gel and gel to solution using table top rheology, and differential scanning calorimetry (DSC) which help to investigate the thermal stability of the organogel.
- Amplitude sweep testing to determine the G′ (solid like behavior), G″ (liquid like behavior), linear viscoelastic region (LVER) and flow point.
- Microscopy studyto show the microstructure of organogels.
- ATR-FTIR to study the hydrogen bonds that are responsible for gelation.
- Evaluation of the organogel mechanical strength by frequency sweep, time dependent recovery tests and creep and recovery tests.

The depot and the slow release of *N*4- myristoyl gemcitabine is the second goal in this study as mentioned before and this evaluated as in Chapter 4

Objectives of Chapter 4

- Study the effect of the addition of *N*4-myristoyl gemcitabine on the selected organogel by executing the following tests: vial inversion, DSC, amplitude sweep and microscopy.
- Drug release studies of *N*4-myristoyl gemcitabine (gemcitabine C14) from the selected organogels.

Chapter two

Optimisation and characterisation of 12-HSA/ oil organogels for localised drug delivery

2. Optimisation and characterisation of 12-HSA/ oil organogels for localised drug delivery

In this chapter, the optimisation of organogels based on 12-HSA in oils will be described, with the aim of creating an organogel for localised drug delivery. The specific focus of this chapter is the selection of the oil and gelator concentration based on the thermal and mechanical characterisation of the 12-HSA organogels by vial inversion, DSC and rheology. Further mechanistic insight in the organogel structure and intermolecular interactions is afforded by light microscopy and ATR-FTIR respectively.

2.1 Introduction

The oily organogels proposed in this chapter, are used to create a depot. Many other researches have considered the use of oils to attain this slow and prolonged release from a depot.

Firstly, diclofenac epolamine was formulated such as a microemulsion of mixtures of oils of capryol (propylene glycol monocaprylate) and of Labrasol (caprylocaproylproyl macrogol-8 glycerides) to control and to slow the drug release through the transdermal route [119]. Also, sesame oil was formulated with sorbitan monostearate and guar gum as a topical drug delivery system to control the release of ciprofloxacin [120]. Additionally, antipsychotic drugs were formulated with oils such as sesame oil, coconut oil and other vegetable oils to prepare long-acting intramuscular injectable formulations [121].

The oils that were selected in our research are a series of pharmaceutically acceptable oils i.e. soybean (SO), medium chain triglycerides (MCT), glyceryl tributyrate (TGB), and glyceryl triacetate (GTA). Figure 2-1 shows the glyceride as a common backbone

structure of the oils and the carbon chain length of the substituted fatty acids. The SO is a mixture of saturated, monosaturated and poly unsaturated fat, where the later represents the major content [122].

The next paragraphs will present examples of where the particular selected oils were utilised in different formulations for intratumoural delivery or for targeted delivery in cancer therapy. SO has been used to prepare emulsions with both large and small particle diameters of 254 ± 5.1 nm and 85.5 ± 18.4 nm where the percentage of SO remaining in the tumour was 70% and 10% respectively [123]. Also, SO was part of the intratumoural injectable microemulsion containing arsenic trioxide to treat human breast cancer and it showed a significant suppression of cell growth in a breast cancer cell line [124]. Also, this oil has also been used with 12-HSA to create an organogel for ibuprofen oral controlled delivery [125].

MCT has been used in many gels such as gels for intratumoural injection were prepared in the following mass proportions (72:17:11) of MCT, phospholipids and ethanol loaded with doxorubicin. The in vitro release study was carried out using different percentage volumes of ethanol in the release media of 0.1M, PBS pH 6.8. It was found the release of doxorubicin was less than 30% of the cumulative amount released after 20 days when the ethanol was 0 and 5% v/v in the release medium [64]. Furthermore, MCT was utilised with soya phosphatidyl choline and ethanol to form an in situ gel to deliver leuprolide for prostate cancer by subcutaneous injection. For this leuprolide gel, the in vitro release study used ethanol as one of the components of the dissolution medium and it was found that approximately 30% of the cumulative amount of leuproilde was released within 28 days when there was no ethanol in the dissolution medium. Additionally, the percentage of the leuprolide released increased to 60% and 90% when

the volume of ethanol in the release medium was 10% and 20% v/v respectively [126]. Also, Strickley has reviewed the excipients used in oral and parenteral preparations where SO and MCT were included in both routes [127]. These examples above support the use of MCT and SO in the organogels.

TGB has been used less extensively in parenteral formulations. An example is an emulsion designed to deliver paclitaxel. TGB was found to be a good solvent for the paclitaxel as this drug has very low water solubility. The emulsion was prepared from 4% of egg-phosphatidyl choline, 3% Tween 80 and 2.25% w/v glycerol [128, 129]. This TGB showed anticancer activity in a murine melanoma model [130].

Additionally the use of GTA as a solvent is in the parenteral administration of many polymeric solutions. Upon injection, the oil diffuses out into the surrounding tissue leaving the polymer as an implant. When the polymeric solutions were injected they formed in situ uniform dense implants with limited holes and this gave slow the release of active constituents such as the combination of poly (DL-lactide) and poly (DLlactide- co-glycolide) in GTA turn solid after in-situ injection [131-133]. Furthermore, the Ahmed group have prepared montelukast as a sustained in situ injectable implant using different polymer concentrations 20%, 30% and 40% w/w of poly-lactic-co-glycolic acid, where they solubilised these polymer concentrations with the solvents NMP, dimethyl sulfoxide, ethyl acetate and GTA. The gels that were subsequently formed were a result of the diffusion out of NMP, dimethyl sulfoxide or ethyl acetate and GTA where the NMP and dimethyl sulfoxide showed a faster release of montelukast compared with gels that prepared with ethyl acetate and GTA [55]. All the above examples of different oils showed that we can use these oils as the liquid part of our organogel formulation which is intended to be

injected into the tumour. Additionally and to the best of our knowledge, no similar research has prepared organogels from 12-HSA in SO MCT, GTA and TGB to deliver anticancer drugs intra-tumourally. Also, we have not found any research exploring the 12-HSA with MCT, TGB and GTA to create organogels. Thus it was interesting to study the effect of these oils on the organogel formulations.

An evaluation of how the liquid component of the organogel influences the physical properties, particularly thermal stability and mechanical strength as these are important for our drug delivery application as they will influence retention at the tumour resection site. Additionally, the selected concentrations of 12-HSA organogel will be for the organogels that give the appropriate mechanical properties and thermal stability for the next step to deliver *N*4-myristoyl gemcitabine.

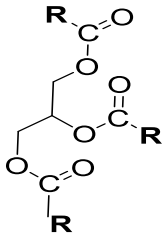

Soybean oil (SO)
$R=(CH)_{16}CH_3$

Medium chain triglyceride (MCT)
$R=(CH)_{4-8}CH_3$

Glyceryl tributyrate (TGB)
$R=(CH)_2CH_3$

Glyceryl triacetate (GTA)
$R=CH_3$

Figure 2-1: The chemical structures of soybean oil, medium chain triglyceride, glyceryl tributyrate and glyceryl triacetate and respective fatty acid chain lengths.

2.2 Materials

The racemic mixture of 12-HSA (99% and CAS number 106-14-9), while the purified soybean oil (SO) and purified medium chain triglycerides (MCT) were kindly donated by Lipoid. The glyceryl tributyrate (TGB) 99% (CAS number 60-1-5 and Lot number BCBL2159V) was purchased from Sigma Aldrich while glyceryl triacetate (GTA) 99% was purchased from Fluka (CAS number 102-76-1 and Lot number BCBD8409V).

2.3 Methods

2.3.1 Organogel preparation

Samples of 12-HSA at 0.5%, 1%, 2%, 3%, 4% to 5% w/w were weighed and mixed with SO, MCT, GTA and TGB to a total weight of 1 g separately in 20 ml scintillation vials. The 12-HSA / oil combinations were screened for gelation at room temperature. The scintillation vials were put into a water bath at 75 °C or 90 °C (some batches of 12-HSA required the higher temperature to solubilise the gelator in the oil) for 30 minutes. After 30 minutes, the vials were taken out of the water-bath and allowed to cool to room temperature. Once cooled, the vials were inverted. When there was no flow upon inversion, the 12-HSA/oil combination was classified as a gel. All organogels for subsequent evaluation by DSC, oscillatory rheology, ATR-FTIR and optical microscopy were prepared using this procedure.

2.3.2 Table top rheology

The solution to gel and gel to solution temperatures were then determined by tilting the vials to 45° for the organogels formed with SO, MCT, GTA and TGB at room temperature. The vials were incubated in a water bath at 75 °C (± 0.1) (melting temperature of 12-

HSA). The temperature was then decreased by 2 °C and the vials were kept at each specific temperature for 15 minutes until reaching 37 °C (the body temperature) and then the temperature increased at the same rate back to 75 °C. The phase transitions from solution to gel and from gel to solution were determined by tilting the vials, and then focusing on whether there was a gelation or not.

2.3.3 Differential scanning calorimetry (DSC)

The temperature and enthalpy of both melting (gel to solution) and solidifying (solution to gel) processes were determined using DSC Q2000 V24.10 (TA Universal) for all the organogels formed above in "table top rheology". A specific amount (7.5 mg to 9.5 mg) of the organogel was put in T zero pan with T zero Hermetic lids. The DSC chamber was flushed with nitrogen. Samples were heated to 100 °C and incubated at this temperature for 30 minutes, then cooled down using a cooling rate of 10 °C/min to 0 °C. After 2 min at 0 °C the samples were then heated to 100 °C using a heating rate 10 °C/min. This was repeated 3 times to determine the enthalpy and the temperature of the phase transitions of melting and solidifying. Data analysis was carried out by using the Universal analysis program. The peak of the curves i.e. maximum heat flow represents the melting and solidifying temperatures, where the area under the curve represents the enthalpy of these transitions.

2.3.4 ATR –Fourier transform infrared spectroscopy

IR spectra were collected using an Agilent Cary 630 spectrometer with ATR crystal at 4 cm^{-1} resolution and 256 scans from 4000 cm^{-1} to 500 cm^{-1}. After being prepared and allowed to gel as described in "organogel preparation", melted organogel samples were placed onto an ATR crystal and scanned after 2 minutes.

2.3.5 Optical microscopy

A drop of the heated organogel was placed on the slide which is already placed on a hot plate at 90 °C and a film of this organogel was formed after gently covering the melted drop with a glass cover slip where this glass cover slip was also on the same hot plate. The slides were then observed using Q IMAGING camera and GX Microscope (Canada). These slides were screened freshly after 2 minutes of preparation using objective X40 at room temperature. The length of fibres was measured using imageJ software by calibrating the images against 100 µm. The images F, G, I and J in **section 2.4.6** were processed with PhotoShop 4 to have better contrast by selecting the option image then select the option Auto contrast as shown in appendix Figure A- 1.

2.3.6 Rheology studies

Rheology experiments were carried out using an Anton Paar MCR302 Modular Compact Rheometer using cone and plate geometry (CP 25-1). Heated organogel samples (~75 °C) were loaded between the plate and cone and then all tests were run at 37 °C.

2.3.6.1 Strain amplitude

Strain oscillatory amplitude sweeps were performed from 0 to 100% strains with angular frequency of 10 rad s^{-1}. Rheoplus 32 V3.61 software was used to evaluate the LVER and flow point. Storage modulus (G′) and loss modulus (G″) were recorded from within the LVER. Four replicate tests were carried out for each organogel.

2.3.6.2 Frequency sweeps

The frequency oscillatory sweeps were executed under an angular frequency from 0.1 rad s^{-1} to 100 rad s^{-1} and selecting a strain from

within the linear viscoelastic region (LVER) of 0.1 %. This test was repeated 4 times.

2.3.6.3 Time dependent structure recovery test

To determine the percentage recovery, the angular frequency was set at 10 rad s^{-1}. Firstly, a low strain of 0.1% was applied for 200 seconds; followed by a high strain of 300% for 60 seconds to destroy the structure of the organogels to the viscous state; and then a third phase of a low strain of 0.1% was applied again for 200 seconds. Reproducibility was ensured by repeating the test five times for the same sample and also repeated with 3 different organogel samples. The instantaneous percentage recovery is the ratio of the first G′ recorded in the third phase to the initial G′ at low strain (first phase) whilst the final recovery is the ratio of last G′ recorded in the third phase to the initial G′ at low strain (first phase) [134].

2.3.6.4 Creep and recovery test

Before executing the creep and recovery test the organogel was held for 25 minutes on the rheometer plate at 37 °C. The yield stress is calculated from log-log plot of shear stress-strain data (i.e. from amplitude sweep data) which is equivalent to the upper region of strain. The value of 50% of yield stress corresponds to the stress that is applied in creep phase (slow constant stress on an organogel to cause progressive deformation) for 60 seconds. The stress is withdrawn in the recovery phase but a strain measurement still made. Compliance (J) is plotted as a function of time in the recovery and creep phases and J represents the ratio of strain to stress [135] . The measurements of this test represent the mean of 3 values. The software Rheoplus was used to determine different parameters of compliance and the Burger model

was used to fit the values of the creep phase as shown in equation 1 which is composed of 3 regions while the recovery phase is fitted to region 4 and region 5 in the equation as shown below. The Burger model consists of Maxwell model and the Kelvin-Voight model as shown in Figure 2-2 which clarifies the 3 regions in the creep phase [136]. Where J_0 is the instantaneous elastic compliance which represents the resistance of the sample to the deformation and J_m represents the retarded elastic region. The J_n defines the viscous flow of the structure or the remaining viscosity after a specific deformation. The time to when the maximum strain is achieved after applying the stress is known as the retardation or delay time $\lambda_{(ret)}$. The materials which are completely elastic show zero $\lambda_{(ret)}$ while the viscoelastic materials have a delay $\lambda_{(ret).}$ The J_{max} is the maximum compliance value in the creep phase. Also the software calculates the recovery phase parameters which are J_E (elastic compliance which is equal to the summation of 2 regions the instantaneous and viscoelastic compliance) and J_v (viscous compliance which equals to $J_{max} - J_E$).

Creep phase

$J(t) = J_0 + J_m(t) + J_n(t)$ (1)

Region 1: Instantaneous compliance J_0

Region 2: Viscoelastic compliance $J_m(t) = J_m^* (1-\exp(-t / \lambda_{(ret)})$

Region 3: Newtonian compliance $J_n(t) = t / eta$

Recovery phase

Region 4: Instantaneous compliance J_0

Region 5: Viscoelastic compliance $J_m(t) = J_m^* (1-\exp(-t / \lambda_{(ret)}))$

(Where is $\lambda_{(ret)}$ the mean retardation time and eta is zero shear viscosity)

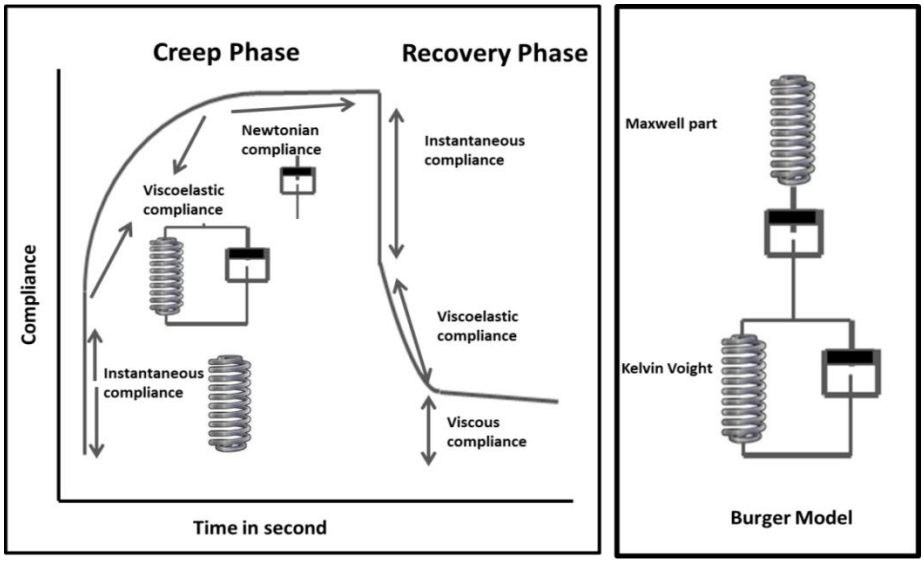

Figure 2-2: The application of the Burger model showing the different regions of each creep and recovery phase.

2.4 Results

2.4.1 12-HSA organogels

12-HSA at 0.5%, 1%, 2%, 3%, 4% and 5 % w/w were mixed with a series of oils i.e. SO, MCT, GTA and TGB at 75 °C for 30 minutes and then left cooling down at room temperature. Visually, gelation was checked by inverting the vials to examine the effect of gravity on the flow of the organogels at room temperature.

As shown in Figure 2-3 organogels were obtained in SO and MCT at all concentration of 12-HSA. In contrast, when GTA and TGB were used as the oil components, organogels were obtained at concentrations of 12-HSA of 1 to 5% w/w and 2 to 5% w/w respectively. This difference in the minimum gelation concentration (MGC) of 12-HSA in the organogels was probably due to the differences in the solubility of 12-HSA in oils. The 12-HSA was less soluble in SO and MCT and needed just 0.5% w/w of 12-HSA to gel SO and MCT. Whilst, the solubility of 12-HSA in GTA and TGB was higher and for this reason at room temperature, there was a need for larger amount of 12-HSA at 1% and 2% w/w to gel the GTA and TGB respectively. In a similar manner, the Patel *et al* prepared organogels by solubilising the sunflower wax, in sunflower oil and the MGC was 0.5% w/w whereas, berry wax and fruit wax gelled sunflower oils at 6% and 7% w/w respectively and they attributed this higher MGC to the higher solubility of berry wax and fruit wax in sunflower oil [137].

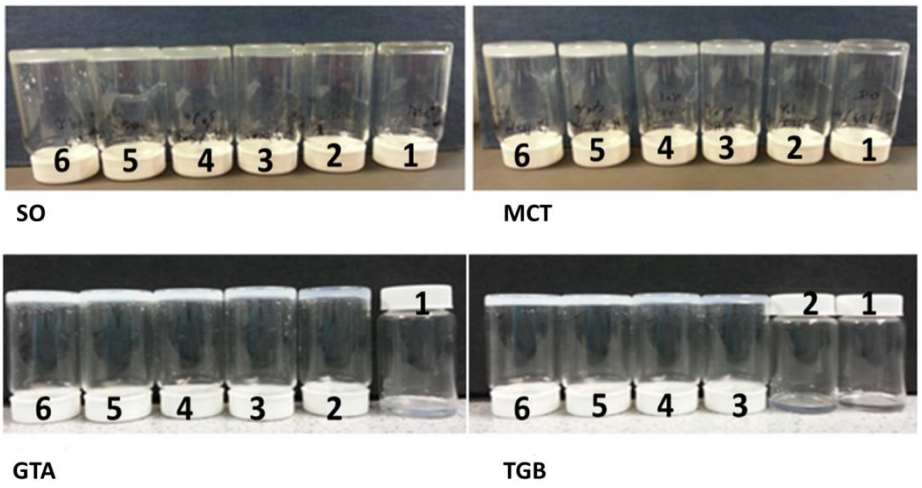

Figure 2-3: Vial inversion of 12-HSA organogels at room temperature in SO, MCT, TGB and GTA where these organogels were prepared by heating to 75 °C or 90 °C for 30 minutes then left to cool to the room temperature and inverted where vial number 6, 5, 4, 3, 2, 1 indicates 5%, 4%, 3%, 2%, 1% and 0. 5% w/w of 12-HSA in different oils. The inverted vials represent the solid organogel and the non-inverted vials represent a solution at room temperature.

2.4.2 Table top rheology

Having established the minimum gelator concentrations for 12-HSA in SO, MCT, GTA and TGB at room temperature, the table top rheology was used to determine the solution-gel and gel-solution transitions temperature of different 12-HSA/oil combinations where the lower temperature set in this experiment was 37 °C. These transitions temperatures were established by simple tilting the vials at different temperatures.

Table 2-1 shows that the solution-gel and gel-solution transitions of temperature of the 12-HSA/oil combinations increased with increasing concentration of 12-HSA. These result are in agreement with those for the N-lauroyl-L-alanine methyl ester gelator when mixed with MCT and SO which showed the same relationship between the concentration of gelator and the transition temperature [138].

However, the following lower 12-HSA concentrations of 0.5% w/w in SO, 0.5% and 1% w/w in MCT, 2% w/w in GTA and 3% w/w in TGB were solutions did not show transitions of temperature at 37 °C or higher where they formed organogels at lower concentrations when a different heating/cooling method and vial inversion were used as described above.

Moreover, Table 2-1 showed a relationship between the minimum amounts that create gels and the length of fatty acid chain of the oils. This relation showed that as the chain length of oil decreased, as the minimum concentration of 12-HSA required to form organogel increased. This relationship holds for all the oils except GTA where the least amount to form organogel in SO was 1% w/w, 2% w/w in MCT, and 4% w/w in TGB as compared to the GTA result (the shortest fatty acid chain length) was 3% w/w. This relationship between the length of fatty acid chain and the minimum amount of gelation is in agreement

with the Hansen solubility parameter study which was carried out by Rogers *et al*. This study showed that as the number carbon atoms of alkane solvent increased, the minimum concentration of 12-HSA to create an organogel decreased [139]. This because the increase in the number of carbon atoms in alkane are accompanied by an increase of steric repulsive of London dispersion forces which represent the main interaction between alkane molecules [140]. This might result in a decrease in the solubility of 12-HSA in SO and in turn decrease the MGC of 12-HSA (18 carbon atoms) with SO (18 carbon atoms of the side chain of glyceride).

Table 2-1: Solution to gel and gel to solution transition temperatures of 12-HSA/oil organogels determined by vial tilting test where the minimum and maximum temperatures were 37 °C and 75 °C. The solidifying and melting rates were 2 °C/15 min. Each value represents the mean of three measurements where --- means liquid or no glation.

Oil	12-HSA (% w/w)	Solution to gel transition temperature (°C)	Gel to solution transition temperature (°C)
MCT	0.5	---	—
	1	—	—
	2	39.00±0.00	45.00±2.00
	3	43.00±2.30	50.33±1.15
	4	49.00±0.00	55.00±0.00
	5	50.33±1.15	55.66±1.15
SO	0.5	—	—
	1	37.00±0.00	45.00±3.46
	2	49.00±0.00	55.00±2.00
	3	56.30±1.15	59.60±1.15
	4	59.00±0.00	63.66±1.15
	5	63.66±1.15	65.66±1.15
GTA	2	—	—
	3	44.33±1.15	53.66±1.15
	4	51.00±0.00	55.00±0.00
	5	53.66±1.15	61.00±0.00
TGB	3	—	—
	4	40.33±3.05	46.33±1.15
	5	44.33±1.15	50.33±1.15

2.4.3 Differential scanning calorimetry

Differential scanning calorimetry (DSC) was used to determine the temperatures and enthalpies of both melting and solidifying process for all the 12-HSA/oil combinations that formed organogels in table top rheology experiment. As shown in Table 2-2 and (Figure 2-4, Figure 2-5, Figure 2-6, Figure 2-7, Figure 2-8, Figure 2-9, Figure 2-10 and Figure 2-11) the transition temperatures and the enthalpies of solidifying and melting processes increased with increasing 12-HSA concentrations. These results are in agreement with those of Rogers *et al* where the DSC transition temperatures and enthalpies from gel to solution increased from 1% to 5% w/w 12-HSA in canola oil organogels [141]. Also, the organogels of 2%,4% and 8% w/w of bees wax in MCT and long chain triglyceride showed the same trend where the solidifying temperature transitions and the enthalpies increased as the gelator increased [142]. Additionally, palladium CNC pincer bis (imidazolylidene) (alkyl C16) in DMSO showed the same trend as our work where increasing the concentration of gelator led to increases in the transition temperatures and the stability of the organogels [143].

Interestingly, the solidifying and melting temperature could not be detected for the following low concentrations of 12-HSA i.e. 1 to 2% w/w in SO and 2% w/w in MCT organogels by DSC but were detected by table top rheology. This difference in the transition temperatures could be attributed the difference in the method's heating/ cooling rates or the difference in the mechanical agitation. Firstly, the cooling/heating rate of DSC was 10 °C/min and the cooling/heating rate in the table top rheology was slower (2 °C/15 min). This effect of cooling rate has been studied on the morphology of the scaffold and it was found, the rapid cooling rate leads to form short branched fibres

and the slow cooling rate forms long with little branching fibres [144]. The second difference in the conditions was the tilting of the vials in table top rheology whilst the DSC experiment was a static method. The effect of mechanical shaking was studied by Cai *et al* who showed that the agitation of cholesteryl derivatives of calix [4] arene with L- or D-phenylalanine in isopropanol decreased the time of gelation from 30 hours to 12 minutes, enhanced the strength by increasing the G′ from 1 x 10^4 to 1x 10^6 Pa and formed shorter and homogenous rod network [145].

In our work, the effect of tilting was to be more dominant than the effect of rapid cooling rate. Since in table top rheology, the tilting might be responsible for forming a denser scaffold at 1% and 2% w/w in SO and MCT organogels and hence showing transition temperatures at these concentrations as compared to DSC with no tilting and no transition temperatures.

Table 2-2: Enthalpies and transition temperatures measured by DSC during melting and solidifying processes of 12-HSA in SO, MCT, GTA and TGB. Each value represents the mean of three measurements ± standard deviation (SD), samples were held for 30 minutes at 100 °C and 2 minutes at 0 °C then the melting and solidifying rates were 10 °C/min.

Oil	12 HSA (% w/w)	Solidifying Temperature (°C)	Enthalpy (solidifying) (J/g)	Melting Temperature (°C)	Enthalpy (melting) (J/g)
MCT	2	—	—	—	—
	3	42.8 ± 0.1	1.5 ± 0.3	51.6 ± 2.4	0.2 ± 0.1
	4	45.3± 0.1	2.5 ± 0.1	52.9 ± 2.1	2.2 ± 0.3
	5	46.4 ± 0.5	3.1 ± 0.5	56.2 ± 1.4	2.8 ± 0.1
SO	1	—	—	—	—
	2	—	—	—	—
	3	48.3 ± 0.6	1.2 ± 0.5	56.6 ± 7.5	0.5 ± 0.4
	4	52.3 ± 0.8	2.1 ± 0.4	62.2 ± 0.1	1.2 ± 0.4
	5	57.6 ± 1.0	3.8 ± 0.8	64.2 ± 1.5	3.3 ± 0.8
GTA	3	54.2 ± 0.2	3.04 ± 0.97	59.7 ± 0.3	1.4 ± 0.2
	4	54.4 ± 1.0	3.89 ± 0.4	59.9 ± 0.3	3.1 ± 0.4
	5	56.1 ± 0.2	4.61 ± 0.5	61.0 ± 0.2	3.7 ± 0.5
TGB	4	40.4 ± 2.0	2.9 ± 0.6	48.2 ± 1.6	2.5 ± 0.7
	5	45.4 ± 1.9	3.2 ± 0.5	51.2 ± 1.6	2.9 ± 0.3

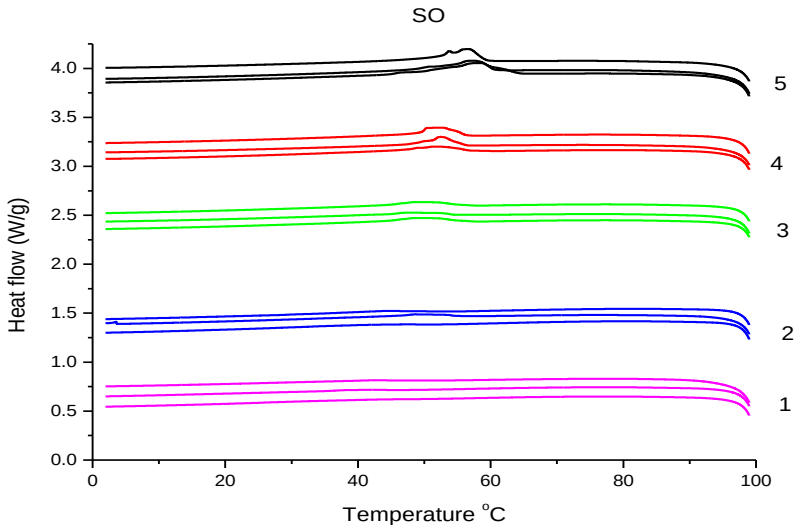

Figure 2-4: Solidifying thermograms of DSC of different concentrations of 12-HSA/SO organogels where rate of cooling was 10 °C/minutes.

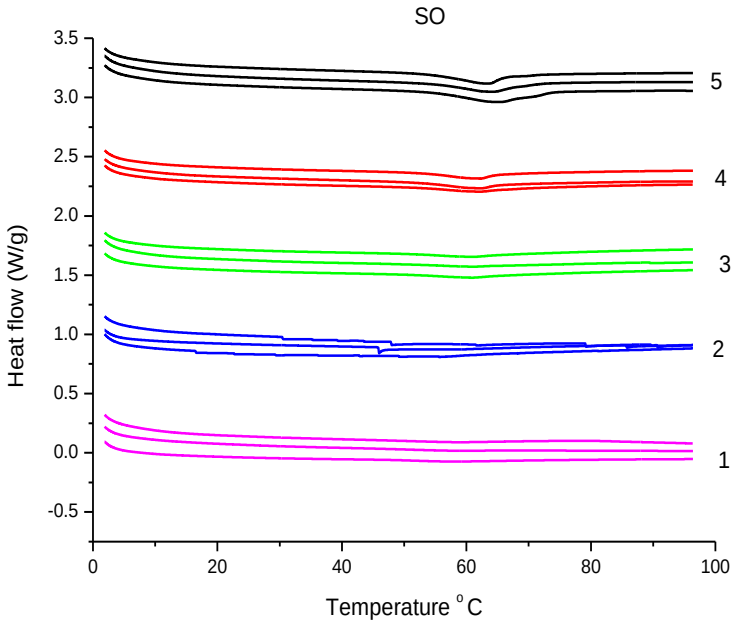

Figure 2-5: Melting thermograms of DSC of different concentrations of 12-HSA/SO organogels where rate of heating was 10 °C/minutes.

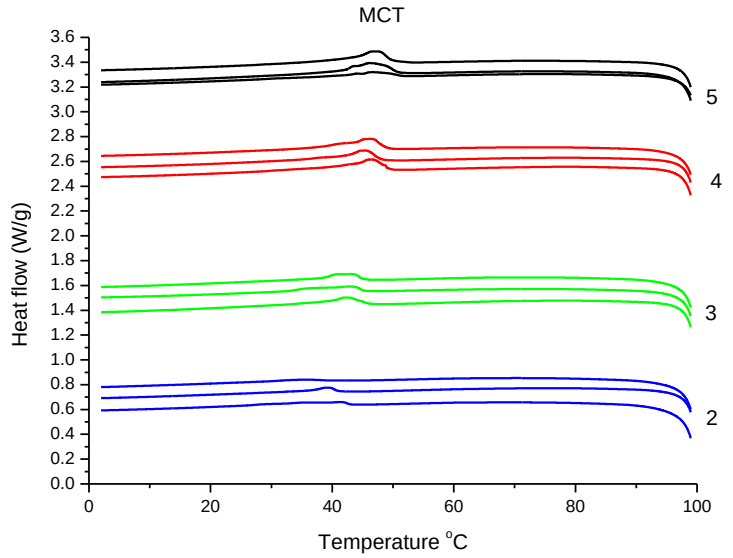

Figure 2-6: Solidifying thermograms of DSC of different concentrations of 12-HSA/MCT organogels where rate of cooling was 10 °C/minutes.

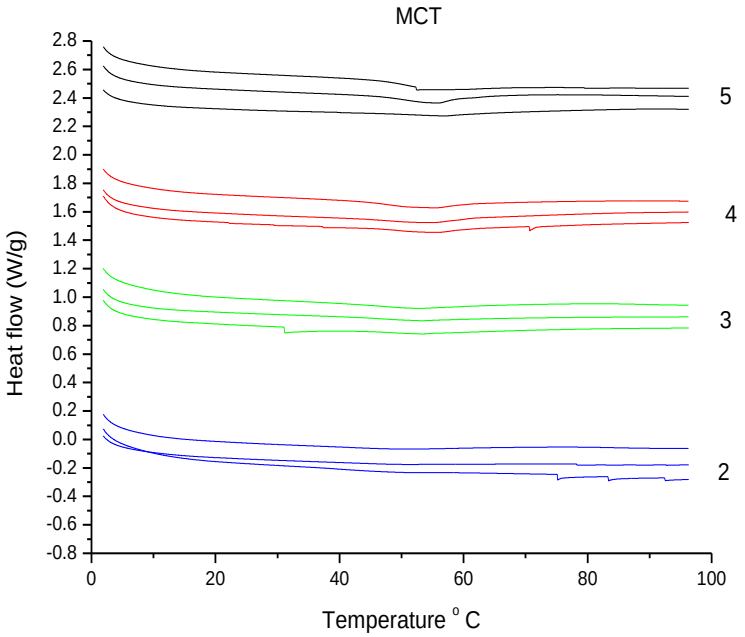

Figure 2-7: Melting thermograms of DSC of different concentrations of 12-HSA/MCT organogels where rate of heating was 10 °C/minutes.

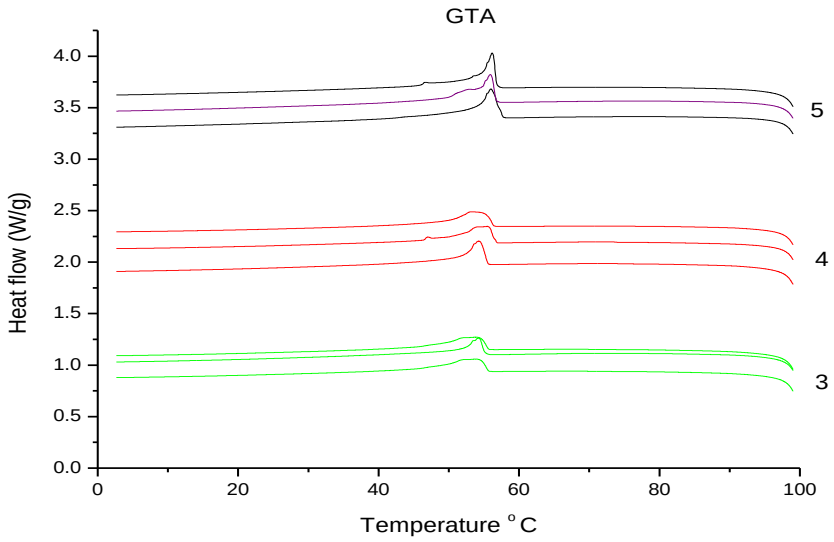

Figure 2-8: Solidifying thermograms of DSC of different concentrations of 12-HSA/GTA organogels where rate of cooling was 10 °C/minutes.

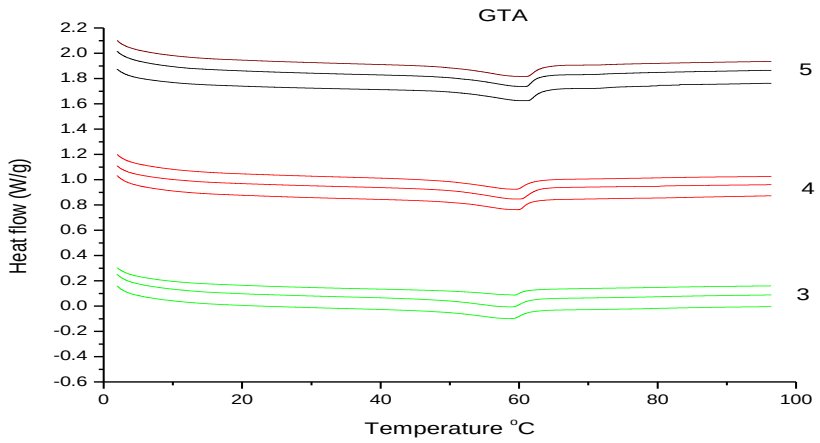

Figure 2-9: Melting thermograms of DSC of different concentrations of 12-HSA/GTA organogels where rate of melting was 10 °C/minutes.

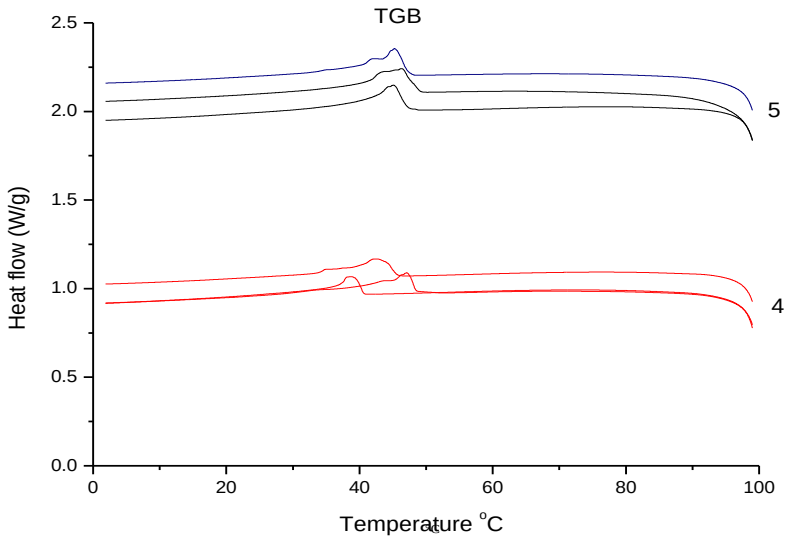

Figure 2-10: Solidifying thermograms of DSC of different concentrations of 12-HSA/TGB organogels where rate of cooling was 10 °C/minutes.

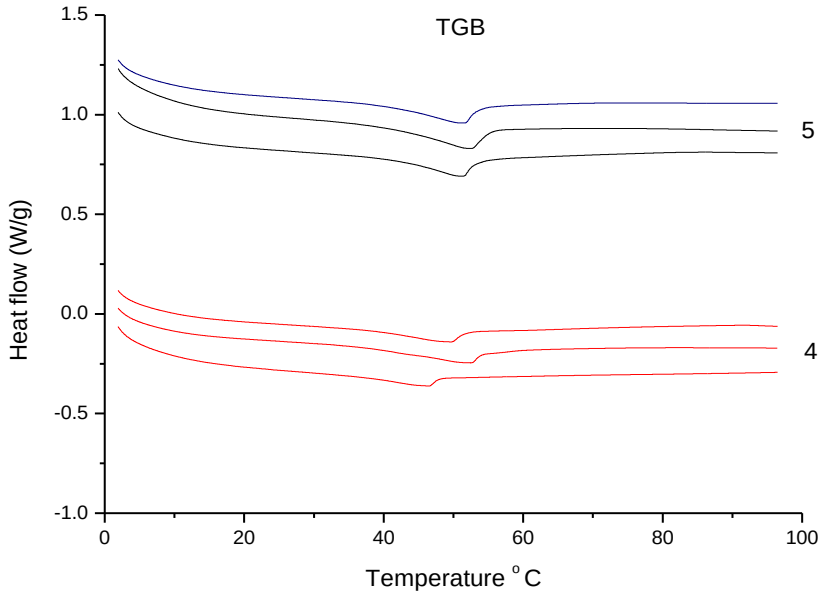

Figure 2-11: Melting thermograms of DSC of different concentrations of 12-HSA/TGB organogels where rate of melting was 10 °C/minutes.

2.4.4 Oscillatory rheology-amplitude sweep

Oscillatory rheology was carried out to characterize the mechanical strength of these organogels 1%, 2%, 3%, 4% and 5% w/w 12-HSA/SO, 2%, 3%, 4% and 5% w/w 12-HSA/MCT, 3%, 4% and 5% w/w 12-HSA/GTA and 4% and 5% w/w 12-HSA/TGB at 37 °C. Amplitude sweep tests were performed to evaluate the storage modulus (G′: solid like behaviour), loss modulus (G″: viscous like behaviour), linear viscoelastic region (LVER: a region at low deformations where both of G′ and G″ are constant and the structure of the sample is in intact). At the end of LVER region the moduli (G′ and G″) start to decrease when the structure of the sample is disturbed. The flow point value is the intersection of the G′ and G″ plots i.e. when G′ is equivalent to G″.

As shown in details in Figure 2-12 (representative figures of organogels in different oils) and Table 2-3. G′ values were higher by one order of magnitude than the G″ values for most of the LVER region for all the organogels. This behaviour is a characteristic of organogels as described by Yan *et al* [146]. Moreover, G′ and G″ values were between 10^3 and 10^6 Pa. A similar range of G′ values was reported for 1% to 5% w/w 12-HSA in canola oil [141]. Also, the value of G′ and G″ increased as the concentration of 12-HSA increased in all oils. This trend in our result is also in agreement with that for organogels of ricinelaidic acid in canola oil where it was found as the concentration of wax increased from 0.5% to 5% w/w, the G′ was increased from 1 x 10^2 to 1 x10^5 respectively [147] .

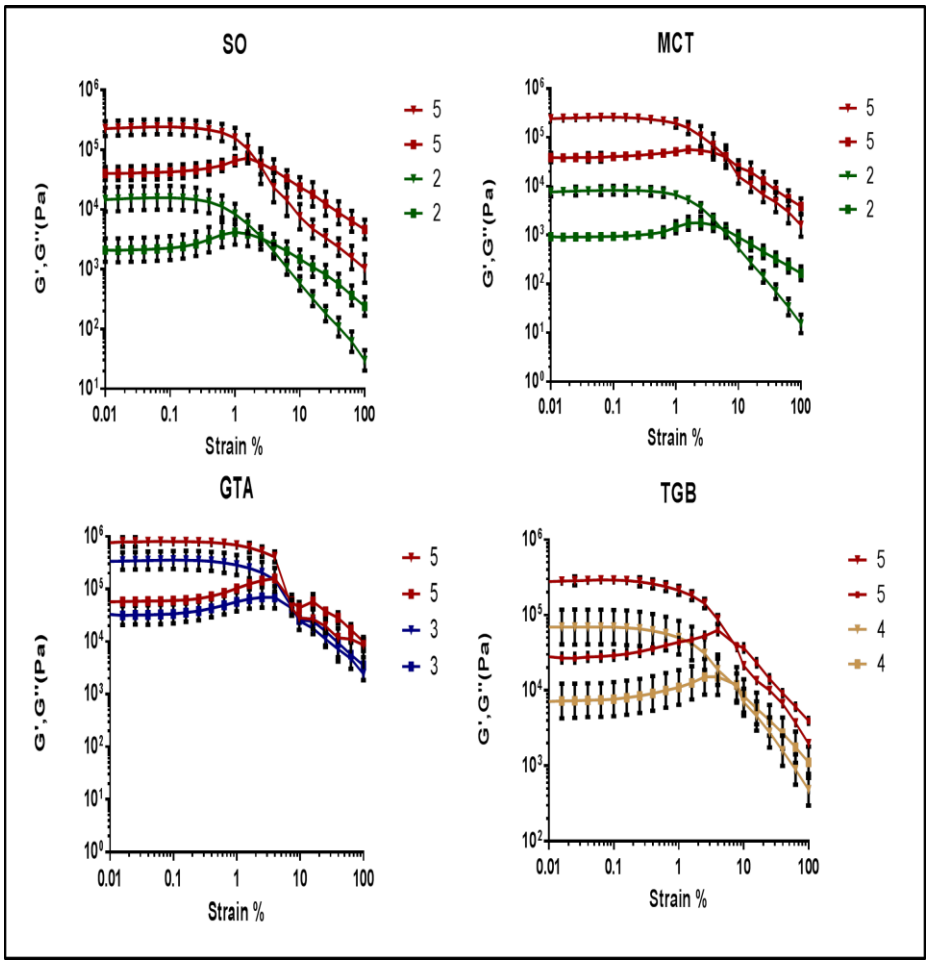

Figure 2-12: Representative figures of amplitude sweep test of different concentrations of 12-HSA in different oils where —●— represents G′ and —■— represents G″ of all organogels. The strain was applied from 0% to 100% and the executed angular frequency was 10 rad s^{-1}. Each figure is a mean of 4 replicates and the standard deviation represented as black bars where note: The amplitude sweep details of all organogels are shown in Table 2-3.

The statistical evaluation of the G′ values generated in the amplitude sweep test was carried out to compare the same solid content of the 12-HSA in different oils as presented in Table 2-3. All G′ values of 3, 4 and 5% w/w of 12-HSA/GTA organogels were statistically higher than the G′ of organogels of the corresponding concentration in SO, MCT and TGB. These higher values of the G′ may be due to the rapid solidifying of all GTA organogels in the narrow gap between the cone

and plate of the rheometer. The organogels were confined in the gap and gave false high values of G′. This narrow gap impact was recorded by Davis and Stokes where they observed a high G′ when they tested carbopol suspensions which became gels upon decreasing the gap [148].

The statistical evaluation of the flow point and LVER parameters was undertaken to compare the concentrations of 12-HSA organogels in the same oils. The flow point values of different concentrations of gelator in MCT and GTA showed no significant difference ($p > 0.05$), whilst the flow point of 1% w/w of 12-HSA/SO had significant difference ($p<0.001$) compared to the higher concentrations of 12-HSA in SO.

Regarding the comparison of the LVER of different concentrations in the same oil, the LVER of 2% w/w of 12-HSA/MCT showed a higher significant value ($p < 0.05$ and $p < 0.01$) compared to 5% w/w and 4 % w/w 12-HSA/MCT respectively. Additionally, the LVER of 5% w/w 12-HSA/GTA had significant different value ($p< 0.01$) compared to the lower LVER of 4% w/w 12-HSA/ GTA. While the LVER values of organogels in SO gave no significant differences. The high value of LVER of 5% w/w 12-HSA/ GTA can be justified by the same reason as used to explain the higher G′ of GTA organogels.

In summary, the higher concentrations of 12-HSA in organogels showed high values of G′ where the lower amounts of 12-HSA in organogels showed higher values of LVER and flow point. Additionally, the statistical analysis did not show significant differences in the flow point and LVER parameters of the amplitude sweep at high concentrations of 12-HSA in SO, MCT and TGB organogels. Thus, further experiment should be undertaken to differentiate between organogels in different oils and different concentrations of organogels in the same oil.

Table 2-3: Amplitude sweep parameters for 12- HSA in SO, MCT, GTA and TGB organogels (values represent the mean of ± SD, (n=4)). One way ANOVA with Tukey's post hoc test was used for statistical analysis.

Oil	12-HSA (% w/w)	G′ x 10^4 (Pa)	G″ x 10^3 (Pa)	Flow point %	LVER %
MCT	2	0.766 ±0.17	0.925 ± 0.18	5.746 ±2.00	0.440 ± 0.16 Δ
	3	3.398 ±0.33	4.770 ± 0.51	3.760 ± 1.05	0.254 ±0.08
	4	11.592±1.48	16.225 ± 1.80	2.789±0.57	0.147 ±0.05
	5	24.025±4.62	38.850 ±9.46	5.240± 2.56	0.231 ±0.01
SO	1	0.312 ± 0.68	0.374 ± 0.08	15.150±6.57 ◊	0.394 ±0.08
	2	1.474± 0.86	2.098 ± 1.21	3.260±1.75	0.270 ±0.24
	3	3.973 ± 0.94	6.610 ± 2.00	2.190±1.28	0.170 ±0.04
	4	10.248±1.44	16.775 ± 1.98	1.320±0.20	0.145 ±0.04
	5	22.800± 7.48	40.375 ± 11.61	1.880±0.69	0.230 ±0.08
GTA	3	33.625±14.99 (**)	33.000 ± 16.87	20.370±17.46	0.300 ± 0.12
	4	43.025±4.43 (****)	47.250 ± 3.54	5.926±0.60	0.161 ± 0.03
	5	76.650±18.31 (****)(***)	57.200 ± 8.18	6.970±1.66	0.540 ± 0.17•
TGB	4	6.925 ± 4.83	7.150 ± 4.60	7.920±4.78	0.230 ± 0.12
	5	27.875 ±3.84	28.075 ± 3.94	6.370±1.00	0.170± 0.00

*** * represents statistically significantly higher G′ of 3% w/w 12-HSA/ GTA as compared to all other 3% w/w 12-HSA in different oils ($p < 0.01$). **** and *** statistically significantly higher G′ of 5% w/w 12-HSA/GTA as compared to 5% w/w12-HSA/SO or MCT ($p < 0.0001$) and 5% w/w 12-HSA/TGB ($p < 0.001$) respectively. **** statistically significantly higher G′ of 4% w/w 12-HSA/GTA as compared to 4% w/w 12-HSA/SO , MCT and TGB ($p < 0.0001$). ◊ statistically significant higher value of the flow point of 1% w/w 12-HSA/SO comparing with flow points of all organogels in SO ($p < 0.001$). Δ represents LVER of 2% w/w 12-HSA/MCT had a higher significant difference ($p < 0.05$) and ($p < 0.01$) as compared to the LVER of 5% w/w 12-HSA/MCT and 4% w/w 12-HSA/MCT respectively. • indicates the LVER of 5% w/w 12-HSA/GTA that showed significant difference compared to the LVER of 4% w/w 12-HSA/GTA ($p < 0.01$).**

2.4.5 Power law

To further understand the link between the mechanical strength of the organogels and their structure, the power law was applied in similar approach to Raeburn *et al* [149].The power law associates the G′ and the gelator concentration as shown in the following equation:

$G' = \gamma \Phi^{m}$. (2)

Plotting the G′ versus Φ (concentration of gelator) yields a curvature line where *m*=1/3-D (D = the fractional dimension) and the y is ɣ. The ɣ value indicates to the size of the primary crystals and the strength of their interactions [150]. ɣ can be defined by the following equation:

$\gamma = mA/6c\pi\sigma\xi\, d^{3}_{0}$ (3)

where

m = the number of neighbouring microstructural elements at the interface

A = Hamaker's constant

c = proportionality constant

σ = the diameter of a microstructural element

ξ = the diameter of one microstructure

d_0 = the average of equilibrium distance between microstructural elements

Raeburn *et al* reports a numerical correlation between the *m* (power law component) and the nature of the scaffold as follows: an *m* value between 3 and 6 equates to a colloidal gel and where a value of 2.5

indicates a cross-linked network and a value of 1.4 an entangled semi-flexible network [149].

The data of the power law correlation is summarized in Figure 2-13 and Table 2-4 which show that the correlation between G′ and concentrations of 12-HSA for MCT and SO where R^2 was 0.9984 and 0.9895 respectively. We also found that *m* was 3.81 and 2.62 for MCT and SO organogels which is indicative of colloidal networks and a cross linked scaffold respectively. Similarly, the power law was applied to the gel of bile acid derived dimeric ester in dichlorobenzene and gave a colloidal gel and flocs of fibres (*m* value was 2.9 i.e. nearly 3) [151]. According to Tang and Marangoni group, colloidal gel means that the close aggregates of fibres are connected by linking fibres as depicted in Figure 2-14 [152].

Regarding the *m* value of the SO organogels which was closed to the m value of the organogel of 12-HSA/ canola oil of 2.5 where this value was derived from the analysis of the log G′ (from a frequency sweep test against the log concentrations where the critical gelator concentration had been subtracted) [153]. The cross-linking is depicted in Figure 2-14 and this illustration relies on the explanation of 12-HSA structure and its impact on the gelation as described in detail in Chapter 1 (section **1.4.**1) where fibres cross link other fibres by the transient junctions formed by hydrogen bonding of the hydroxyl groups.

Also, as shown in Table 2-4 the fractional dimension values for MCT and SO organogels were 2.73 and 2.61 respectively. Lam *et al* detailed how the fractional dimension in the power law equation can be used to gain information about the solid content of gelator in the scaffold [154]. Indeed both SO and MCT organogels showed fractional dimension values indicative of a high proportion of the gelator 12-HSA incorporated in the 3D scaffold.

We could not evaluate the GTA and TGB organogels because of limited values of G′ (3 and 2 values respectively) to build the relationship between the G′ and the concentration of gelator.

To summarize, the application of power law equation is indicative of colloidal and cross linked organogels for MCT and SO organogels respectively.

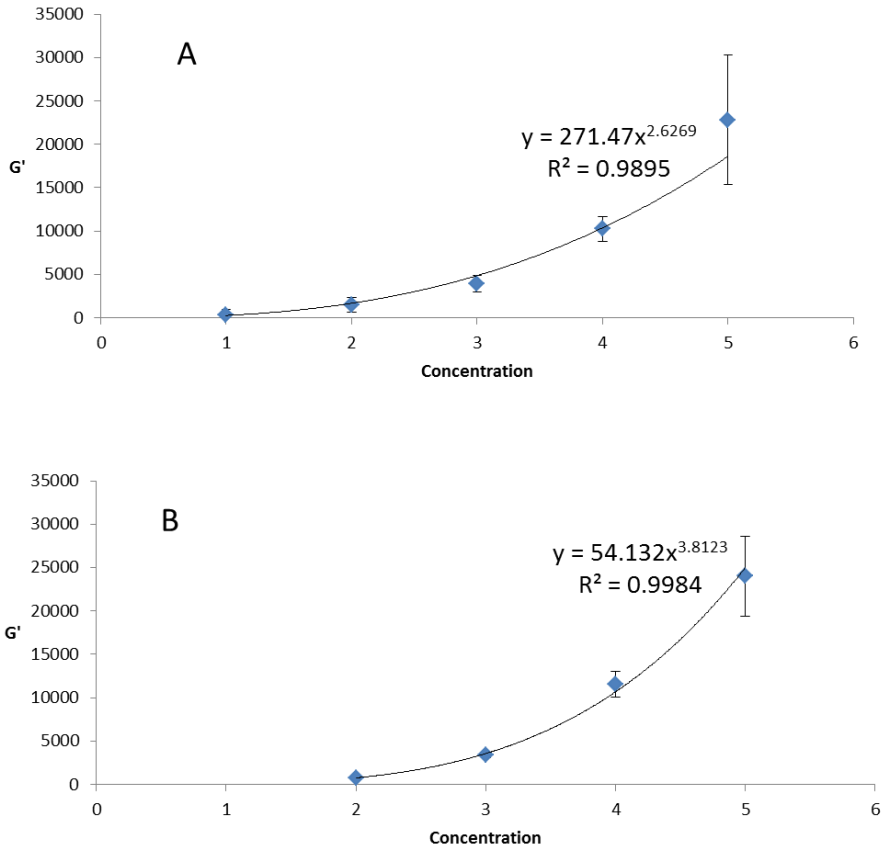

Figure 2-13: Application of power law, A G′ versus corresponding concentrations of all 12-HSA organogels in SO. B represents G′ versus corresponding concentrations of 12- HSA organogels in MCT.

Table 2-4: Numerical values from application of the power (G′ versus corresponding concentrations of 12-HSA in organogels of SO and MCT) where, D = the fractional dimension of the scaffold, ɣ= indicates to the size of the primary crystals and the strength of their interactions, R^2= the regression of G′ versus concentration of organogels in different oils and m the power law component of the correlation of G′ versus concentration of organogels.

Oil phase of 12-HSA Organogels	Fractional Dimension (D)	Power law component (m)	Correlation R^2	Magnitude the strength of the interactions and the size of primary crystals ɣ
MCT	2.73	3.81	0.9984	54.132
SO	2.61	2.62	0.9895	271.47

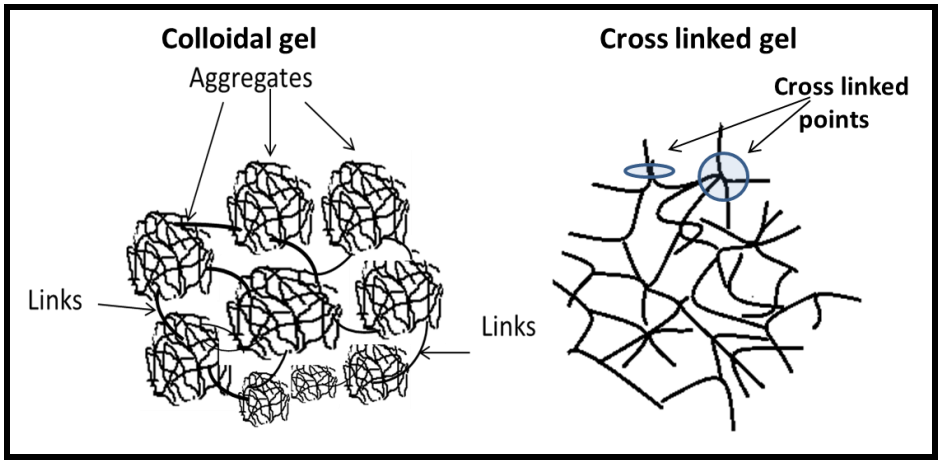

Figure 2-14: Schematic illustration of the colloidal network and cross linked scaffold.

2.4.6 Optical light microscopy

Organogel morphology in different oils and with different concentration of 12-HSA was studied with optical microscopy. The optical images of 12-HSA in different oils were captured by melting the organogels from 90 °C then cooling down to room temperature and then taking images after 2 minutes. As shown in Figure 2-15, organogels were characterized by fibre networks. Moreover, organogels prepared in SO and MCT oils displayed an increase in fibre density with increasing concentrations of 12-HSA. Similarly, the SEM images of conjugated carbamate with an alkyl C8 side chain in benzonitrile showed an increase in the density of the organogel fibre with increasing concentrations from 0.04 to 0.08 and then to 0.1M [155]. The software ImageJ was used to measure the fibre length between branching points of the fibre scaffold using the optical images of 12-HSA in different oils as shown in appendix Figure A- 2. Fibre length of all organogels showed in Figure 2-16 a decrease in the fibre length as the concentration of 12-HSA in SO, MCT and TGB increase. In contrast, organogels prepared in GTA showed an increase in fibre length with the increase in 12-HSA concentration. This opposite outcome agrees with the results of pentafluorophenyl-functionalized in *n*-decane where their TEM images showed an increase in the fibre length as the concentration increased from 2.5 $x10^{-5}$ to 7.5 $x10^{-5}$M [156]. The growth of fibres to form a scaffold can be explained according to crystallographic mismatch branching mechanism as depicted in Figure 2-17. The fibre formation starts by nucleation then grow to form fibres; followed by tip branching (the branching could be at the tip of the fibre or at the side of the fibre as mentioned in the section **1.3.4** (**3D structure of Gelators**) and this progression continues to branch the fibre that create a specific degree of mismatch. The supercooling/ supersaturation effect on the degree of mismatch was studied by Li and

Lam and they found the higher supercooling led to a denser branching network. The parameter to measure the branching density was the correlation length ξ, which is defined as the distance between two closed branching points along a fibril and this correlation length of fibres decreased as the cooling rate increased [157, 158]. Also, the length or the correlation length in our study shortened as the concentration of the 12-HSA increased in all organogels which is indicative of forming denser scaffolds at higher concentrations of the gelator. The exception was with GTA organogels, where the fibre length lengthened as the concentration increased. This means the fibre segment is long and the growth to from the scaffolds by junctions or by the crystallographic mismatch occurred away from the primary nucleation or the primary fibres. This indicated a less dense scaffold due to the less branching fibres. The trend of the decrease in the correlation length was similar to Lam *et al* where they studied the effect of supercooling on the density of the scaffold by measuring the correlation length. The inverse relation between rapid cooling rate and short fibres was obtained with the 2.5 % w/w of 12-HSA in mineral oil. This was done by analysing different polarised images and the range started at around 100µm then decreased to around 25µm. This range of fibre length was close to the range of fibre lengths observed in our study from 70µm ±4.3 to 13.5µm ±1.17 and was a result of increasing the concentration of 12-HSA (supersaturation).

In summary, all organogels showed a fibre scaffold. The fibre length decreased as the concentration of 12-HSA increased in SO, MCT and TGB organogels and created a denser scaffold. However, an opposite relationship was found with the GTA organogels where the correlation length of 12-HSA/GTA organogels increased as the 12-HSA increased creating low density scaffolds.

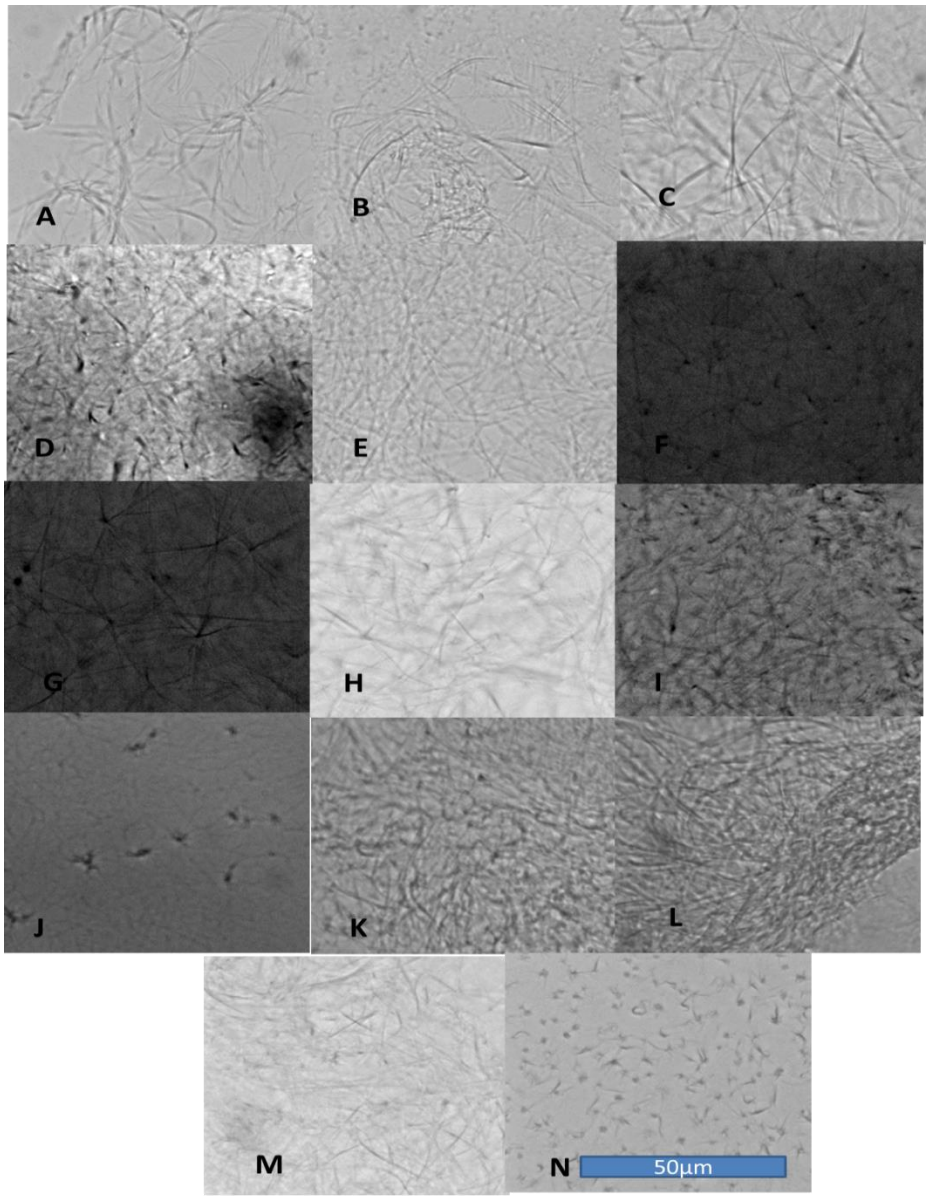

Figure 2-15: Optical microscopy images of organogels of different concentrations of 12-HSA in SO, MCT, TGB and GTA. Where A,B,C,D,E represent 1%, 2%, 3%, 4%, 5% w/w 12 –HSA/SO and F,G,H,I represent 2%, 3%, 4%, 5% w/w 12-HSA/MCT . Also, J, K, and L represents 3%, 4%, 5% w/w 12-HSA/GTA where M, N represent 4%, 5% w/w 12-HSA/TGB respectively. These images were taken after 2 minutes of slide preparation using X40 objective and magnification bar is 50 µm.

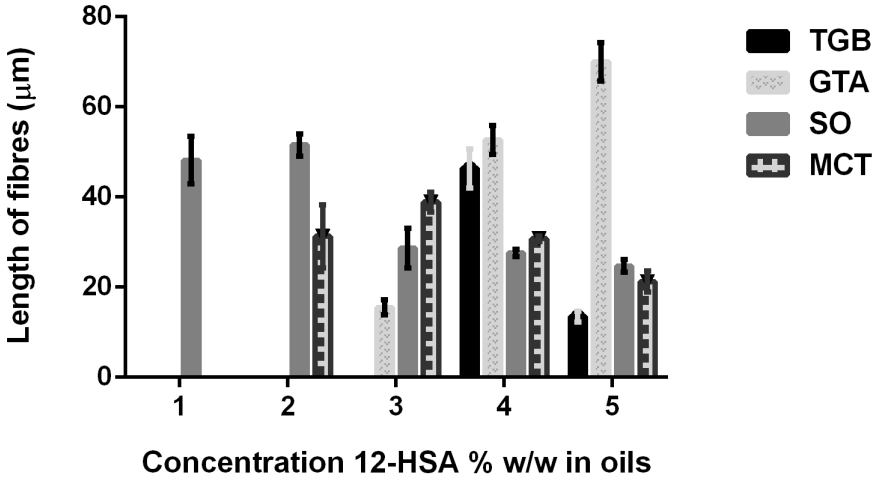

Figure 2-16: Relationship between the correlation length of fibres and the concentration (% w/w) of 12-HSA in organogels of MCT, SO, GTA and TGB. The length of fibres of each organogel represents the average of 3 optical microscopy images where 25 fibres were analysed per image using ImageJ software.

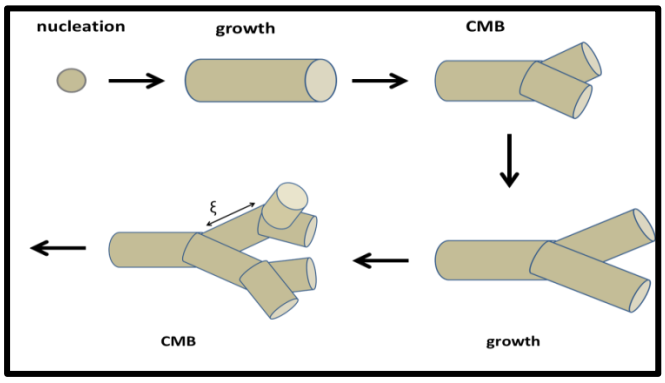

Figure 2-17: Crystallographic mismatch theory, the nucleation, the crystal growth and the growth with crystal mismatch. This figure is adapted from reference [142].

2.4.7 ATR –Fourier transform infrared spectroscopy

FTIR spectroscopy measurements were carried out to monitor the hydrogen bonding between hydroxyl and carbonyl groups of 12-HSA which are responsible for the formation of 3D fibre networks. The FTIR spectra in previous studies of 12-HSA organogels showed different peaks associated with the carbonyl group. Peaks at 1700 cm^{-1} or 1690 cm^{-1} are indicative of 12-HSA dimerisation to form fibres, whilst peaks at 1720 cm^{-1} indicated a spherulite scaffold [112]. Whilst, peaks of 1730 cm^{-1} in the spectra represent interactions of the carbonyl group with the solvent as the monomer [159]. Also, the peak at 3200 cm^{-1} represents the hydroxyl group in 12-HSA [112].

ATR FTIR spectra of all the organogels showed a peak between 1738 cm^{-1} and 1744 cm^{-1} which represented the carbonyl interactions of 12-HSA with oils and the carbonyl group of all oils overlapping as shown in Figure 2-18 (representative figure shows the 5% w/w of 12-HSA in different oils and the pure 12-HSA) (Oil spectra of SO, MCT, GTA and TGB are shown in Appendix Figure A- 3). Similarly, the carbonyl group of methyl oleate appeared at 1740 cm^{-1} and overlapped with the carbonyl peak that appeared at 1700 cm^{-1} of 12-HSA in methyl oleate [113]. Peaks associated with carbonyl of 3%, 4%, 5% w/w 12-HSA in GTA and 4% and 5% w/w 12-HSA in TGB were at 1695 cm^{-1} and close to the carbonyl of pure 12-HSA. Whilst peaks that associated with the carbonyl of 3%, 4% and 5% w/w 12-HSA in MCT and SO shifted to a higher wave number at 1697 cm^{-1}. The 1% w/w 12-HSA/SO and 2% w/w 12-HSA in SO and MCT showed peaks associated with the carbonyl at 1699 cm^{-1}. Also, the hydroxyl (3200 cm^{-1}) groups appeared in all organogels. The hydrogen bond interactions amongst 12-HSA- 12-HSA are responsible for gelation [160, 161]. Correspondingly, our studies are comparable to that of Wu

et al who correlated the 3D fibre network with the peaks of IR of carbonyl and hydroxyl at 1690 cm^{-1} and 3200 cm^{-1} respectively [112].

IR peaks associated with the carbonyl group of 12-HSA and oil	IR peaks associated with the hydroxyl group of 12-HSA
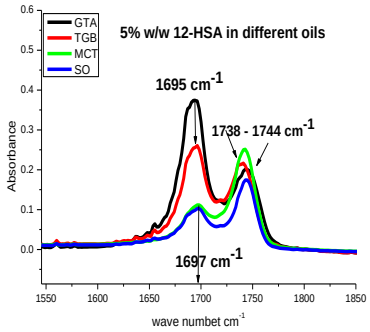	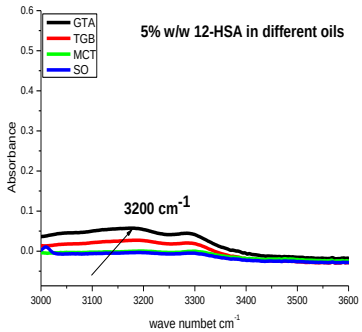
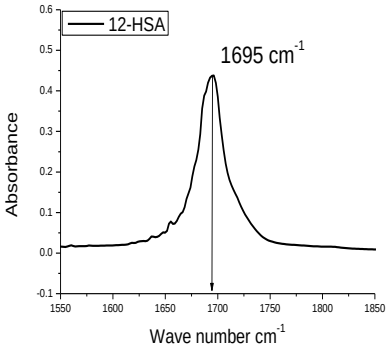	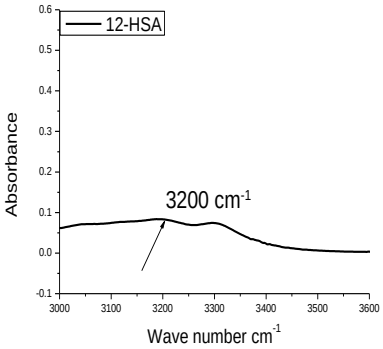

Figure 2-18: Representative figure of ATR-FTIR spectra of 12-HSA in SO, MCT, GTA and TGB to show the peaks associated with carbonyl and hydroxyl that are responsible for dimerization where the last row represent the pure solid 12-HSA.

2.4.8 Frequency sweep

A dense fibre scaffold as observed for SO and MCT by microscopy is important for achieving the goal of an organogel depot for controlled drug release as will be demonstrated by the following example. Behera *et al* reported that an increase in the concentration of Span 60 in sunflower oil led to increase in the density of the fibre network where, 25% w/w of Span 60 in sunflower oil slowed down the release of 1% w/w salicylic acid after 8 hours to 35.95% compared with an organogel containing 18% w/w Span 60 which released 40.62% of salicylic acid in the same time frame [162]. To compare this theory and our findings with attainment of our goals, all further work is focused on the organogels of MCT and SO were a dense fibre network was demonstrated and has excluded GTA organogels and TGB organogels.

The elasticity of the organogel is also important in selecting the combination of 12-HSA and oil for the organogel as higher elasticity will help to keep the organogel as an intact solid into the tumour. Thus, frequency sweep, time dependent recovery test and creep and recovery testing were carried out on organogels with 1%, 2%, 3%, 4% and 5% w/w 12-HSA in SO and with 2%, 3%, 4% and 5% w/w 12-HSA in MCT.

Frequency sweeps were conducted for further examination of the organogel's mechanical strength by applying different angular frequencies. Firstly, the analysis of the frequency sweep results of both oils showed G′ values greater than G″ as shown in Figure 2-19 (representative figures) and Table 2-5.

Similarly, the organogels of 13% of glyceryl monostearate and fractionated coconut oil showed a higher G′ than G″ along the applied range of frequency from 0.1 to 10 Hz where the applied stress was 5 Pa [163]. Also, these results are consistent with the work of Terech *et al*

who evaluated 0.88 % w/w of 12-HSA in dodecane and the result showed higher values of G′ than G″ values as a function of frequency [164].

More detailed analysis of the frequency sweep results can be undertaken by taking the slope of log G′, log G″ versus log angular frequency [165]. When this analysis was carried out for gels of acrylamide/sodium acryloyldimethyl taurate copolymer in isohexadecane and the results of 3% and 5% w/w gels showed solid like behaviour when the slopes of log G′ versus log angular frequency were between 0.06 and 0.056 and the slopes of log G″ versus log angular frequency were between 0.102 and 0.12 [166]. The same analysis was undertaken for the current results of organogels starting with log G′ versus log angular frequency and the slopes of the straight lines as shown in Table 2-6 is within this range 0.02 to 0.06 (near zero). This data indicates that the G′ values were independent of angular frequency. This was similar to the work of Laupheimer *et al*, where they applied a frequency sweeps to organogel of 12-HSA in *n*-decane. They showed greater G′ than G″ values and that the slope of the relationship of log G′ versus log angular frequency was 0.07 and 0.06 for the organogels of 5% and 2.5% or 1.5% w/w 12-HSA in n-decane respectively [167].

The curves of log G″ versus log angular frequency did not show straight lines and instead, these lines exhibited a “u” or “v” shape of the lower frequencies below 2.5 rad s^{-1} as shown in Figure 2-20. Table 2-7 presents the results of log G″ versus log angular frequency where the analysis was carried out for the angular frequency range from100 to 2.5 rad s^{-1} i.e. excluding the low frequency data and showed good correlations for all organogels of SO and MCT. The G″ values as shown in Figure 2-20 decreased from 100 to 1 rad s^{-1} of the angular

frequency and then showed a slight increase in G″ value until reaching 0.1 rad s^{-1} of the angular frequency. This kind of frequency sweep was similar to that of 4% w/v of (peptide protected by a benzyloxycarbonyl group at its N-terminal end and by a hydrazine-naphthalimide group at its C-terminal end) in tetraline that showed a similar pattern of G′ and G″ to our work. This gel showed the same G′ plot and a decrease in the values of G″ as the angular frequency decreased. This means the G′ was frequency independent. This can be attributed to the aggregate behaviour and transient junctions between aggregates or transient junctions at cross-links between fibres [168, 169].

In summary, all tested organogels G′ revealed frequency independent and showed an increase in G′ and G″ values as the concentration of 12-HSA increased. Hence, further analysis is needed to elucidate differences, if any in the strength of the organogels.

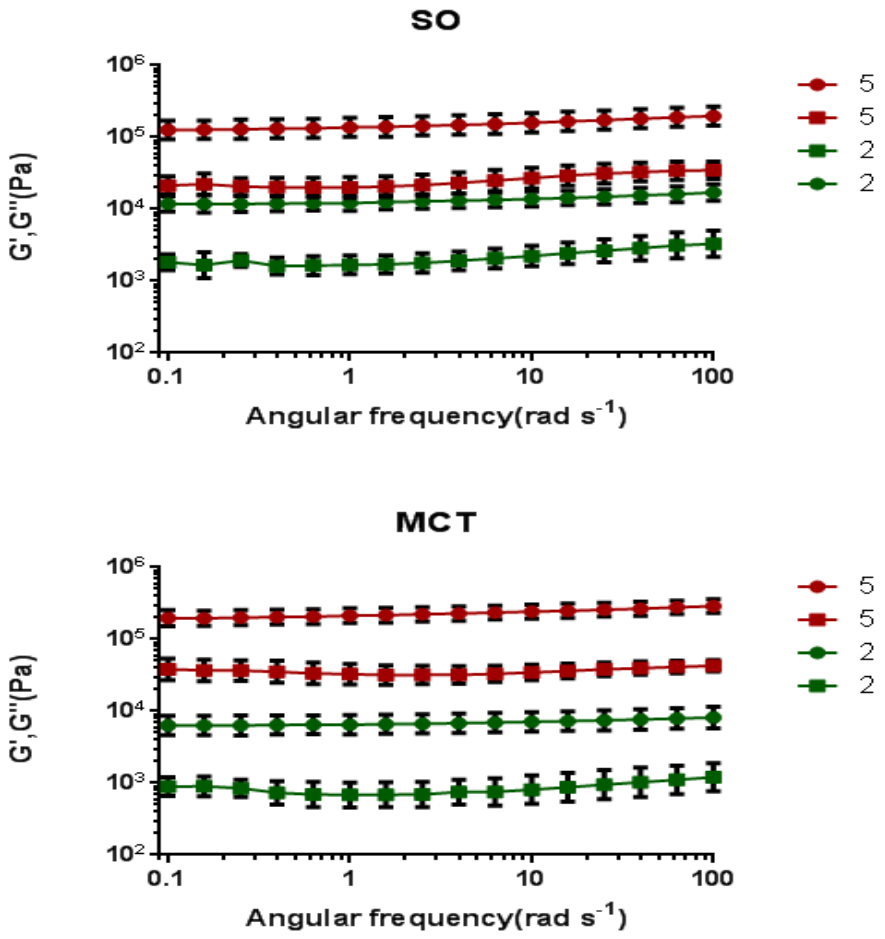

Figure 2-19: Representative frequency sweeps of organogels of different concentrations of 12-HSA in SO and MCT where the applied strain was 0.1% and the angular frequency applied was from 0.1 rad s^{-1} to 100 rad s^{-1}. Each figure represents 4 replicates where —●— represents G′ and —■— represents G″.

Table 2-5: **Frequency sweep G′ and G″ (Pa) of 12-HSA in SO and MCT where each value represents the mean ±SD, (n=4). Where the applied strain was 0.1% and the G′ and G″ were measured at an angular frequency of 10 rad s^{-1}.**

12-HSA Concentration % w/w	(12-HSA/SO) G′ x10^4	(12-HSA/SO) G″ x10^3	(12-HSA/MCT) G′ x 10^4	(12-HSA/MCT) G″ x10^3
1	0.3823± 0.5450	0.444± 0.123	-	-
2	1.3870± 0.3612	2.232± 0.879	0.7085± 0.2609	0.809± 0.464
3	1.9125± 0.4954	2.897± 0.287	2.8350± 0.7945	3.960± 1.123
4	7.9050 ± 2.5844	12.785± 5.684	9.3475± 2.3875	13.667± 3.519
5	15.8950± 5.8064	27.100± 10.685	24.1750± 6.1220	34.500± 9.766

Table 2-6: Log G′ versus log angular frequency of 12-HSA in SO and MCT organogels: data for the slope and the correlation of this relationship where the angular frequency analysis was carried for the whole range from 100 to 0.1 rad s^{-1} of the frequency range.

12-HSA concentration % w/w	12-HSA/SO Slope	12-HSA/SO Correlation	12-HSA/MCT Slope	12HSA/MCT Correlation
1	0.020	0.866	-	-
2	0.052	0.923	0.036	0.928
3	0.045	0.843	0.058	0.959
4	0.057	0.945	0.062	0.979
5	0.066	0.963	0.056	0.979

Table 2-7: Log G″ versus log angular frequency of 12-HSA in SO and MCT organogels: where data for the slope and the correlation of this relationship where the angular frequency range analysis from 100 to 2.51 rad s^{-1} of the angular frequency range.

12-HSA concentration % w/w	12-HSA/SO Slope	12-HSA/SO Correlation	12HSA/MCT Slope	12-HSA/MCT Correlation
1	0.21	0.971	-	-
2	0.17	0.998	0.15	0.983
3	0.17	0.990	0.14	0.990
4	0.13	0.995	0.13	0.995
5	0.13	0.979	0.08	0.981

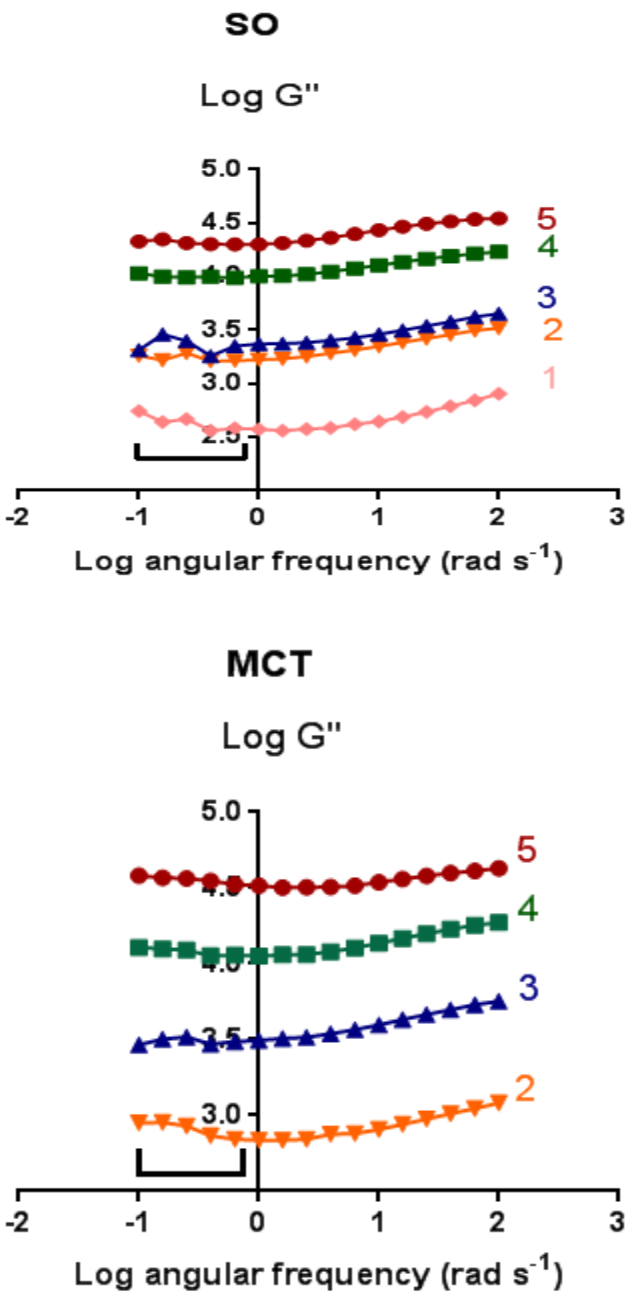

Figure 2-20: Log G″ versus log angular frequency of MCT and SO organogels where the labeled area represents the low angular frequency where each value represents the mean of 4 measurements.

2.4.9 Time dependent recovery

The time dependent recovery test was carried out to test the thixotropic behaviour of 12-HSA in SO and MCT to help in differentiating between the organogels of different concentrations in the same oil. Firstly, a low strain of 0.1% was applied for 200 seconds; followed by a high strain 300% for 60 seconds to destroy the structure of the organogels to the viscous state; and then a third phase of a low strain of 0.1% was applied again for 200 seconds (Figure 2-21) (representative figures). The instantaneous recovery is the ratio of the first G′ recorded in the third phase to the initial G′ at low strain (first phase); whilst the final percentage recovery is the ratio of last G′ recorded in the third phase to the initial G′ at low strain (first phase). As shown in Figure 2-21, the third phase showed straight curves of G′.

This means all MCT and SO organogels reform their 3D structure after removal of high strain i.e. “self-healing”. Indeed, the recovery of the organogel structure was very rapid and all organogels gave a higher G′ than G″ in the third region of this test. In other words, there was not complete destruction of the organogel structure throughout the sample allowing the organogels to recover quickly.

The instantaneous recovery and the final percentage recovery are reported in Table 2-8. Both 12-HSA/SO and 12-HSA/MCT organogels showed quick recovery which increased as the concentration of 12-HSA increased. MCT organogels showed a quicker recovery and higher values. Also, in both oils the 1% w/w 12-HSA/SO and 2% w/w 12-HSA/MCT showed higher percentage of instantaneous recovery compared with the higher concentrations of organogels. The final percentage of recovery values showed good recovery values where the least value was 85.35% and the highest percentage recovery was 97.48%.

These recovery values representing excellent self-healing gels as compared with the gel of 5 mg/ml FMOC-leucine-glycine which were prepared in different compositions of DMSO/water and were reported to have a good range of recovery between 75% and 80% when DMSO volume proportions were less than 0.25 [170]. Also, Mallia *et al* observed a rapid recovery and the percentage recovery was 90 % after applying an external strain on organogels of 2 % w/w primary amide derivatives of 12-HSA in silicone oil. This rapid recovery was attributed to the hydrogen bond strength between 12-HSA molecules [171]. Additionally, all organogels showed a higher value of final recovery than instantaneous recovery. This can be explained by the transient junctions between fibres where they stayed as an active site even after the deformation phase and which helped in the reunion of closed fibres as depicted in Figure 2-22.

In summary, thixotropic behaviour and high percentages values of instantaneous and final recovery were achieved for all organogels.

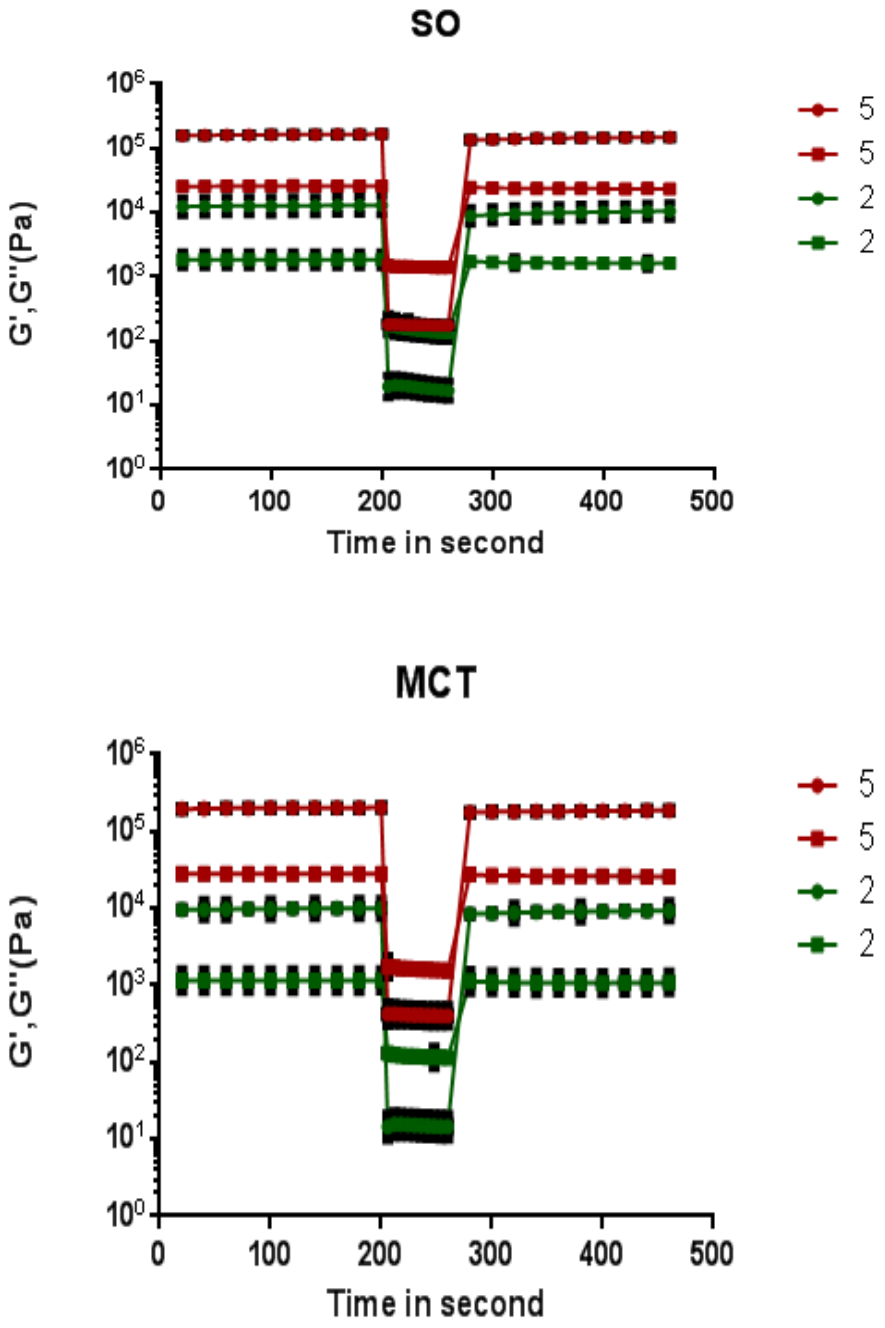

Figure 2-21: Representative figures of time dependent recovery profiles of organogels of 12-HSA in SO and MCT where each figure represents a mean of 3 samples where each sample represented the mean of 5 cycles, where —●— represents G′ and —■— represents G″.

Table 2-8: Time dependent recovery tests for 12-HSA in SO and MCT organogels where the instantaneous recovery and the final percentage recovery values represent the mean± SD (n= 15) (mean of 3 samples and 5 cycles per sample).

Oil	SO					MCT			
12-HSA (% w/w)	1	2	3	4	5	2	3	4	5
Instantaneous recovery%	82.08 ± 3.3	70.88± 3.2	78.72 ± 5.2	84.46 ±2.0	85.06 ±0.5	88.19 ±0.5	87.86 ±0.8	89.25 ±2	89.44 ±1.3
Final recovery %	89.90 ±9.9	85.35 ±4.7	91.16 ±2.9	93.72 ±2.0	93.97 ±0.9	97.48 ±0.5	96.12 ± 1.6	95.13 ± 0.7	95.24 ± 1.6

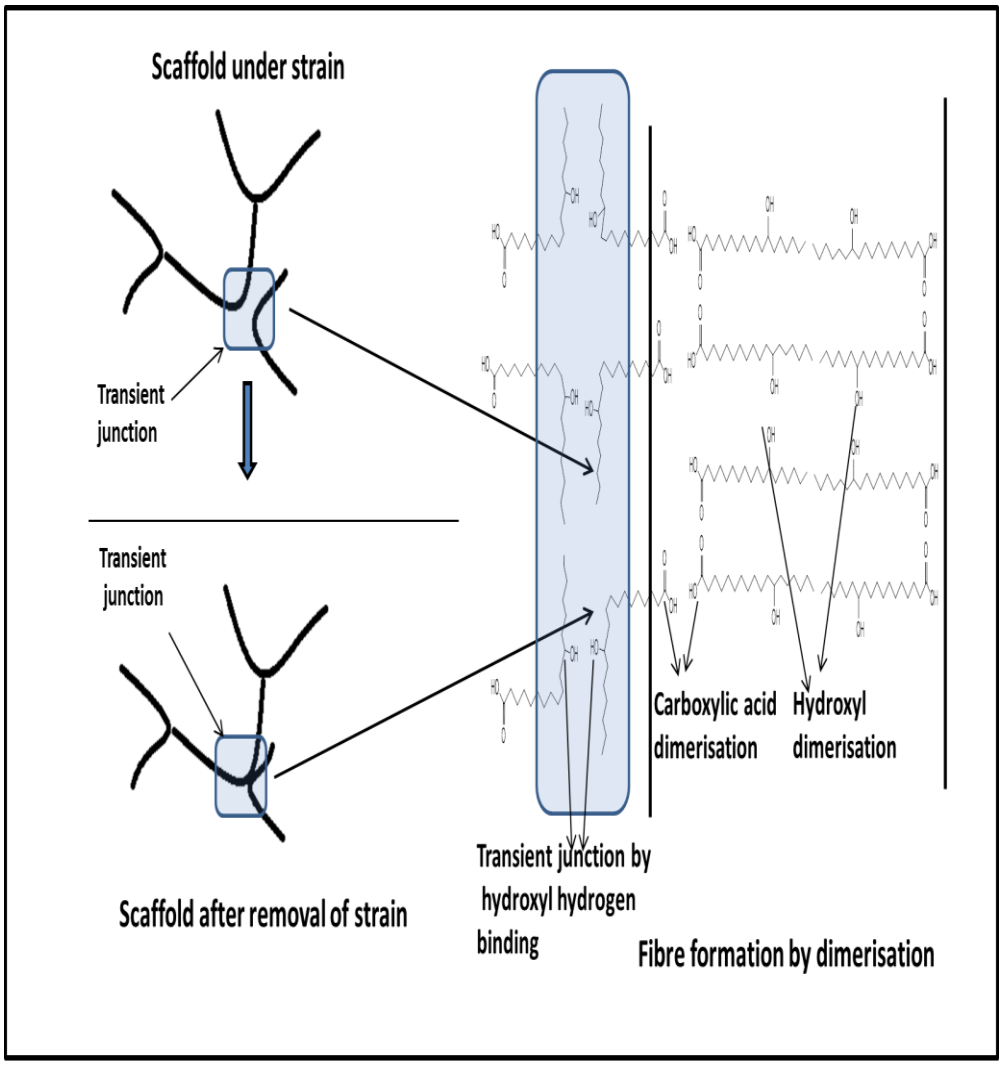

Figure 2-22: Schematic illustration of the transient junctions that connected fibres in different conditions, under the strain and after removal the strain where fibre formation diagram was taken from reference [113].

2.4.10 Creep and recovery tests

The goal behind our work was to select organogels to be injected into the tumour or tumour resection site. Since, the tissues have their own constant stress, creep and recovery was selected to apply a constant stress and mimic the in situ conditions of the tissue [172]. The creep and recovery tests were carried out on 12-HSA in MCT and SO organogels as shown in Figure 2-23 where the stress was applied for 60 seconds. Table 2-9 shows the creep parameters which includes instantaneous compliance that represents the primary resistance to the stress applied on the organogels; and where viscoelastic compliance indicates the deformation of the solid or the elasticity of organogels; and the shear viscosity gives an indication of the last step of the deformation.

All organogels gave high correlation to the Burger model and generally showed that the instantaneous and viscoelastic compliance decreased when increasing the concentration of the gelator 12-HSA. While shear viscosity increased as the concentration of 12-HSA increased. This means the highest concentrations of 12-HSA were more resistant to deformation.

Table 2-10 shows the recovery parameters which includes firstly the maximum compliance that represents the last point in the deformation of the creep phase and secondly the instantaneous compliance which means the initial recovery after removing the applied stress. Thirdly the instantaneous compliance is the portion of elastic compliance which indicates the recovery of the elastic structure and lastly, the viscous compliance means the extent of deformation. All recovery parameters showed a high correlation to the equations of region 4 and 5 as shown in **2.3.6.4** and their values decreased as the concentration of gelator increased as shown in Table 2-10. There were exceptions in the

recovery table and did not follow the above trend where the elastic compliance of 4% w/w 12-HSA/MCT was higher than 3% w/w 12-HSA/MCT. Also, the elastic compliance and viscous compliance values of 5% w/w 12-HSA/SO were larger than the 4% w/w 12-HSA/SO and this is shown in Figure 2-23 where the recovery curves of these 2 organogels are overlapped. These recovery parameters when they decreased indicate that the organogels are more resistant to the deformation. Specifically, the low value of maximum compliance means the minimum deformation which in turn reflects the strength of the permanent and transient junctions of the scaffold. The same reverse relationship between the stress applied and the creep recovery parameters for SO and MCT organogels, was also found for 2% w/w of 12-HSA and the 2% w/w R-N-octadecyl-12-hydroxyoctadecanamide in safflower oil organogels where the stress applied was 175 Pa and 189 Pa respectively. Also, the creep recovery parameters of 2% w/w 12-HSA/safflower oil were higher than 2% w/w R-N-octadecyl-12-hydroxyoctadecanamide in safflower oil [135].

Generally, there was decrease in compliance in both creep and recovery phases as the concentration of gelator increased in SO and MCT which lead us to select 5% w/w 12-HSA in SO and MCT for progression as basis of the organogel depot formulation. Specifically these organogels showed the lowest values of the maximum compliance and instantaneous compliance in the recovery phase.

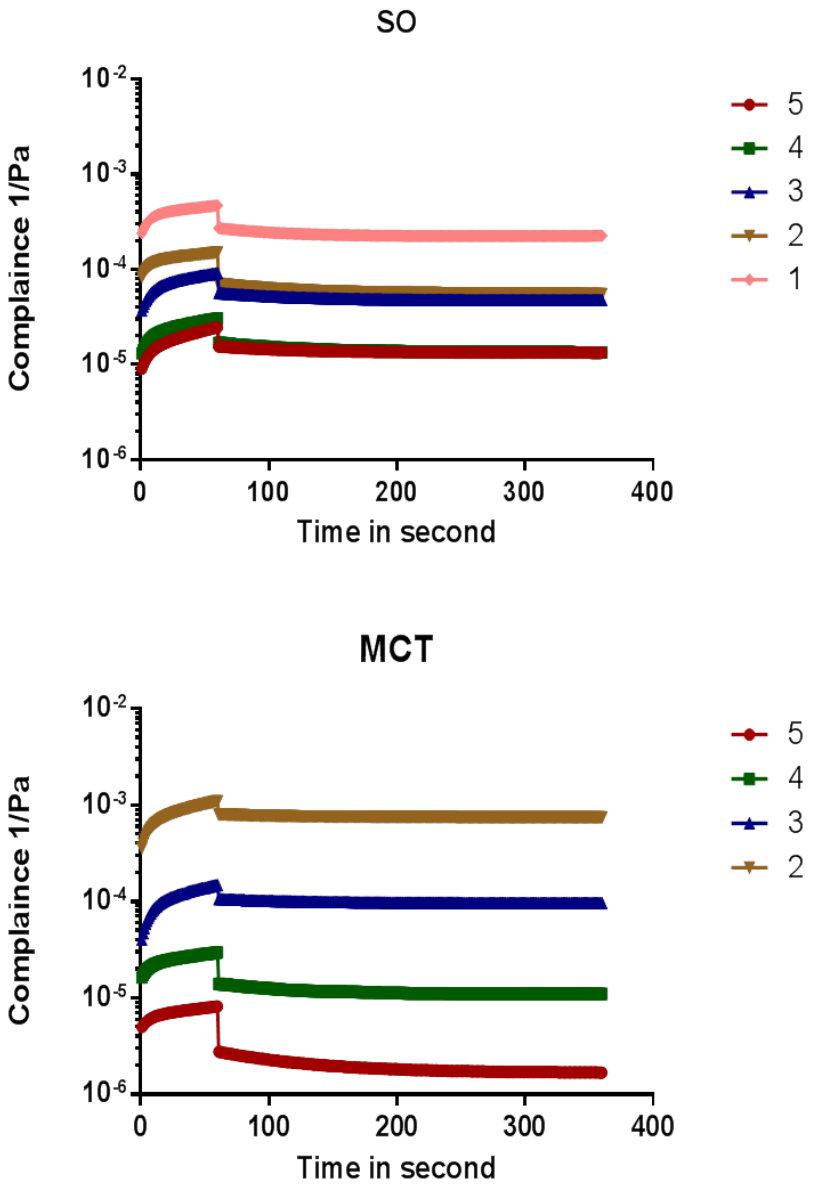

Figure 2-23: Creep recovery compliance of 12-HSA in SO and MCT organogels, where each figure represents a mean of 3 replicates. Where the stresses (see Table 8) were applied to each the oragnogel for 60 seconds and then theses stresses were removed for the remainder 300 seconds of the test .

Table 2-9: Creep parameters for organogels of 12- HSA in MCT and SO where the stress is applied for 60 seconds and then these stresses were removed for the remainder 300 seconds of the test.(The values represent mean ± SD,(n = 3)).

Oil	12-HSA % (w/w)	Stress applied (Pa)	Instantaneous Compliance J_0(1/Pa)	Viscoelastic compliance J_m(1/Pa)	Zero shear viscosity eta (Pa·s)	R^2 Correlation
MCT	5	941.82	$4.720 \times 10^{-6} \pm 4.300 \times 10^{-7}$	$1.700 \times 10^{-6} \pm 1.100 \times 10^{-7}$	$35197 \times 10^3 \pm 5869 \times 10^3$	0.998
	4	331.87	$1.517 \times 10^{-5} \pm 5.390 \times 10^{-6}$	$7.360 \times 10^{-6} \pm 7.360 \times 10^{-6}$	$10613 \times 10^3 \pm 5069 \times 10^3$	0.987
	3	123.58	$3.309 \times 10^{-5} \pm 1.400 \times 10^{-5}$	$5.694 \times 10^{-5} \pm 6.400 \times 10^{-5}$	$1890 \times 10^3 \pm 2024 \times 10^3$	0.993
	2	34.59	$3.148 \times 10^{-4} \pm 1.700 \times 10^{-4}$	$3.419 \times 10^{-4} \pm 2.700 \times 10^{-4}$	$4268 \times 10^2 \pm 5736 \times 10^2$	0.997
SO	5	530.00	$8.130 \times 10^{-6} \pm 1.180 \times 10^{-6}$	$5.716 \times 10^{-6} \pm 2.300 \times 10^{-6}$	$8776 \times 10^3 \pm 7982 \times 10^3$	0.997
	4	289.00	$1.194 \times 10^{-5} \pm 3.000 \times 10^{-6}$	$8.606 \times 10^{-6} \pm 3.700 \times 10^{-6}$	$7352 \times 10^3 \pm 3508 \times 10^3$	0.995
	3	92.00	$3.315 \times 10^{-5} \pm 1.390 \times 10^{-5}$	$3.186 \times 10^{-5} \pm 1.900 \times 10^{-5}$	$2643 \times 10^3 \pm 1328 \times 10^3$	0.989
	2	62.00	$7.710 \times 10^{-5} \pm 1.900 \times 10^{-5}$	$4.438 \times 10^{-5} \pm 2.700 \times 10^{-5}$	$2382 \times 10^3 \pm 1112 \times 10^3$	0.972
	1	47.50	$2.189 \times 10^{-4} \pm 8.100 \times 10^{-5}$	$1.594 \times 10^{-4} \pm 0.001$	$803 \times 10^3 \pm 466 \times 10^3$	0.996

Table 2-10: Recovery parameters for organogels of 12-HSA in MCT and SO when the stress is applied for 60 seconds and then these stresses were removed for the remainder 300 seconds of the test (The values represent the mean ± SD,(n=3)).

Oil	12-HSA % (w/w)	Maximum compliance J_{max} (1/Pa)	Instantaneous compliance J_0 (1/Pa)	Elastic compliance J_E (1/Pa)	Viscous compliance J_V (1/Pa)	R^2 Correlation
MCT	5	$8.200 \times 10^{-6} \pm 1.200 \times 10^{-7}$	$5.420 \times 10^{-6} \pm 6.100 \times 10^{-7}$	$6.537 \times 10^{-6} \pm 6.900 \times 10^{-7}$	$1.667 \times 10^{-6} \pm 5.900 \times 10^{-7}$	0.913
	4	$2.967 \times 10^{-5} \pm 1.500 \times 10^{-5}$	$1.558 \times 10^{-5} \pm 5.240 \times 10^{-6}$	$1.864 \times 10^{-5} \pm 6.500 \times 10^{-6}$	$1.658 \times 10^{-5} \pm 9.900 \times 10^{-6}$	0.883
	3	$1.476 \times 10^{-4} \pm 1.400 \times 10^{-4}$	$4.129 \times 10^{-5} \pm 1.300 \times 10^{-5}$	$5.123 \times 10^{-6} \pm 1.400 \times 10^{-5}$	$9.637 \times 10^{-4} \pm 1.300 \times 10^{-4}$	0.793
	2	$1.089 \times 10^{-3} \pm 7.600 \times 10^{-4}$	$2.893 \times 10^{-4} \pm 1.300 \times 10^{-4}$	$3.443 \times 10^{-4} \pm 1.600 \times 10^{-4}$	$7.449 \times 10^{-4} \pm 6.100 \times 10^{-4}$	0.953
SO	5	$2.441 \times 10^{-5} \pm 9.400 \times 10^{-6}$	$8.872 \times 10^{-6} \pm 1.300 \times 10^{-6}$	$1.466 \times 10^{-5} \pm 3.600 \times 10^{-6}$	$1.417 \times 10^{-5} \pm 8.200 \times 10^{-6}$	0.938
	4	$3.062 \times 10^{-5} \pm 1.200 \times 10^{-5}$	$1.438 \times 10^{-5} \pm 2.700 \times 10^{-6}$	$1.717 \times 10^{-6} \pm 4.900 \times 10^{-6}$	$1.340 \times 10^{-6} \pm 7.600 \times 10^{-6}$	0.883
	3	$9.232 \times 10^{-5} \pm 4.200 \times 10^{-5}$	$3.554 \times 10^{-5} \pm 9.300 \times 10^{-6}$	$4.484 \times 10^{-5} \pm 1.200 \times 10^{-5}$	$4.740 \times 10^{-5} \pm 3.200 \times 10^{-5}$	0.796
	2	$1.514 \times 10^{-4} \pm 5.300 \times 10^{-5}$	$8.054 \times 10^{-5} \pm 1.800 \times 10^{-5}$	$9.616 \times 10^{-5} \pm 2.200 \times 10^{-5}$	$5.519 \times 10^{-5} \pm 3.500 \times 10^{-5}$	0.796
	1	$4.667 \times 10^{-4} \pm 2.200 \times 10^{-4}$	$1.944 \times 10^{-4} \pm 9.100 \times 10^{-5}$	$2.300 \times 10^{-2} \pm 0.400 \times 10^{-1}$	$2.300 \times 10^{-2} \pm 0.400 \times 10^{-1}$	0.941

.

2.5 Conclusions

The goal of this chapter was to select the best organogel with the thermal stability and sufficient mechanical strength to ensure an intact organogel upon injection into the tumour. Thus the selection was 5% w/w 12-HSA in SO or MCT. This selection was due to 5% w/w of 12-HSA in both oils showing the highest thermal stability. Also, the optical microscopy showed 5% w/w of 12-HSA in SO or MCT organogels had denser 3D fibre scaffolds. Also, time dependent recovery tests showed all the concentrations of organogels in SO and MCT, gave high percentages of instantaneous and final recovery and hence could be injected and would reform. The conclusive decision was by the aid of creep and recovery parameters which showed the 5% w/w 12-HSA in SO and MCT were the less compliant compared to the other concentrations and hence most likely to resist deformation to stresses applied within the tumour resection site. This confirmed the 5% w/w 12-HSA/SO and 5% w/w 12-HSA/ MCT as organogel depots for controlled release and progression to incorporation of *N*4-myristoyl gemcitabine in chapter 4.

Chapter 3

Optimisation and characterisation of 12-HSA/Propylene glycol organogels for localised drug delivery

3. Optimisation and characterisation of 12-HSA/Propylene glycol organogels for localised drug delivery

In chapter two, the best-selected organogels were the 5% w/w 12-HSA in SO and MCT where these organogels will be explored further in the next step in our work which is to incorporate *N*4-myristoyl gemcitabine (chapter 4). However, before these investigations, we have evaluated an alternative solvent to form the organogel in propylene glycol (PG). Thus the focus in the current chapter is to establish the concentration of 12-HSA needed for appropriate thermal stability and mechanical strength of the propylene glycol organogels for the controlled release depot by vial inversion, DSC and rheology. Further mechanistic insight in the organogel structure and intermolecular interactions is afforded by light microscopy and ATR-FTIR respectively.

3.1 Introduction

In this chapter, the organogels proposed for intratumoural delivery where the liquid part is the PG as shown in Figure 3-1 and the main gelator is 12-HSA. PG has also been used by other researchers such as Jones *et al* where poly acrylic acid was the polymeric gelator used to prepare the organogels exploiting the mucoadhesive property of the gelator, for oral local delivery. This organogel was prepared with the following percentages of poly acrylic acid 3%, 5% and 10% w/w and showed solid like behaviour [173]. Also, Lim *et al* used PG with 2% to 10% w/v dibutyllauroylglutamide as a gelator to prepare organogels containing haloperidol for transdermal delivery. The highest concentration of gelator showed the highest storage moduli and the

lowest rate of the haloperidol permeation [174]. Additionally, Liu *et al* used β-cyclodextrin with propylene glycol to prepare an organogel and this organogel showed both solid and liquid phases in the presence of potassium carbonate. The first reversible transition was repeated several times from solid to liquid, whilst the second irreversible transition occurred by increasing the temperature of the organogel to the boiling point of PG (188 °C) leading to a solid gel [175]. Moreover, Wang prepared organogels using 1,3:2,4-di-O-benzylidene-D-sorbitol as a gelator and propylene glycol as a liquid phase incorporating 5-fluorouracil [176].

Additionally, PG has been in of many parenteral formulations as a solvent such as the parenteral formulation of etomidate for the treatment of hypercortisolism. In this study, the daily PG dose was 7g / day in patients with renal failure [177]. Also, PG has been used as a co-solvent to increase the solubility of hydrophobic drugs such as celecoxib, rofecoxib, meloxicam, and nimesulide in parenteral formulations [178]. Moreover, PG was one of the co-solvents that were used in preparation of a parenteral microemulsion. However, it was found the high concentration of PG led to pain at the site of injection and haemolysis [179, 180].

These examples show that the PG has been used in many organogels and it is also very well known as a co-solvent in many parenteral formulations which supports our choice to use it in our studies. Also, according to our knowledge, no research is available about the organogels of 12-HSA in PG to date. It is thus of interest to study 12-HSA as a gelator with the PG as the liquid part of the organogel.

The aim of this chapter was to select the best organogel to incorporate *N*4-myristoyl gemcitabine to prepare an organogel intended for injection into tumours. Thus, organogels of 12-HSA in PG were

prepared at different concentrations and their temperature transitions from liquid to solid and vice versa were studied using table top rheology and DSC. Also, rheology was used to assess the mechanical strength of the organogels (amplitude sweep, frequency sweeps, time dependent recovery and creep and recovery test). All these tests were important to select the best gelator concentration of 12-HSA in PG for progression.

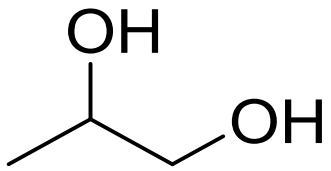

Figure 3-1: Propylene glycol chemical structure

3.2 Materials

The racemic mixture of 12-HSA (99% and CAS number 106-14-9) was purchased from Sigma Aldrich, and high purely grade PG (CAS number 57-55-6 and Lot number Q1484) was bought from MP Biomedicals, LLC.

3.3 Method

3.3.1 Organogel formulation

Organogel formulations of 12-HSA were prepared using the following concentrations 0.5%, 1%, 2%, 3%, 4%, 6%, 8%, 10%, 12%, and 14% w/w of 12-HSA in PG and the same method of preparation followed as in section **2.3.1.**

3.3.2 Table top rheology (Vial inversion).

This experiment was carried out as described in **section 2.3.2**.

3.3.3 Differential scanning calorimeter (DSC)

The same experimental conditions were used as the DSC study in **section 2.3.3,** where the weight of organogels in the pans was between 9.5 mg to 11.5 mg.

3.3.4 Polarised light microscope

A drop of melted organogel was placed on the already heated slides at 90 °C and covered gently by the glass cover slip, which was also heated at 90 °C to form a film. All these slides were examined 5 minutes after preparations then after 3 hours, 1 day and 6 days using PriorLux POL microscope (Prior Scientific, Fulbourn, and Cambridge, UK). The images were captured using the camera Q IMAGING that was connected to the microscope with the aid of the software Q capture. The objective used was X10 and all images were scaled against 200µm.

3.3.5 ATR –Fourier transform infrared spectroscopy

The samples of organogels were scooped as a solid gel onto the of ATR-FTIR crystal 24 hours after organogel preparation. All the other experimental details are as described in **section 2.3.4.**

3.3.6 Optical light microscopy

The slide preparation was as described in **section 2.3.5**, and each prepared slide was observed after the following periods of time: 5 minutes after preparation, 3 hours, and daily until day 6.

3.3.7 Rheology studies

All the details are the same as described in section **2.3.6.**

3.3.7.1 Strain amplitude

This test was run as described in section **2.3.6.1** where the samples were held for 10 minutes on the rheometer plate before running the test.

3.3.7.2 Frequency sweeps

This test was carried out as described in section **2.3.6.2** and where the samples were held for 10 minutes on the rheometer plate before running the test and the applied strain was 0.01%.

3.3.7.3 Time dependent structure recovery test

This test was executed as described in section **2.3.6.3.** The samples were held for 10 minutes on the rheometer plate before each cycle of the test i.e. first phase. The applied strain in the first phase and the third phase was 0.01%.

3.3.7.4 Creep and recovery test

The test was performed as described in section **2.3.6.4.**

3.4 Results

3.4.1 Organogel formation by table top rheology (vial inversion)

The first step to check organogel formation is by vial inversion. If there is no flow of the vial contents, this indicates an organogel. To investigate the solidifying of 12-HSA in PG, the following concentrations : 0.5, 1, 2, 3, 4, 6, 8, 10, 12 and 14% w/w 12-HSA in PG were incubated in a water bath for 30 minutes then cooled to room temperature. As shown in Figure 3-2 the lowest concentration of 12-HSA that can form an organogel with PG was 4% w/w 12-HSA. Similarly, Burkhardt *et al* studied 12-HSA with different solvents where only the diethylene glycol gave a close result to 12-HSA in PG and the lowest amount of 12-HSA to solidify the diethylene glycol was 3% w/w [110]. Also, the solidifying of gels took different periods of time where 4 and 6 % w/w 12-HSA in PG needed 90 minutes to gel. While 8% and 10% w/w 12-HSA took 15 minutes to solidify and the last 2 concentrations 12% and 14% w/w gelled after 7 minutes.

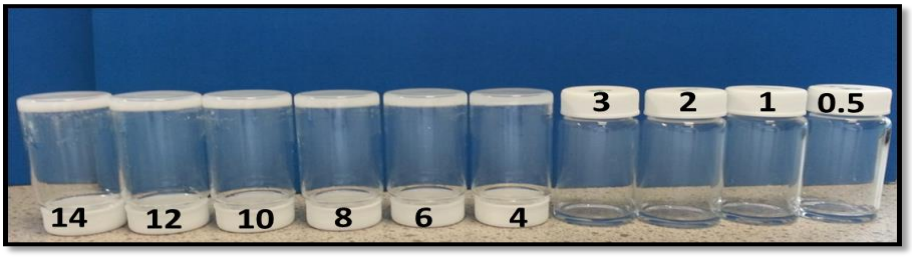

Figure 3-2: Vial inversion at room temperature of organogels of 12-HSA in PG of 14%, 12%, 10%, 8%, 6%, 4%, 3%, 2%, 1%, 0.5 % w/w 12-HSA as labeled. These organogels were heated to 75 °C for 30 minutes then cooled down to the room temperature. Inverted vials mean solid organogels and non-inverted vials mean solutions at room temperature.

3.4.2 Solution to gel transitions by table top rheology

The visual examination of the organogels as solid or viscous liquid at different temperatures was investigated by table top rheology, using simple vial tilting. This test monitored the following heating - cooling - heating cycles starting at 75 °C (melting point of 12-HSA) then cooled down to 37 °C (body temperature) and then increased back to the 75 °C. Table 3-1 presents the concentration of 12-HSA in PG and the transition temperatures of the solution to gel and gel to the solution which shows as the concentration of 12-HSA increases so does the transition temperatures. This result was in agreement with the gelator 2, 3-dihydroxycholestane which gelled different solvents such as cyclohexane, carbon tetra chloride and dichloromethane and table top rheology test was used to investigate the solution to gel transition temperatures. This test showed a direct relationship between the concentration of gelator and the temperature of gelation where cyclohexane showed the highest solution to gel transition temperatures and hence were the most thermally stable gels. Specifically, the lowest concentration of 2, 3-dihydroxycholestane that gelled cyclohexane at 64 °C was 0.13% w/w [181].

Additionally, 4% and 6 % w/w 12-HSA in PG were not solid at 37 °C, but the higher concentrations 8 %, 10%, 12% and 14% w/w gelled at 37 °C. Indeed, the most thermally stable organogel within the selected range of our work was 14% w/w 12-HSA in PG with the highest solution to gel transition temperature of 43 °C.

Table 3-1: Transitions temperature from solution to gel and from gel to solution of different concentrations of 12-HSA/ PG organogels. Each value is a mean of 3 replicates. The maximum and minimum temperatures used in table top rheology were 75 °C and 37 °C, whilst the rate of heating or cooling was 2°C/15 minutes.

12-HSA/PG % w/w	Transition temperature from solution to gel (°C)	Transition temperature from gel to solution (°C)
14	43.00±0.00	51.00±0.00
12	42.00±1.40	50.00±0.00
10	40.00±1.41	48.00±1.41
8	37.00±0.00	45.00±0.00
6	-	-
4	-	-

3.4.3 DSC

Further to table top rheology, thermal characterisation by DSC was carried out with a 10 °C/min cooling/heating rates used to investigate the gelation behaviour. The solidifying/ melting temperature transitions were characterised and by onset, peak maximum and enthalpy.

Table 3-2 shows firstly there was a relationship between the concentration of 12-HSA in PG and solidifying/melting temperatures where the onset, the peak of solidifying/melting and the enthalpy increased as the concentration of gelator in PG increased. Similarly, the concentrations 2%, 3%, 5%, 7%, 10%, 15%, 20%, 25% w/w of 1,3:2,4-di-*O*-benzylidene-D-sorbitol in ethylene glycol gave correspondingly an increase in the peak and enthalpies of the

melting/solidifying temperatures by DSC [182]. Moreover, a similar observation was reported for organogels of sorbitan monostearate in sesame oil where an increase in the enthalpy of melting temperature with concentration, was an indicator of more thermally stable organogels [92].

Also, Table 3-2 shows that all concentrations of 12-HSA in PG had onset and peak of solidifying temperatures lower than body temperatures, but all organogels peaks of melting temperatures showed a higher temperature than 37 °C and this means these organogels are capable of staying intact as a solid at body temperature where, the 14% w/w 12-HSA/PG organogel showed the highest melting temperature (transition from gel to liquid) at 48.11 °C.

These solidifying/ melting transitions temperature were different from transitions temperature of solidifying/ melting of table top rheology and this led to different minimum gelation concentrations (MGC). The difference in MGC in these 2 methods could be justified according to the differences in the cooling rate of the 2 methods [183], or the differences in the extent of agitation of the 2 methods i.e. agitation in table top rheology versus no agitation or shaking in DSC. We have already made this observation for 12-HSA oil organogels in Chapter 2 and rationalised it to be due to the difference in mechanical agitation between the methods. Indeed, our results are in agreement with Herpt *et al* who found that the MGC of the organogel of 1,1′-(9- tetradecyl-9H-carbazole-3,6-diyl)bis(3-ethylurea) in DMSO was 40 mg/ml and it decreased to 20 mg/ml after shaking the organogels. This decrease in MGC was because shacking helped to shorten, fragment and accelerate the growth of fibres. All these helped to form a scaffold capable of retaining DMSO at a lower concentration as an organogel [184].

Also, Figure 3-3 and Figure 3-4 show in addition to the peaks of solidifying and melting, there are other small peaks in both

thermograms. The additional peaks appear in the solidifying thermogram (Figure 3-3) are at 70.5 °C ± 0.78 whilst the melting thermograms (Figure 3-4) shows the additional peaks at 79.7 °C ± 0.42. As a result of the presence of these additional peaks, the DSC experiment was carried out on the pure 12-HSA using the same conditions used with the organogels. The results are shown in Figure 3-5. The solidifying temperature of pure 12-HSA was 72.79 °C ± 0.61 and the melting temperature was 81.73 °C ± 0.24 and hence the additional peaks in DSC thermograms are crystals of 12-HSA.

The additional peaks in DSC did not show an order in their appearance and they were not found in all thermograms. Thus, it is possible that the additional peaks were not observed in all DSC thermograms due to the short cooling cycle of 10 minutes was not enough to form the crystals or to start nucleation.

2 peaks in DSC thermograms (the main peak plus additional peaks) indicate that the scaffold has crystals and fibres. Different studies have reached the same conclusion of having fibres and crystals but used synchrotron time-resolved small-angle X-ray scattering to investigate the scaffold growth of the 12-HSA gels in dodecane, xylene and toluene. They found 2 stages of the scaffold formation, where the first stage included developing a fibre network, and the second stage when the crystalline nucleation occurred and this prevented the growth of fibre network [185]. However, solidifying thermograms of DSC showed the appearance of additional peaks before the main peaks which infers the appearance of crystals before fibres.

In summary, the DSC study showed that the most thermally stable organogel was 14% w/w 12-HSA/PG with a melting temperature of 48.11 °C. Also, crystals of 12-HSA were present in the organogel as shown by additional peaks in the DSC thermograms.

Table 3-2: Thermal properties (solidifying and melting) of 12-HSA/PG organogels. Each value represents the mean of 3 replicates ±standard deviation (SD). The rate of heating and cooling was 10 °C/minutes and the samples were held at 100 °C and 0 °C for 30 minutes and 2 minutes respectively.

% w/w 12-HSA in PG	Onset of solidifying temp (°C)	Peak of solidifying temp (°C)	Enthalpy of solidifying temp (J/g)	Onset of melting temp (°C)	Peak of melting temp (°C)	Enthalpy of melting temp (J/g)
14	28.10± 2.24	19.31± 3.06	20.78± 2.98	38.75± 0.15	48.11± 0.13	14.31± 2.61
12	27.10± 1.93	17.91± 5.92	15.92± 3.83	37.69± 0.41	47.03± 0.25	10.38± 1.20
10	26.53± 0.74	15.17± 1.08	14.61± 1.28	35.77± 0.81	45.78± 0.16	11.14± 2.11
8	21.90± 0.47	10.56± 3.10	11.08± 0.50	33.50± 0.12	43.47± 0.22	7.56± 0.66
6	21.71	9.92	6.26	32.92± 0.75	43.16± 1.18	5.50± 0.97
4		-	-	31.53± 0.67	38.85± 0.26	2.71± 1.02

Note: the solidifying parameters of 6% 12-HSA/PG were an average of 2 values.

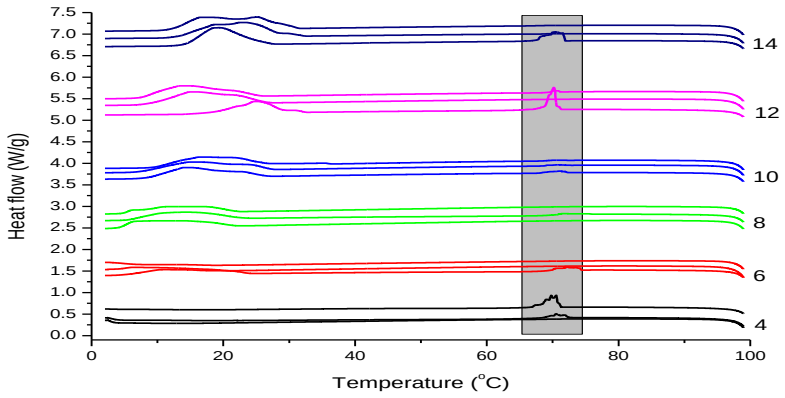

Figure 3-3: Solidifying thermograms of DSC of different concentrations of 12-HSA/PG organogels and the label points to the additional peaks at 70.5 °C ± 0.78 where rate of cooling was 10 °C/minutes.

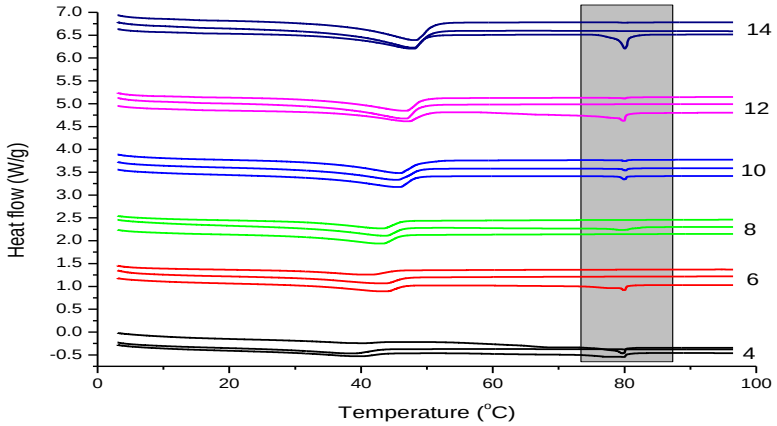

Figure 3-4: Melting thermograms of DSC of different concentrations of 12-HSA/PG organogels and the label points to the additional peaks at 79.7 °C ± 0.42 where the melting rate was 10 °C/minutes. .

Solidifying of pure 12-HSA	Melting of pure 12-HSA
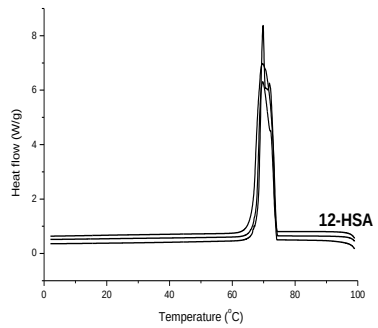	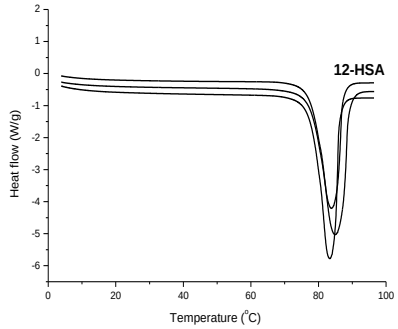

Figure 3-5: Solidifying and melting thermograms of pure 12-HSA where the cooling and melting rate was 10 °C/minutes and the samples were held for 30 minutes at 100 °C and 2 minutes at 0 °C.

3.4.4 Polarised light microscope

Having shown the presence of 12-HSA crystals in the organogels by DSC, a polarised light microscope was then also used to confirm their presence. As shown in Figure 3-6, the images of all tested organogels 5 minutes after preparation gave a spherulite fibre scaffold at all concentrations and particularly evident at the higher concentration with no crystals. However the images after 3 hours of slide preparation clearly show the crystals; then at day1, a distinctive crystal growth was observed with large crystals especially at 4%, 6% and 8 % w/w 12-HSA /PG whilst 10%, 12%, and 14% w/w 12-HSA/PG micrographs show numerous small crystals throughout the sample. The slides were followed daily until day 6 and the images did not show any differences, thus the observations were not continued beyond this point.

In summary, it was found the crystal appearance in the organogels was time dependant and the time to when crystals were observed was 3 hours.

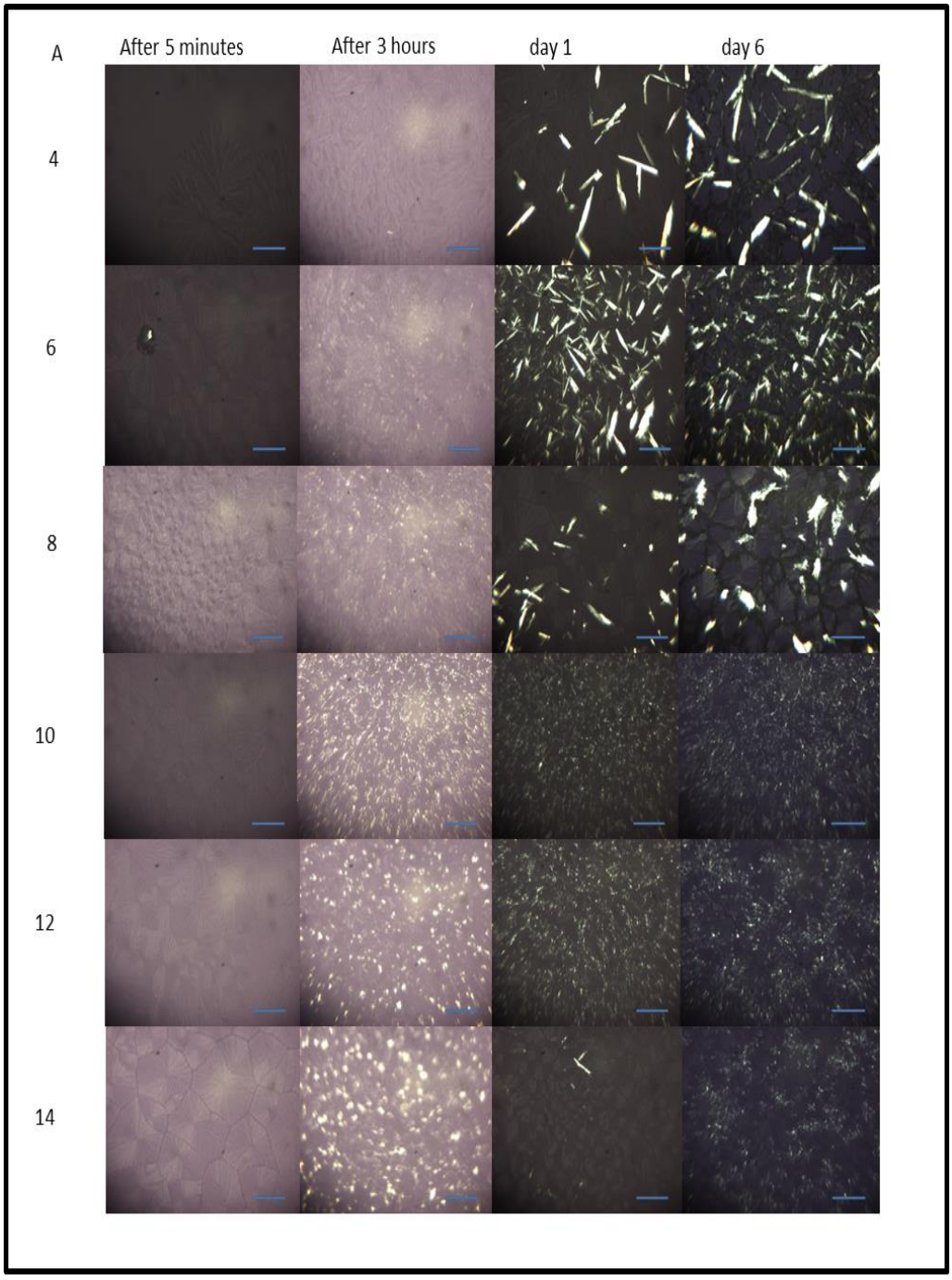

Figure 3-6: Polarised light microscopy images of organogels. Column A represents the % w/w of 12-HSA/PG organogels where the other columns represent the time periods after cooling. The objective was X10 and the magnification bar is 200 µm.

3.4.5 Amplitude sweep

The viscoelasticity is another key characteristic of organogels, where it can be examined by amplitude sweep testing. This test provides many parameters such as the G′ value (solid-like behaviour), G″ value (viscous like behaviour), LVER (Linear viscoelastic region) which region at low deformations where both of G′ and G″ are constant and the structure of the sample is in intact). At the end of LVER region, the modulli (G′ and G″) start to decrease when the structure of the sample is disturbed. The flow point means when the plot of G′ intersects with the plot of G″ at a point where G′=G″.

Figure 3-7 and Table 3-3 (representative figures) show that the G′ was higher than G″ by one order of magnitude in the LVER region of all organogels except the 4% w/w 12-HSA/PG which was a weak gel and had no LVER value. The G′ values compared with G′ values in 12-HSA/oils organogels in Chapter 2 showed the same trend. Whilst, the range of G′ values in Chapter 2 for the gelator concentrations range from 1% to 5% w/w 12-HSA in SO and MCT were lower and within the range from 10^3 to 10^5.

Furthermore, as exhibited in Figure 3-7 and Table 3-3, the increases in the concentration of 12-HSA in the organogels led to greater values of G′, G″ and LVER, whilst flow point values did not show a specific order. Statistically, G′ of 14% w/w 12-HSA/PG was significantly higher ($p<0.0001$) in comparison with G′ of 4% and 6% w/w 12-HSA in PG. Also, LVER value of 14% w/w 12-HSA/PG organogels was significantly greater ($p<0.0001$) in comparison with 6%, 8%, 10%, and 12 % w/w 12-HSA/ PG organogels. The LVER of 4% w/w 12-HSA/PG organogel was excluded because this organogel had no LVER as shown in Figure 3-7. In a similar manner, Wright and Marangoni reported the storage modulus within the LVER of ricinelaidic acid in a canola oil organogels was concentration dependent and increased as these

concentrations 0.5%, 1%, 2.5%, 4% and 5% w/w of ricinelaidic acid increased [186]. The 14% w/w 12-HSA/PG gave a great LVER value compared with the lower concentrations of 12-HSA/PG organogels and this reflects the strength or the elasticity of the highest concentration of organogel. Likewise, the G′ trend of the organogels of 0.5,1, 2, 3, 6 % w/w of a paramagnetic D-homosteroidal nitroxide free radical (D-3b-hydroxy-17,17-dipropyl-17a-azahomoandrostanyl-17a-oxy) in cyclohexane, showed the same trend which was an increase in the LVER values as a function of concentration [96]. Also, Laupheimer *et al* investigated the LVER by applying stress amplitude sweep and they found the same order to our work where 1.5%, 2.5% and 5% w/w of 12-HSA/ *n*-decane organogels gave an increase in the LVER values which were 18, 50 and 75 Pa respectively [167].

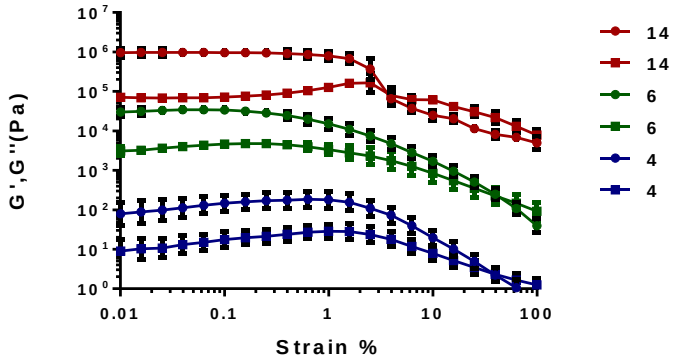

Figure 3-7: Representative figures of amplitude sweep of 12-HSA/PG organogels, where ⟶ represents G′ and ⟶ represents G″ and the applied strain was from 0% to 100% and the angular frequency was 10 rad s^{-1}. Each plot is an average of 4 replicates and the SD represented as black bars. The amplitude sweeps details of all organogels are shown in Table 3-4.

Table 3-3: Amplitude sweep parameters of 12-HSA/PG organogels. Each value represents the mean ± SD (n=4). Statistical analysis was done using one way ANOVA with Tukey's post hoc test where the significant value is (p< 0.05).

12HSA % w/w	G′ x 10^4 (Pa)	G″ x 10^3 (Pa)	Flow point(%)	LVER (%)
14	95.8500±27.7206 •••• ••• ••	70.625±18.136	3.27±1.14	0.43±0.09 ****
12	47.5750±28.7507	40.075±19.321	17.47±14.97	0.14±0.01
10	43.6000±7.0109	41.975±3.956	10±4.5	0.06±0.01
8	31.8500±3.4229	32.500±2.423	16.34±3.5	0.059±0.005
6	2.9975 ±0.8876	3.100±0.890	47.25±20.99 ◊◊	0.051±0.02
4	0.0078± 0.0074	0.009±0.008	40.66 ±20.0 ◊	-

•••• represents a higher significant G′ value of 14% w/w 12-HSA/PG compared with 4% and 6% w/w of 12-HSA/PG. (*p* < 0.0001)
••• represents a higher significant G′ value of 14% w/w 12-HSA/PG compared to 12% w/w and 10% w/w of 12-HSA/PG. (*p* < 0.001)
•• shows a higher significant G′ value of 14% w/w 12-HSA/PG compared to G′ of 8% w/w 12-HSA/PG. (*p* < 0.01)
****** represents a higher significant LVER value of 14% w/w 12-HSA/PG correspond to the other LVER of 12%,10%,8% ,6% w/w 12-HSA/PG. (*p* < 0.0001)**
◊ shows a higher significant flow point value of 4% w/w 12-HSA/PG compared to 14% w/w 12-HSA/PG. (*p* < 0.05)
◊◊ exhibits a higher significant value flow point of 6% w/w 12-HSA in compared to 14% w/w 12-HSA/PG. (*p* < 0.01)

3.4.6 Power law

To examine the microscopic nature of the organogels, the power law was implemented by plotting the storage modulus versus different concentrations of organogels where all the details of this law are explained in section **2.4.5**. The 4% w/w 12-HSA in PG was excluded in this test due to the weak gel behaviour as shown in amplitude sweep test. Figure 3-8 shows a regression relationship (R^2= 0.845) of G′ versus concentrations, where the *m* (the power law component) was 3.6335 which indicates a colloidal gel. The colloidal gel means clusters or aggregates of fibres and these aggregates are connected by fibres as described in **2.4.5** section of the power law in Chapter 2. The fractional dimension was obtained from *m* where *m*=1/3-D (D means the fractional dimension) which was 2.72. This value identifies the spatial distribution of the scaffold. The ɣ value was 77.631 and indicates to the sizes of the primary crystals and the strength of the interactions. Organogels of 12-HSA/MCT as reported in Chapter 2 are also colloidal gels. Colloidal organogels were also reported for organogels of the equimolar of 1-adamantanecarboxylic acid and 1-adamantylamine / dimethyl sulfoxide by executing power law and where *m* value was 4.2 [187]. Terech and Friol stated that the colloidal gel structure promotes the elasticity of organogel which is a result of links between the aggregates rather than the elasticity of the aggregates themselves as depicted in Figure 2-6 in Chapter 2 [96]. This can be related to the high LVER values of 14% and 12% w/w 12-HSA/PG compared to the lower concentrations of the 12-HSA/PG organogels, where the higher concentration of gelator led to a higher number of spherulites and this, in turn, increased the number of links between spherulites and after applying an increasing strain in amplitude sweep test, the organogel showed a resistance to the deformation with a high LVER value.

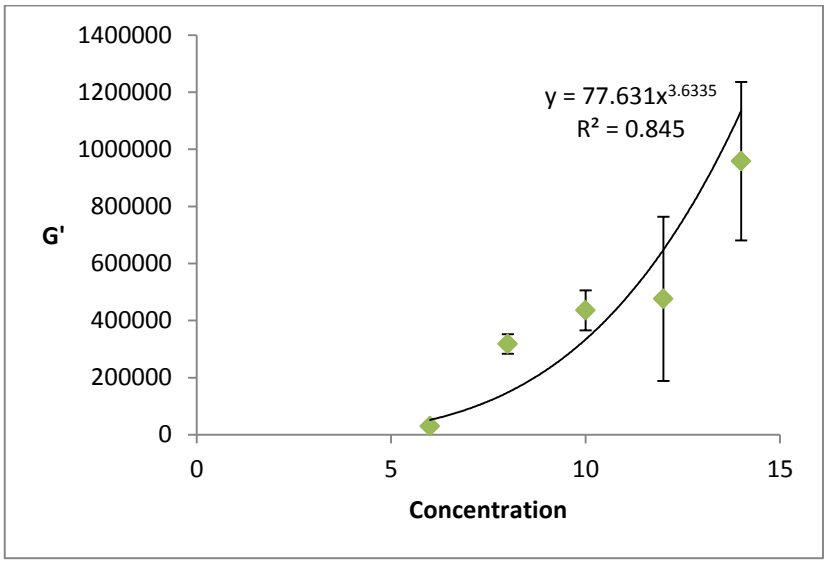

Figure 3-8: Application of the power law by plotting G′ versus corresponding concentrations % w/w 12-HSA in PG organogels .

3.4.7 Optical light microscopy

Microscopy study was carried out to evaluate the microstructure and the scaffold morphology of the organogels of 4%, 6%, 8%, 10%, 12% and 14% w/w 12-HSA in PG. The optical images demonstrate 5 minutes after preparation (Figure 3-9) a frond-like structure and present rising from a central nucleus to form spherulites. In addition, the spherulite density is visually low in 4% and 6% w/w 12-HSA/PG organogels, whilst the density of spherulites increased as the concentration of the gelator increased. Also, after 3 hours only the growth of the spherulites in 4% w/w 12-HSA/PG organogels was observed, whilst the images for the same time period for 6%, 8%, and 10% w/w of 12-HSA/PG organogels showed fibres appearing over the spherulite scaffold. Also, the organogels 12% and 14% w/w 12-HSA/PG exhibited growth of fibres in the borders between spherulites. Additionally, the main changes that happened at day 1 were gaps appearing between adjacent spherulites and producing fibres that linked the neighbouring spherulites. At day 2, more growth was shown which appeared as darker areas. Observation of slides continued until day 6 and the slides did not show any further changes.

It was noted that 12-HSA/ PG organogels formation is time dependent, thus a further investigation into the time dependency was undertaken as shown in Figure 3-10. The selection of the organogel with 6% w/w of 12-HSA in PG was due to their slow gelation which helped to follow the spherulites configuration with time. At 1:07 minutes the fibre nucleation centre started and images at time 1:54, 2:07, 2:11, 2:22, 2:28 minutes all showed the spherulite growth. By 2:33 minute, the growth stopped when the margins of the single spherulite faced the margins of the neighbour's growing spherulite. Likewise in another study, the spherulites structures were obtained from the organogel of *N*-lauroyl-L-

glutamicacid di-*n*-butylamide in PG and the spherulites formation was followed from the first moments of the formation [85]. The growth of these spherulites of *N*-lauroyl-L-glutamicacid di-*n*-butylamide in PG started from the fibre nucleation centre and, then arms radiated from the centre and with time the structure developed branched arms which led to the spherulite structure. These spherulites organogels have been noted in other studies such as the gelator of 2% w/w 1,3:2,4-dibenzylidene-D-sorbitol in poly(propyleneglycol) [188].

In summary, all organogels showed a spherulites network and the changes in structure occurred within 2 days from preparation.

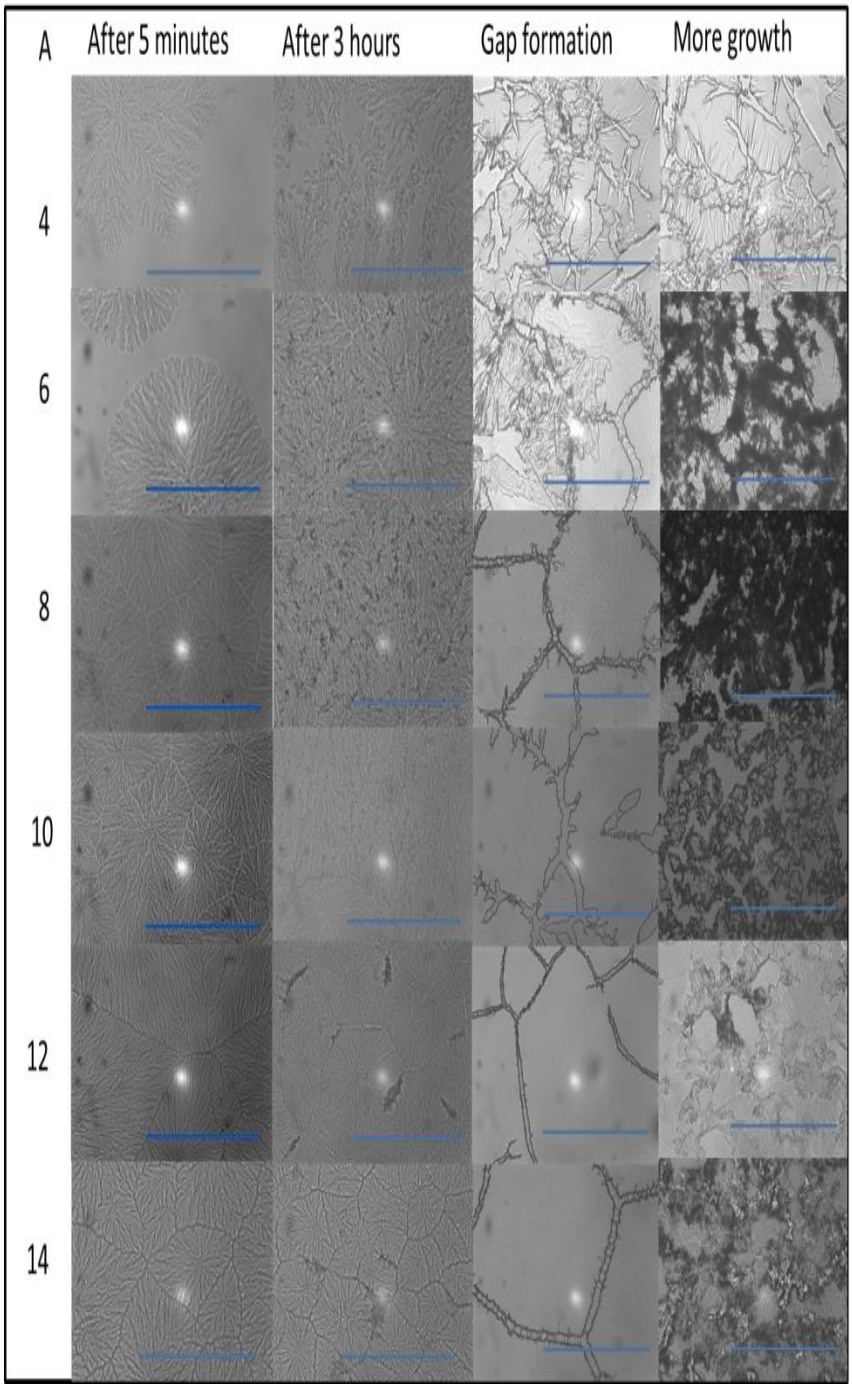

Figure 3-9: **Optical microscopy images of the growth of 12-HSA/PG organogels, where column A represents the percentage of solid content of 12-HSA in PG. The column "after minutes" and "after 3 hours" present images at those times. Column "gap formation" presents the gap between neighbour spherulites and started at day 1 while column "more growth" presents darker areas and this started at day 2. The objective was X40 and the scale: 200 µm. The light reflection of the microscope appears as a white dot in most images**.

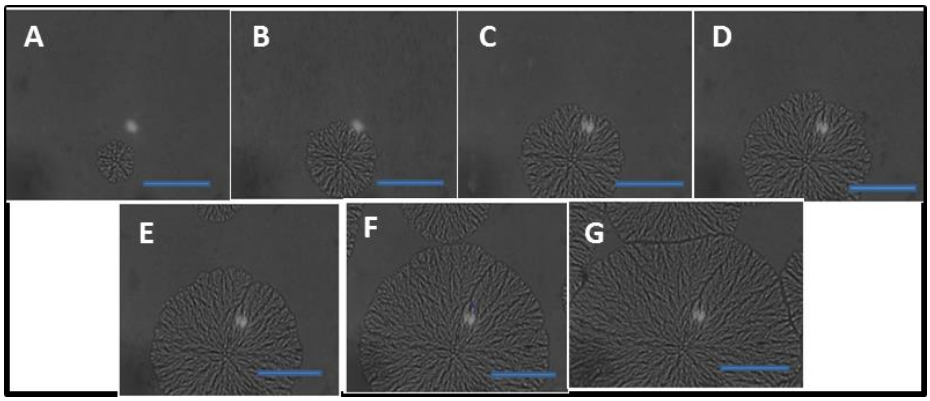

Figure 3-10: Formation of spherulites of 6% w/w 12-HSA/PG organogels with time where A, B, C, D, E, F, G represents the images at the following times 1:07, 1:54, 2:07, 2:11, 2:22, 2:28, 2:33 minutes respectively. ObjectiveX40 and the scale bar is 100 µm. The light reflection of the microscope appears as a white dot in most images.

3.4.8 ATR-FTIR

ATR-FTIR was used to investigate the hydrogen bonding between 12-HSA molecules which are responsible on scaffold formation. Figure 3-11 which shows peaks in the ATR-FTIR spectra associated with the carbonyl (1695 cm^{-1}) of 12-HSA and hydroxyl groups (3306 cm^{-1}) of 12-HSA and PG in 12-HSA/PG organogels. For all organogels there was a peak associated with carbonyl group of 12-HSA (Figure 3-11). The highest peak was for the pure 12-HSA then the peak intensities gave the following rank order 14% >12% > 10% > 8%> and 6% w/w for 12-HSA/ PG. Also, the disappearance of the peaks at 1730 cm^{-1} (Figure 3-11) is indicative of no interactions between 12-HSA and PG. To clarify, the peak appearance at 1730 cm^{-1} of 12-HSA was attributed to the carbonyl group of the free monomer which means the existence of the gelator in solution as a soluble form and indicates the interactions between gelator and PG [159]. This peak was also observed in 12-HSA/mineral oil organogels besides the main peak associated carbonyl at 1700 cm^{-1} that is responsible dimerisation of 12-HSA-12-HSA molecules and subsequent for gelation [189]. Also, 1730

cm^{-1} was noticed with 1700 cm^{-1} in the organogel spectrograms of 12-HSA/alcohol using alcohols with different chain lengths [161]. To form organogels, the process of forming the fibre scaffold should be a balance between the interactions of gelator-gelator (dimerization) and gelator-solvent molecules [146]. Additionally to carbonyl group investigation, the organogel spectra of the hydroxyl group are shown in Figure 3-11. However, the hydroxyl group exists in both molecules of the PG and 12-HSA and thus this makes it difficult to interpret the hydroxyl spectra.

As can be seen, the increase in the 12-HSA concentration showed an increase in the intensities of carbonyl peaks and this means a more hydrogen bonded 3D network between 12-HSA molecules in the organogels.

Furthermore, there was a focus in previous studies on the relation between infrared data and optical images. These studies revealed that the presence of carbonyl peaks at 1700 cm^{-1} or 1690 cm^{-1} means the dimerisation of the carbonyl groups that are responsible for hydrogen bonding and a fibre network formation [157, 161]. The optical images of our work of all 12-HSA/PG organogel exhibited formation of spherulites network and fibres where the spectrograms of the organogels showed peaks associated with carbonyl at 1695 cm^{-1}. This is different from the result of Songwei *et al* where they revealed that the organogel of 12-HSA in ketone led to spherulites network and its carbonyl group appeared at 1720 cm^{-1} [112]. This difference in infrared peaks might be due to no or weak interactions between 12-HSA and PG as shown in Figure 3-11 which suggests the 12-HSA molecules assembled to constitute the spherulite scaffold and are not in solution.

IR peaks associated with the carbonyl group of 12-HSA	IR peaks associated with the hydroxyl group of 12-HSA
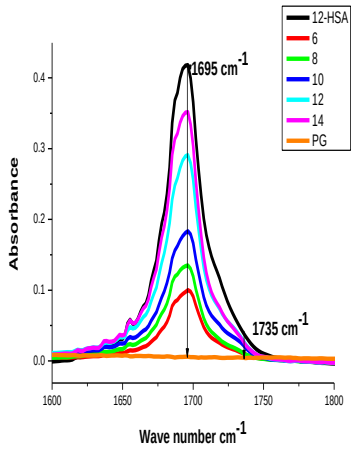	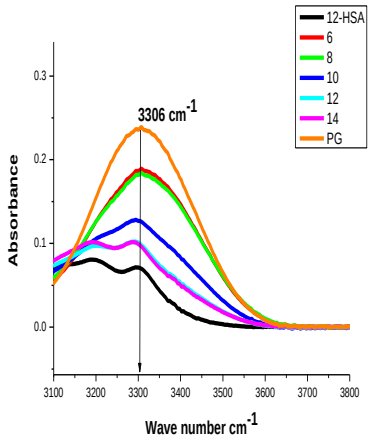

Figure 3-11: ATR-FTIR spectra showing the peaks associated with the carbonyl and hydroxyl groups of 12-HSA/ PG organogels.

3.4.9 Frequency sweep

The strength of the organogel is an important criterion since it is the intention to use this organogel to deliver *N*4-myristoyl gemcitabine as a depot in the solid tumour where Leunig *et al* have reported that the tumour develops a high interstitial fluid pressure [190]. Thus, the organogels need sufficient strength for intratumoural delivery to resist deformation from the pressure within the tumour. Therefore, the following tests were undertaken to determine the mechanical strength: frequency sweep, the time dependant recovery and creep and recovery. These were used to determine the strength of the different organogels according to the differences in their solid content.

Frequency sweep test gives the ability to screen G′ and G″ at different frequencies and at constant strain which was selected from within the LVER. Firstly, frequency sweep as presented in Figure 3-12 (representative figure) and Table 3-4 shows for all organogels G′ values are higher than G″ at high angular frequencies; where all data in Table 3-4 were recorded at an of the angular frequency 10 rad s^{-1} and shows an increase in the G′ and G″ values as the 12-HSA concentration in PG increased. Also, the G′ value was higher value than G″ value by one order of magnitude. This result is consistent with the 1.5%, 2.5% and 5% w/w of 12-HSA/ *n*-decane which showed an increase in G′ as the concentration of gelator increased [167]. The increase in G′ while increasing the concentration of 12-HSA was within the range of 10^5 to 10^6 Pa for the 6% to 14% w/w 12-HSA respectively. This result was similar to the frequency sweep results of 12-HSA in dicaprylyl ether where G′ increased from 10^5 to 10^6 Pa for organogel concentrations of 6% to 15% w/w 12-HSA [191].

This was the first step in the analysis of the frequency sweep results. The second step in the analysis, as discussed in **2.4.8** section, was carried out by taking the log G′, log G″ versus log angular frequency. Starting with the analysis of log G′ versus log angular frequency, showed a straight line plot with high correlation values within the range from 0.917 to 0.987; and where the slope ranged from 0.043 to 0.029. This analysis was done from 100 to 1 rad s^{-1} of the angular frequency and this range of slopes indicated that G′ values were frequency independent. It was found that the G′ values decreased then increased at low frequencies (1 to 0.1 rad s^{-1}). Secondly, the analysis of log G″ versus log angular frequency showed a variation and it depended on the concentration of the 12-HSA in the organogels where, the slope was 0.04, 0.076 and 0.079 for 14%, 12% and 10% w/w 12-HSA/PG respectively (Figure 3-13). However, the correlation values of these

plots were 0.88, 0.6 and 0.967 for 14%, 12% and 10% w/w of 12-HSA/PG organogels respectively. These slopes were as a result of the analysis of angular frequency from 100 to 2.51 rad s^{-1}. Thereafter, the values of G″ increased in the region of angular frequency from 2.51 to 0.1 rad s^{-1}. The increase in the G′ and the G″ values at low frequency could be due to the transient junctions in the scaffold or to the links between the adjacent spherulites or aggregates that could have the opportunity to connect again and show this increase in both G′ and G″.

Whilst, the organogel with 8% w/w 12-HSA/PG showed a negative slope with increasing G″ values the angular frequency decreased and where, the 6% w/w 12-HSA/PG organogels showed a variation in the values of G″ i.e. values decreasing until 25.1 rad s^{-1} then increasing as the angular frequency decreased. These results were difficult to justify or explain when G′ has not crossed the G″ curves through the whole range of angular frequency. Basak *et al* pointed out that the soft like solid materials tolerate the applied force by exhibiting curves of G′ that had not crossed the G″ curves [75]. According to Jean-Michel Guenet, further testing is needed to explore the solidity of the organogel [169].

To conclude, this test showed an increase was observed in G′ and G″ values as the concentration of PG increased. Also, the G′ of all tested organogels was frequency independent in the frequency range from 100 to 1 rad s^{-1}.

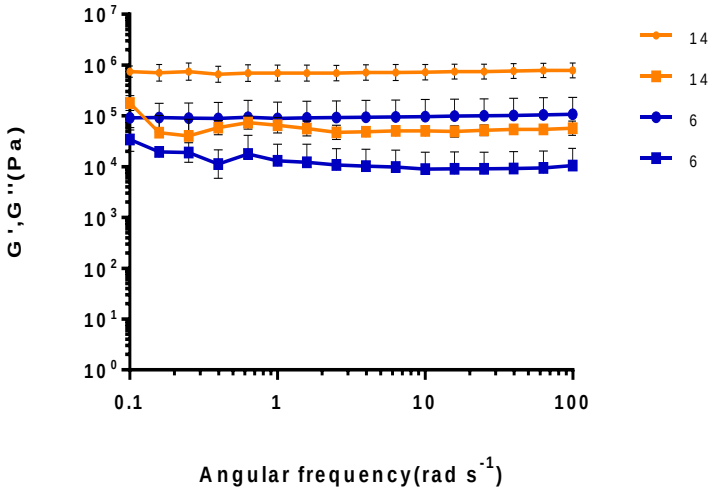

Figure 3-12: Representative figures of frequency sweeps of 12-HSA/PG organogels. The applied strain was 0.01, and the angular frequency was from 0.1 rad s^{-1} to 100 rad s^{-1}. Each plot is an average of 4 where ⟶● represents G′ and ⟶■ represents G″.

Table 3-4: **Frequency sweeps G′ and G″ of 12-HSA/ PG organogels where each value represents the mean ± SD (n=4). All these values taken at 10 rad s^{-1} angular frequency and the angular frequency applied were from 0.1 rad s^{-1} to 100 rad s^{-1} using 0.01% strain and where, the slope of log G′ versus log angular frequency was from 100 to 1 rad s^{-1}.**

12-HSA in PG (% w/w)	G′ x 10^4 (Pa)	G″ x 10^3 (Pa)	Slope of log G′ versus log angular frequency	R^2 correlation of the log G′ versus log angular frequency
14	72.7000 ± 30.0310	50.400 ± 12.163	0.029	0.957
12	34.8000 ± 14.7550	29.900 ± 10.531	0.043	0.987
10	23.4000 ± 8.0289	21.700 ± 7.536	0.041	0.974
8	22.1000 ± 16.6253	22.300 ± 15.459	0.023	0.917
6	9.6700 ± 11.2697	9.000 ± 10.223	0.038	0.985

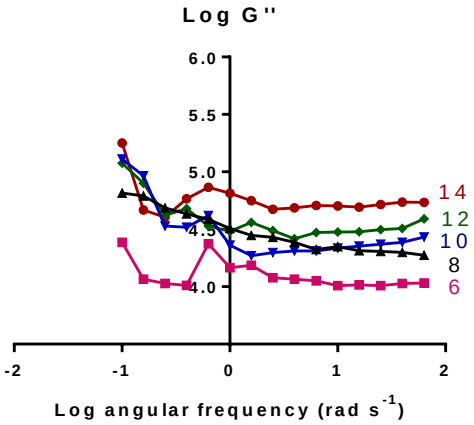

Figure 3-13: Log G″ versus log angular frequency of different concentrations of 12-HSA/ PG organogels.

3.4.10 Time dependent recovery test

The time dependant recovery test was carried out to evaluate the self-healing properties of the organogel scaffold by applying different strain values with time. Indeed this test was executed in our work and by others work to show the thixotropic behaviour which means the capability of the gels to be injected through a syringe and then reform in-situ once the strain is removed [192]. In our studies, a low strain of 0.01% was applied for 200 seconds; followed by a high strain of 300% for 60 seconds to destroy the structure of the organogels to the viscous state, and then the third phase of a low strain of 0.01% was applied again for 200 seconds. The instantaneous percentage recovery is the ratio of the first G′ recorded in the third phase to the initial G′ at low strain (first phase); whilst the final percentage recovery is the ratio of the last G′ recorded in the third phase to the initial G′ at low strain (first phase).

Within the 200 seconds of the first phase of 6% w/w 12-HSA/PG, there was an increase in both G′ and G″ curves and this might be due to the constant low strain which was 0.01% that encouraged the transient junctions to rebound again. The third phase of the time dependent recovery test of the 6%, 8% and 10% w/w of 12-HSA/PG organogels (see Figure 3-14 representative figure) gave instantaneous recovery percentage values of 12%, 30% and 31% respectively, then those organogels showed a slow recovery over the remainder of the relaxation phase until the end of the cycle. The final percentages of recovery are shown in Table 3-5 were 82%, 90% and 86% for 6%, 8% and 10% w/w of 12-HSA/PG organogels respectively. Whilst, 12% and 14% w/w of 12-HSA in PG gave instantaneous recovery percentage values of 65% and 66% respectively. These instantaneous recovery percentages were close to the 50 % of the initial recovery percentage of

10 % w/w of *N*,*N*'-disubstituted urea/glycerol organogels, however, the applied strain in the deformation phase was 10000% [193].

Increases in G′ values of 12 % and 14% w/w 12-HSA/PG for the rest of the cycle were observed and where their final percentage recoveries were 95% and 86% respectively (Table 3-5). Furthermore, for all organogels, their final recovery percentages were higher than their instantaneous recovery and this could be explained by after deformation, the fibre links between closed spherulites were capable of reforming. Additionally, Table 3-5 shows that the final percentages recoveries of all organogels were within the range between 82.75% ± 12 and 95.94 ± 1.3 for G. This magnitude of recovery represents a self-healing gel and similar to the percentage recoveries of 12-HSA organogels in MCT and SO in Chapter 2. Both types of 12-HSA organogels show good recovery compared to the gels of 5 mg/ml FMOC-leucine-glycine which was prepared in different compositions of DMSO/water and showed recoveries between 75% and 80% when DMSO solvent fractions in water were less than 0.25 [170].

In summary, all organogels showed thixotropic behaviour and the 12% and 14% w/w 12-HSA/PG organogels showed good instantaneous recovery after the deformation period in comparison to the lower concentrations of organogels.

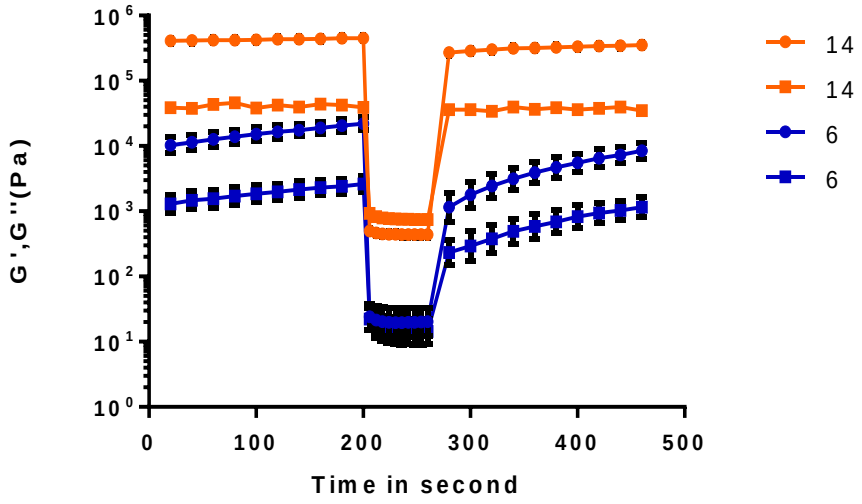

Figure 3-14: Representative figures of time dependent recovery profiles of organogels of 12-HSA/PG where each figure represents a mean of 3 samples and 5 cycles per sample, where ⟶ represents G′ and ⟶ represents G″.

Table 3-5: **Time dependent recovery tests of 12-HSA/PG organogels where the instantaneous percentage recovery and final percentage recovery values represent the mean± (n= 15) (mean of 3 samples and 5 cycles per sample)**

12-HSA/PG (% w/w)	14	12	10	8	6
Instantaneous recovery (%)	66.00±2.5	65.55±25.3	31.28±2.3	30.68±10.5	12.1±2.5
Final recovery (%)	85.72±1.6	95.94±1.3	86.25±5.9	90.02±3.1	82.75±12.0

3.4.11 Creep and recovery test

The goal behind our work is to select the organogels to be injected into the tumour or tumour resection site. Since the tissues have their own constant stress, creep and recovery was selected to apply a constant stress that mimics the in situ conditions of the depot in the tissue. Thus, creep and recovery was carried out by applying a stress for 60 seconds on the organogels as shown in Figure 3-15. All data in Table 3-6 were fitted to Burger model and showed high correlation values. The first two parameters in the creep phase reflected the initial response after applying the stress where the instantaneous compliance represents the primary resistance to the deformation and viscoelastic compliance represents the magnitude of elastic deformation. These 2 parameters the instantaneous compliance and the viscoelastic compliance decreased with the increases in 12-HSA concentration in PG as shown in Table 3-6, although values for 10% and 12% w/w 12-HSA/PG were similar. Generally, this order of the instantaneous compliance and the viscoelastic compliance means more viscoelastic behaviour of

organogels with higher concentrations. The last step in describing the deformation in the creep phase for the organogels is zero shear viscosity which indicates changes in the scaffold. As presented in Table 3-6, there was an increase in the values of zero shear viscosity as the concentration increased for 12-HSA in PG and where 8% w/w 12-HSA/PG showed an unexpectedly high value compared with other concentrations. Table 3-7 reports the recovery phase parameters, where the maximum compliance reflects the last point in the deformation creep phase; the instantaneous compliance represents the first recovery after removal the stress and where the instantaneous compliance is part of elastic compliance which indicates the recovery of the elastic structure, and finally the viscous compliance reflects the deformation magnitude. All these recovery parameters decreased as the concentration of gelator increased. The creep and recovery test showed an inverse relationship between the stress applied on the organogels and the compliance parameters. This was similar to the organogels of 3% w/w candelilla wax/ safflower oil (organogel 1) and 3% of candelilla wax and 1% tripalmitin/safflower oil (organogel 2) that were investigated by a creep and recovery test. The stresses that applied were (55.64 Pa) and (62.37 Pa) for organogels 1 and 2 and all creep phase parameters values of organogel 2 were less than organogel 1[194].

To conclude, the increase in the 12-HSA concentrations in PG organogels showed a decrease in compliance values and especially the 14% w/w 12-HSA/PG which exhibited a good recovery and their structures gave more solid or elastic-like behaviour.

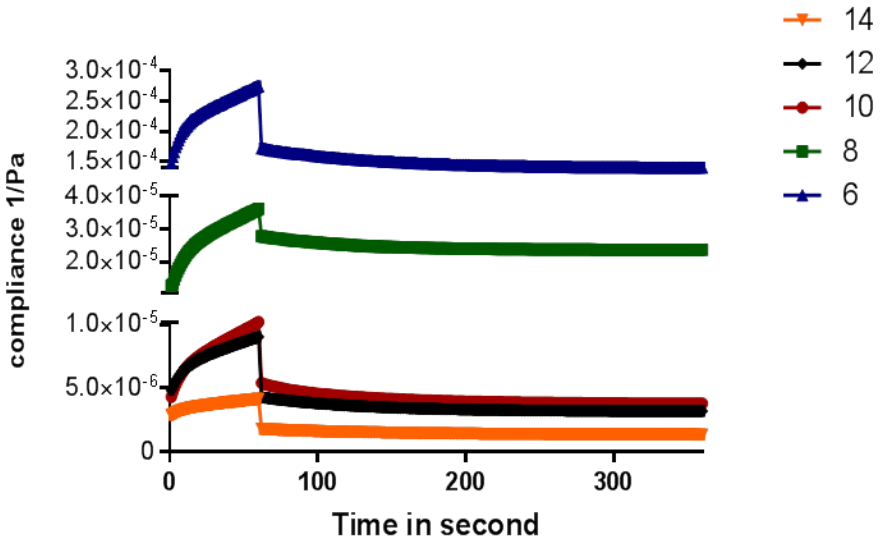

Figure 3-15: Creep recovery test of 12-HSA/PG organogels. Each figure is the average of 3 triplicates. Different stresses were applied for 60 seconds for each organogels and then removed for the remainder 300 seconds of the test.

Table 3-6: **Creep phase parameters of 12-HSA/PG organogels where the stress was applied for 60 seconds and removed for the remainder 300 seconds of the test. The values are an average of 3 replicates ± SD.**

12-HSA/ PG % w/w	Stress applied (Pa)	Instantaneous compliance J_0(1/Pa)	Viscoelastic compliance J_m (1/Pa)	Zero shear viscosity eta (Pa·s)	R^2 Correlation
14	2240	2.79×10^{-6}± 9.58×10^{-7}	5.89×10^{-7}± 2.88×10^{-7}	92473×10^{3}± 445775×10^{2}	0.99
12	1405	4.52×10^{-6}± 2.98×10^{-6}	2.17×10^{-6}± 2.09×10^{-6}	70666×10^{3}± 307171×10^{2}	0.99
10	820	3.92×10^{-6}± 2.22×10^{-6}	2.60×10^{-6} ± 2.54×10^{-6}	50109×10^{3}± 553126×10^{1}	0.99
8	600	10.00×10^{-5}± 0.2×10^{-5}	1.30×10^{-5} ± 90×10^{-6}	589676×10^{3}± 976290×10^{3}	0.99
6	66	1.36×10^{-4}± 76.1×10^{-5}	6.99×10^{-5}± 4.26×10^{-5}	1058×10^{3}± 570373	0.99

Table 3-7: **Recovery phase parameters of 12-HSA/PG organogels. The values are an average of 3 replicates ±SD where the stress was applied for 60 seconds and removed for remainder 300 seconds.**

12-HSA in PG % w/w	Maximum compliance J_{max} (1/Pa)	Instantaneous compliance $J_{\circ}$ (1/Pa)	Elastic compliance J_E (1/Pa)	Viscous compliance J_V (1/Pa)	R^2 Correlation
14	$4.13 \times 10^{-6} \pm 8.04 \times 10^{-7}$	$2.33 \times 10^{-6} \pm 5.71 \times 10^{-7}$	$2.80 \times 10^{-6} \pm 0.75 \times 10^{-6}$	$1.19 \times 10^{-6} \pm 8.21 \times 10^{-7}$	0.96
12	$8.99 \times 10^{-6} \pm 7.32 \times 10^{-6}$	$4.69 \times 10^{-6} \pm 2.83 \times 10^{-6}$	$5.82 \times 10^{-6} \pm 3.61 \times 10^{-6}$	$3.16 \times 10^{-6} \pm 3.73 \times 10^{-6}$	0.96
10	$1.00 \times 10^{-5} \pm 8.08 \times 10^{-6}$	$4.59 \times 10^{-6} \pm 3.27 \times 10^{-6}$	$6.29 \times 10^{-6} \pm 4.59 \times 10^{-6}$	$3.76 \times 10^{-6} \pm 3.51 \times 10^{-6}$	0.96
8	$3.60 \times 10^{-5} \pm 2.10 \times 10^{-5}$	$8.00 \times 10^{-6} \pm 1.00 \times 10^{-6}$	$1.20 \times 10^{-5} \pm 3.00 \times 10^{-6}$	$2.40 \times 10^{-5} \pm 1.80 \times 10^{-5}$	0.98
6	$2.71 \times 10^{-4} \pm 1.46 \times 10^{-4}$	$9.88 \times 10^{-5} \pm 4.96 \times 10^{-5}$	$1.32 \times 10^{-4} \pm 6.57 \times 10^{-5}$	$1.39 \times 10^{-4} \pm 8.22 \times 10^{-5}$	0.98

3.5 Conclusions

The aim of this chapter was to select the best organogel for incorporating with *N*4-myristoyl gemcitabine. The selection depended on the elasticity and thermal stability of organogel and the choice was the 14% w/w 12-HSA/PG. The 14% w/wn12-HSA/PG organogel meets the requirements due to its highest thermal stability and high elasticity by showing high LVER values and thixotropic behaviour i.e. ability to be injected by syringe and reform in-situ. Moreover, this organogel was the least compliant in creep and recovery tests in comparison to other organogels with lower concentrations. Hence, 14% w/w 12-HSA in PG organogel will be progressed as a depot for controlled release of *N*4-myristoyl gemcitabine in Chapter 4.

Chapter four

12-HSA organogels to deliver

*N*4-myristoyl gemcitabine

4. 12-HSA organogels to deliver *N*4-myristoyl gemcitabine

The best organogels in terms of thermal stability and mechanical strength in Chapter 2 and 3 were the 5% w/w 12-HSA in SO or MCT and the 14% w/w 12-HSA/PG. Hence these organogels were progressed in this chapter for the controlled release of *N*4-myristoyl gemcitabine (gemcitabine C14). This gemcitabine C14 is a lipophilic form of GEM and was selected to overcome the drawbacks of gemcitabine which are the hydrophilicity, rapid metabolism and the active diffusion. Thus, the amid prodrug of gemcitabine protects the amine group of GEM from rapid hydrolysis. Also, the gemcitabine C14 provide the lipophilicity that helps the molecule to diffuse passively. The gemcitabine C14 cytotoxicity was tested (the gemcitabine C14 was synthesised by Katheryn Skilling as mentioned in declaration page) and showed a growth inhibition to PaCa-2 (pancreatic adenocarcinoma) and MKN-7 (gastric adenocarcinoma) cell lines in addition to HCT-116 (colon adenocarcinoma) and MCF-7 (breast adenocarcinaoma).

4.1 Introduction

Many researchers have explored the possibility of incorporating drugs into organogels and using them for controlled drug delivery via different routes of administration [195-197]. For example, the L-alanine derivative in safflower oil organogel was used to deliver subcutaneously leuprolide which is a leutinizing hormone for prostate

cancer where the organogels of 7.5 % w/v and 10% w/v of N-Stearoyl-l-alanine methyl ester in safflower oil released 30% and 20% leuprolide after 4 days respectively [62, 70]. Also, for nasal delivery, the 7.5% w/w of sorbitan monostearate in isopropyl myristate and Tween 80 organogel released 40% of propranolol after 6 hours whilst the aqueous solution released 100% of propranolol within 1 hour [198]. Moreover, Ibrahim *et al* formulated different organogels for transdermal delivery where the liquid part was soybean oil and was mixed with Span 60, lecithin-pluronic and cetyl alcohol to create organogels which delivered 49.4%, 43.7% and 50.4% of diltiazem hydrochloride respectively [199]. All the above examples show that organogels are a suitable dosage forms for controlled release, thus this chapter will focus on the incorporation of gemcitabine C14 as shown in Figure 4-1 using different concentrations (0.1%, 0.3% and 0.5% w/w) and the impact of these additions on the selected organogels. Also, the gemcitabine C14 in the selected organogels was part of the novelty of our work where according to our knowledge these combinations have not been reported before.

This chapter is divided into 2 sections, where the first section **A** includes the addition of gemcitabine C14 to the selected organogels 5% w/w 12-HSA in SO and MCT. While, section B focuses on the addition of gemcitabine C14 to the organogel of 14% w/w 12-HSA in PG. These sections A and B are a progression from the results in chapters 2 and 3 respectively where these organogels were evaluated without drug and will be used as our baseline data.

Thus, the following studies were executed to study the changes that might affect the organogels after the addition of gemcitabine C14: DSC, light microscopy and oscillatory rheology (amplitude sweep) and optical microscopy. At the end of each section, an in vitro drug release

study was carried out to examine the organogel's ability to control the release of gemcitabine C14. In addition to the in vitro release, a simulation of the injection of the organogel into chicken breast was carried out to show the ability of the selected organogels to stay as a solid intact gel.

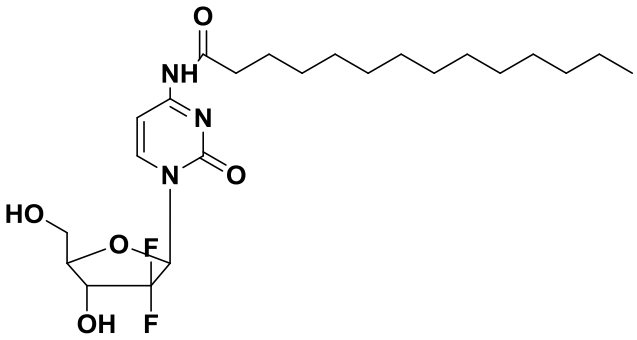

Figure 4-1: Chemical structure of *N*4-myristoyl gemcitabine (gemcitabine C14).

4.1.1 Section A (gemcitabine C14 with the 5% w/w 12-HSA in SO and MCT)

4.1.1.1 Materials

N-methyl pyrrolidone 99.5% (NMP CAS number 872-50-4 and Lot number C29Z974) and disodium hydrogen phosphate 99.9% (Na_2HPO_4, CAS number and Lot number 41k0148) were purchased from Sigma Aldrich, where dodecyl sulphate sodium salt 85% (SDS, CAS number 151-21-3 and Lot number A0352510) was bought from Acros. *N*4-myristoyl gemcitabine (gemcitabine C14) was synthesised by K. Skilling as mentioned in the declaration page.

Also, Nile red (CAS number 7385-67-3 and Lot number QR10555) was brought MP Biomedical, France.

4.1.1.2 Experimental work

4.1.1.2.1 Organogel formation

To the selected organogels 5% w/w 12-HSA in SO and MCT, 0.5%, 0.3% and 0.1% w/w of gemcitabine C14 was added to 20 ml scintillation vials separately and placed in a water bath at 90 °C. This method of organogel preparation was used in all the studies below.

4.1.1.2.2 DSC

This experiment was carried out as described in **2.3.3** part.

4.1.1.2.3 Amplitude sweep

This test was undertaken as described in **2.3.6.1** section.

4.1.1.2.4 Light Microscopy

Optical images were obtained as described in **2.3.5** section.

4.1.1.2.5 *In vitro* release study

4.1.1.2.5.1 In vitro release study method 1 (constant volume of drug release medium)

Solid organogel: 0.5 g of an organogel containing 0.3% and 0.5 % w/w of gemcitabine C14 in 5% w/w 12-HSA/ MCT was placed in 500 ml of sodium phosphate buffer pH 6.8, 0.01 M with 0.1 % w/v sodium dodecyl sulphate to simulate drug release *in vivo* in the tumour tissue. 0.1 % w/v SDS was used to ensure sink conditions as gemcitabine C14 is very insoluble but soluble at 0.0456 mg/ml in 0.1 % w/v SDS in sodium phosphate buffer pH 6.8 (the pH of extracellular matrix of tumour tissue [200]) 0.01M. The minimum concentration of SDS was used to prevent solubilisation of the oil. The organogel in the release medium was shaken at 100 rpm and at 37 °C in a water bath. This system was sealed to inhibit the loss of release medium by evaporation. One millilitre was withdrawn from release medium and then replaced with the same volume of buffer at 1 and 3 hours then at 1, 2, 3, 4, 8, 12, 17 and 30 days. One millilitre of methanol was added to the sample before analysing using HPLC. The drug release from the organogel was repeated in triplicate. The remaining organogels were collected after 30 days to analyse the remaining amount of gemcitabine C14 in the organogel to calculate the percentage of recovery. Also, the initial amount of gemcitabine C14 in the organogels for both concentrations 0.3% and 0.5% w/w was determined by preparing the organogels as in the method of organogel preparation then, the organogels were solubilised directly in methanol. This was carried out as very lipophilic compounds such as gemcitabine C14 are known to adsorb readily to the glass wall of vials or containers. The amount remaining in the organogel and the initial amount were analysed using the HPLC method as shown below.

Liquefied organogel: 0.5 g of an organogel containing 0.3% and 0.5 % w/w of gemcitabine C14 in 5% w/w 12-HSA / MCT was solubilised in 50 µL of NMP and heated at 90 °C. This liquefied organogel was injected using a syringe and 21 gauge needles into 500 ml of sodium phosphate buffer pH 6.8, 0.01 M with 0.1 % w/w sodium dodecyl sulphate. The remaining details of the drug release method are as described for solid organogel above.

4.1.1.2.5.2 *In vitro* release study: method 2 (sample and separate)

0.5 gram of organogel was solubilized using NMP and was heated at 90 °C to guarantee the solubility of gemcitabine C14 and then injected using a syringe with a 21 gauge needle into 25 ml of sodium phosphate buffer pH 6.8, 0.01 M with 0.1 % w/w sodium dodecyl sulphate in 50 ml tubes with a screw. This 25 ml was replaced completely by another 25 ml of phosphate buffer after 3 hours and then after 24 hours. This process was followed daily for 30 days. For stability purposes, the release medium samples were kept in a freezer at -80 °C. This experiment was run in triplicate for each concentration. To analyse the samples, a 25 ml of methanol was added to the 25 ml of the sample and mixed well using the agitator then injected directly to the HPLC. The remaining gels after 30 days were then collected; dissolved and were analysed using the same HPLC method.

4.1.1.2.6 Analysis of in vitro release kinetics

The release of drug was modelled using the Korsemeyer-peppas following equation [201]:

$M_t / M_0 = kt^n$

The M_t represents the drug amount released at time t where M_0 is the initial amount of drug loading, the rate constant is k and n is the exponent. The n value is calculated by taking the $\log_{10}$ of M_t / M_0 versus

$\log_{10}$ t where the slope (the exponent n) indicates the release mechanism. The slope should be taken from the linear portion of 60% of drug released. When the value of n is ≤ 0.45, this drug release is Fickian diffusion. Anomalous drug release is when n is between 0.45 and 1 and if n is more than 1, then there is zero order release kinetics.

4.1.1.2.7 HPLC

The HPLC analysis was performed using the Agilent, Hewlett Packard series 1050 with a C8 column (Agilant-Zorbax Sclipse XDB, 4.6 X 150 mm - 5 micron). The mobile phase was water/methanol mixture (20: 80 v/v %) and the flow was set at 1 ml/min. The wavelength of detection was fixed at 250 nm (the wavelength of maximum absorption of the *N* 4-myristoyl gemcitabine in methanol). The instrument temperature was maintained at 30 °C and the injection volume was 20 µL.

4.1.1.2.8 Calibration curves of gemcitabine C14

4.1.1.2.8.1 Gemcitabine C14 calibration curve in methanol

The following concentrations were used to prepare the calibration curve in methanol (0.02, 0.004, 0.0016, 0.00064, 0.00032, and 0.000256) mg/ml and these concentrations were prepared in triplicate. This standard curve used to analyse the amount of gemcitabine C14 remaining in the organogels and the initial loading of the organogels.

4.1.1.2.8.2 Gemcitabine C14 calibration curve in methanol: buffer

The following concentrations (0.008, 00048, 0.00288, 0.001728, 0.0010368, 0.00062208, 0.000373248, and 0.000223949) mg / ml were prepared in 50: 50 methanol: buffer that used to analyse the samples in the release study.

4.1.1.2.9 *In vitro* injections simulation

A hole was made in a piece of fresh chicken breast then this tissue was incubated in water at 37 °C for 3 hours. Solid 5% w/w 12-HSA/MCT organogel with 0.005 % w/w Nile red was injected into the hole using a syringe. Also, the same organogel now with DiD incorporated at 0.051 % w/w was injected directly into chicken breast using a syringe with a 25 gauge needle.

Also, 0.2 ml of the organogel liquefied with NMP was injected followed by 0.1 ml of buffer into the hole in chicken breast. The addition of buffer helped the diffusion of NMP from the organogel. In all cases, the tissue was left for 15 minutes and then cut open to examine the status of the organogel.

4.1.1.3 Results

4.1.1.3.1 Organogel formation

Gemcitabine C14 was added to both SO and MCT, and then heated in a water bath to 90 °C then left to cool down to room temperature. The 0.1 %, 0.3 % and 0.5 % w/w gemcitabine C14 were not soluble in SO when heated and hence were not progressed further. However gemcitabine C14 was soluble in MCT and formed transparent gels after cooling down the vials to room temperatures as shown in Figure 4-2A. Indeed gemcitabine C14 is a gelator and this is not unexpected based on its nucleoside structure and structural similarity to the cytidine and 2′-deoxycytidine gelators of Skilling *et al* [202].

These three *N*4-myristoyl gemcitabine concentrations were then mixed with 12-HSA to formulate oragnogels. These organogels were then screened by vial inversion to ascertain whether gemcitabine C14 disturbed the formation of the 5 % w/w 12-HSA/MCT organogel. Figure 4-2B shows that the three organogels were solid and did not flow upon vial inversion.

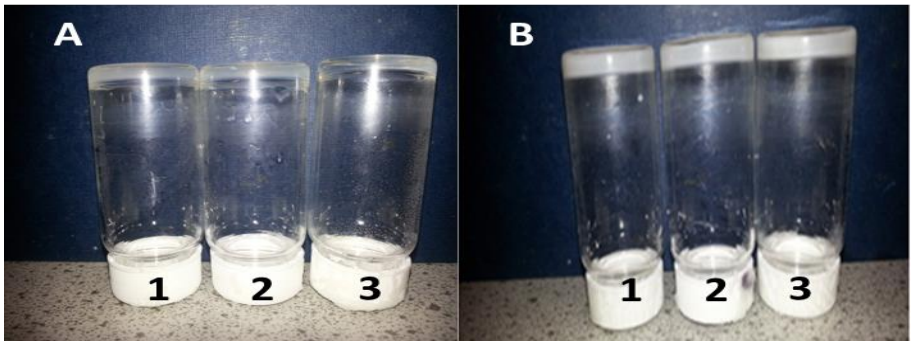

Figure 4-2: A- Vial inversion of organogels where 1, 2 and 3 represents 0.5%, 0.3% and 0.1% w/w gemcitabine C14 in MCT as labeled. B- Vial inversion of organogels where 1, 2, and 3 represents 0.5%, 0.3% and 0.1% w/w gemcitabine C14 in 5% w/w 12-HSA/MCT as labeled. These organogels were heated at 90 °C for approximately 5 hours then cooled to the room temperature. Inverted vials mean solid organogels.

4.1.1.3.2 Amplitude sweep

Amplitude sweep was used to study any changes to the organogel strength upon addition of gemcitabine C14 (Figure 4-3: representative data). This was done by comparing the amplitude sweep parameters (G′, G″, LVER and flow point) of the organogels that contained gemcitabine C14 with the parameters of the selected organogel without drug. As shown in Table 4-1 the addition of different concentrations of gemcitabine C14 did not change the amplitude sweep parameters and this is supported statistically where no significant differences could be detected upon addition of gemcitabine C14 to 5 % w/w 12-HSA/MCT. The only exception was the LVER of the organogel after addition of 0.1 % w/w of gemcitabine C14 which was significantly shorter in comparison with other concentrations ($p < 0.0001$). No change in the mechanical strength and the elasticity of the 5% w/w 12-HSA/MCT upon addition of gemcitabine C14 could be simply explained by the solid content differences between 12-HSA and gemcitabine C14 where 0.5% w/w gemcitabine C14 amount was 10 times less than 5% w/w 12-HSA. This meant these small quantities were not capable of disrupting or strengthening the bonding in the rapid formation of 5% w/w 12-HSA/MCT scaffold. Also, Sintang *et al* executed amplitude sweep test and found that the G′ of the 10% w/w of monoglycerides in a sunflower oil organogel did not change after the addition of phytosterol to the monoglycerides in these proportions (monoglycerides /phytosterol) 70:30 and 40:60 where the solid content was kept at 10% w/w [203].

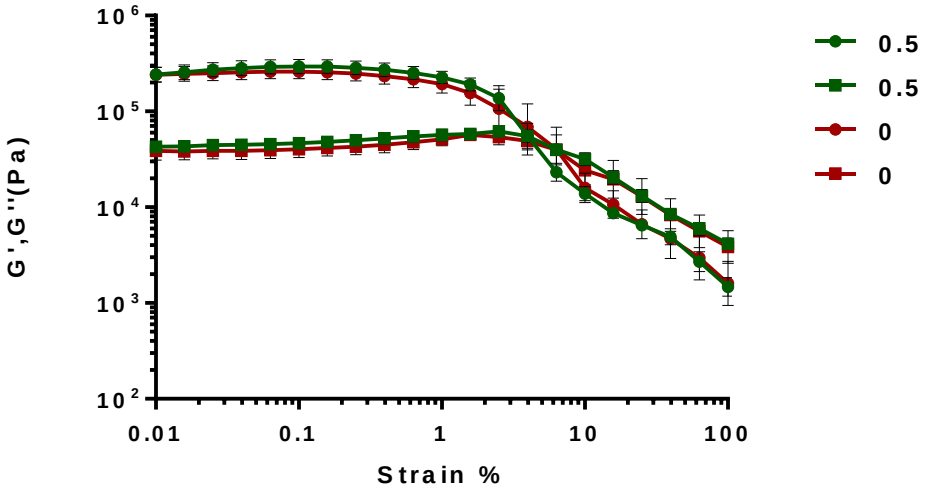

Figure 4-3: Amplitude sweep of different concentrations % w/w of gemcitabine C14 in 5% w/w 12-HSA/MCT, where ⟶● represents G′ and ⟶■ represents G″ and the applied strain was from 0% to 100% and the angular frequency was 10 rad s^{-1}. Each plot is a mean of 4 replicates and the standard deviation represented as black bars. All the amplitude sweeps details of the organogels are shown in Table 1.

Table 4-1: Amplitude sweep parameters of gemcitabine C14 in 5% w/w 12-HSA organogels. (Values represent the mean of ± SD, (n=4)). Statistical analysis was carried out using one way ANOVA with Tukey's post hoc test.

Gemcitabine C14 (% w/w)	G′ x 10^4 (Pa)	G″x 10^4 (Pa)	LVER (%)	Flow point (%)
0	24.025 ± 4.620	3.885 ± 9.462	0.231 ± 0.014	5.240 ± 2.560
0.1	35.275 ± 13.423	6.060 ± 2.676	0.099± 0.00004 ****	3.725 ± 0.419
0.3	30.750 ± 6.459	5.252 ± 1.370	0.156 ± 0.003	3.906 ± 0.535
0.5	24.200 ± 4.685	4.272 ± 0.608	0.157 ± 0.001	3.833 ± 1.051

****** significantly lower LVER value of 0.1% w/w gemcitabine C14 as compared to all other gemcitabine C14 concentrations ($p < 0.0001$).**

4.1.1.3.3 DSC

The addition of gemcitabine C14 to 5% w/w 12-HSA/ MCT organogels was further evaluated using DSC to study the peak and the enthalpy of solidifying and melting transitions as shown in Table 4-2. Statistically, the solidifying and melting temperatures of the gemcitabine C14 organogels and their associated enthalpies did not show a specific order and there were no significant differences compared to 5% w/w 12-HSA/MCT organogel ($p > 0.05$). This also can be explained by the low solid content of gemcitabine C14 as compared to that of 12-HSA.

Table 4-2: Thermal properties (solidifying and melting) of different concentrations % w/w of gemcitabine C14 in 5% w/w 12-HSA/MCT. Each value is a mean of 3 replicates ± standard deviation (SD). The rate of heating and solidifying was 10 °C/minutes and the samples were held at 100 °C and 0 °C for 30 minutes and 2 minutes respectively.

Gemcitabine C14 % (w/w)	Solidifying temperature (°C)	Enthalpy (solidifying) (J/g)	Melting temperature (°C)	Enthalpy (melting) (J/g)
0	46.40 ± 0.50	3.10 ± 0.50	56.20 ± 1.40	2.80 ± 0.10
0.1	46.12 ±0.73	3.75 ± 0.80	55.17 ±1.40	2.70 ± 0.37
0.3	45.95 ±1.14	3.51 ± 0.70	53.71 ±0.46	3.04 ± 0.26
0.5	46.18 ±0.14	2.75 ± 0.58	54.71 ±1.64	2.59 ± 0.34

4.1.1.3.4 Optical microscope

Moreover, the fibre scaffold of the organogels containing gemcitabine C14 was imaged using optical microscopy to identify any changes in its structure in comparison to the organogel without gemcitabine C14. As shown in Figure 4-4, all gemcitabine C14 loaded organogels displayed fibres approximately of the same density as the 5% w/w 12-HSA/MCT. Furthermore, there was no significant difference between the fibre length of organogels having gemcitabine C14 and the organogel without gemcitabine C14 ($p > 0.05$) as shown in Figure 4-5.

Again this can be explained by difference in the solid contents between gemcitabine C14 and the 12-HSA where these small quantities were not able to change the 12-HSA network. Also, there were trials to capture optical images of the gemcitabine C14 in MCT organogels but we could not see the scaffold that was generated by gemcitabine C14 and this was probably due to the high transparency of these organogels.

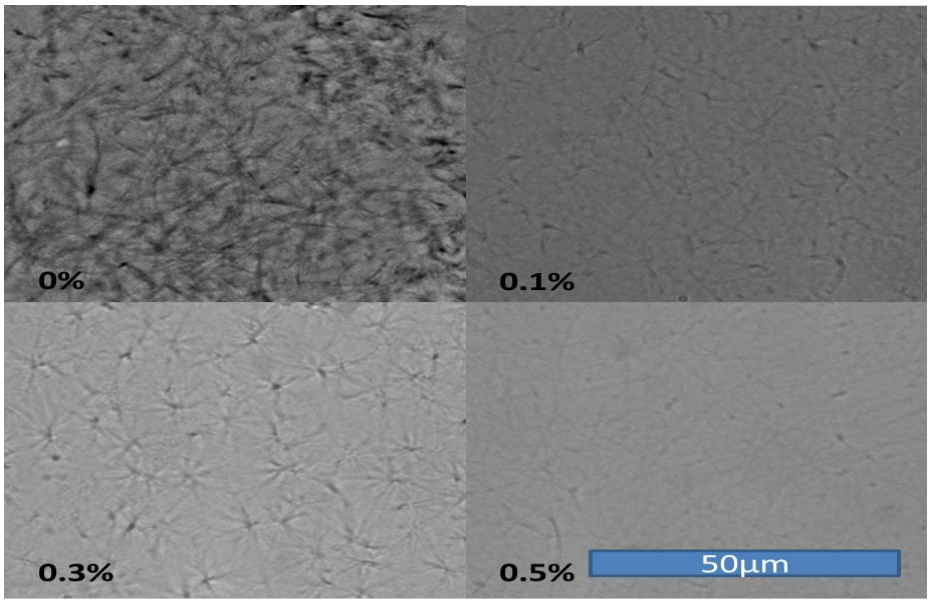

Figure 4-4: Optical microscopy images of 0%, 0.1%, 0.3% and 0.5% w/w gemcitabine C14 in 5% w/w 12-HSA/MCT organogels as labeled were taken after 2 minutes of slide preparation using magnification X40.

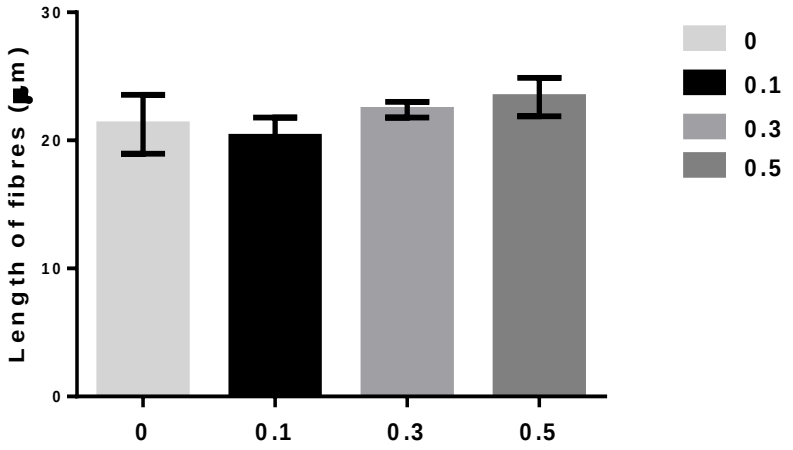

Figure 4-5: Relationship between the length of fibres and different concentrations of gemcitabine C14 % w/w in 5% w/w 12-HSA/ MCT organogels. The length of fibres of each organogel represents the average length of 3 optical microscopy images, 25 fibres were analysed per image using ImageJ software where the length of fibre measurement was made away from margins of the image.

4.1.1.3.5 Calibration curves of gemcitabine C14

A calibration curve prepared in methanol was used to quantify the amount remaining and the initial drug loading of the organogels. This curve showed a high correlation 0.9999 and gave the following equation (y = 36996x - 2.4103) as shown in Figure 4-6. Whilst, the calibration curve prepared in 50: 50 methanol: buffer was used to analyse the drug released from the organogels which gave a high correlation value 0.9984 and gave the following equation (y = 38392x - 7.4481) as presented in Figure 4-7.

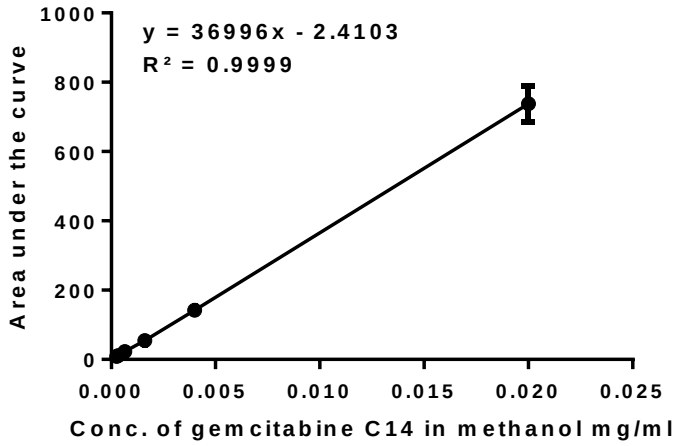

Figure 4-6: Calibration curve of gemcitabine C14 in methanol where each point is a mean of 3 replicates and the black bar represents the standard deviation.

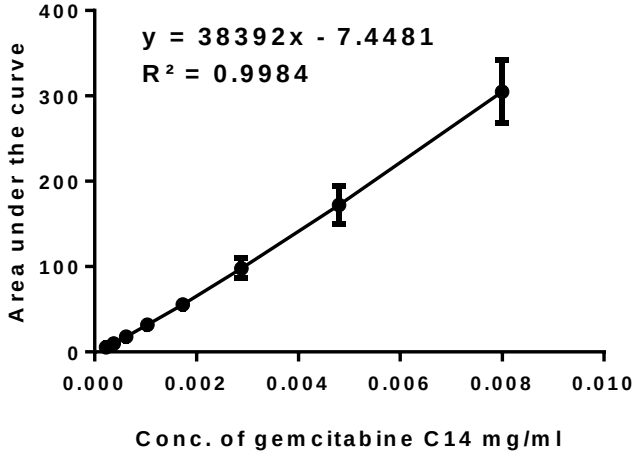

Figure 4-7: Calibration curve of gemcitabine C14 in 50:50 methanol: buffer where each point is a mean of 3 replicates and the black bars represent the standard deviation.

4.1.1.3.6 Release studies

Firstly we will describe how the organogels can be injected. Indeed the selected organogel 5% w/w 12-HSA/MCT showed an ability to be delivered by 2 methods. The first method (solid organogel) depends on the elasticity and syringability that 5% w/w 12-HSA/MCT organogel demonstrated with a syringe or with a syringe and 25 gauge needle as shown in Figure 4-8. Also, the selected organogel can be injected by a different method by liquefying the organogel with the aid of NMP, where the NMP within seconds rapidly solubilised the gemcitabine C14, the 12-HSA and MCT. This solvent liquefied the whole organogel contents and disturbed the bonding responsible for gelation. This liquefied gel can be injected using a syringe and 21 gauge needle. Once this is injected in buffer or *in vivo*, the NMP diffuses out leading to a solidified organogel again as shown in Figure 4-8. The release data below will further evaluate the effect of NMP on drug release from the organogels. NMP has been used in many studies for the same purpose as in our work such as the 5% w/w *N*-behenoyl L-tyrosine methyl ester in safflower oil organogel which contained 0.045 w/v rivastigmine for treatment of Alzheimer's disease. This organogel was liquefied by NMP and injected using 500 µL subcutaneously in rats, where after diffusion of NMP, a solidified organogel implant led to the controlled release of rivastigmine for 35 days [63].

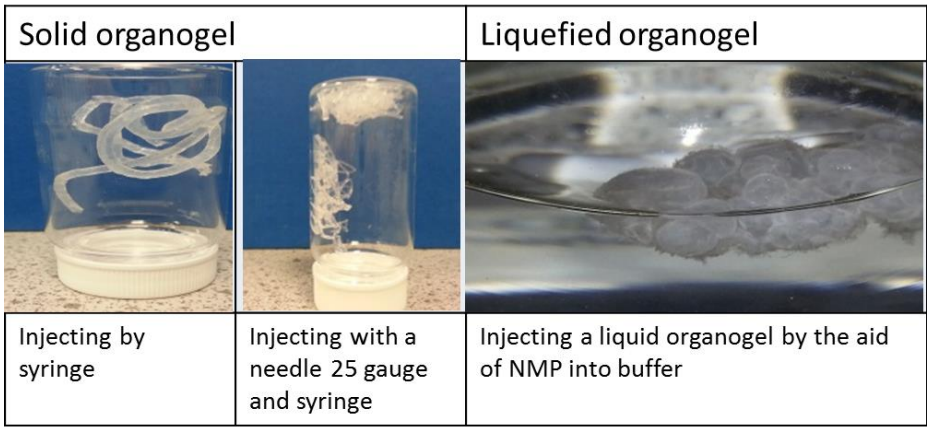

Figure 4-8: Delivery of 5% w/w 12-HSA/MCT organogel using different methods.

The aim of this work is to formulate an organogel for controlled drug release intra-tumourally and hence the focus of the drug release studies was to investigate whether the organogels gave slow, controlled release of gemcitabine C14 over 30 days. The amount released using method 1 (constant volume release medium) as shown in Figure 4-9 and injected as solid organogel of 0.3% and 0.5% w/w gemcitabine C14 after 4 days was (0.18 mg ±0.007) and (0.24 mg ±0.01) whilst the amount released after 30 days was (0.25 mg ±0.01) and (0.29 mg ±0.06) respectively. For the liquefied delivery of the organogel, the release study gave a higher amount released from the organogels loaded with 0.3% and 0.5% w/w of gemcitabine C14, where the amount released after 4 days was (0.36 mg ±0.01) and (0.59 mg ±0.03) and after 30 days, (0.46 mg ±0.02) and (0.65 mg ±0.03) respectively. The higher amounts of gemcitabine C14 released into the buffer using a liquefied organogel was probably due to the NMP which increased the solubility of gemcitabine C14 in the release medium.

The cumulative percentage of gemcitabine C14 released by both delivery methods is presented in Figure 4-10. The cumulative percentage released from the organogels with 0.3% and 0.5% w/w of gemcitabine C14 (liquefied with NMP) in 5% w/w 12-HSA/MCT organogels was 34.37 % ± 1.48 and 35.02 % ± 1.8 after 30 days. Indeed, the cumulative percentages released from both concentrations were almost the same after 30 days.

The liquefied organogels exhibited similar behaviour to those of Bastiat *et al* where they solubilised 2.3% w/w N-stearoyl L-tyrosine methyl ester in safflower oil organogel with NMP. The organogel was also loaded with the rivastigmine. The burst release of drug was 18% in the first day due to the NMP and the release was followed for 7 days where only a further 2 % was released [204].

The cumulative percentage released from the organogels with 0.3% and 0.5 % w/w gemcitabine C14 (delivered by injecting and shearing solid organogels) was 26.62 % ± 1.28 and 18.95 % ± 3.88 after 30 days respectively as shown in Figure 4-10. The organogel that contained the 0.3% w/w of gemcitabine C14 showed a higher percentage release than the organogel with 0.5% w/w. This can be rationalised by the fact that release was the same from both organogels but with different initial loadings of gemcitabine C14. This result was in agreement with the release study of arachidic acid in soybean oil organogel which contained paliperidone used in schizophrenia treatment. This study followed the release for 14 days and 100 % was released for 2 mg/ml organogel; 80% for the 4mg/ml organogel, whilst only 70% was released for the 6 mg/ml organogel over the same period of time [205].

The two delivery methods gave good percentage recoveries as shown in details in Table 4-3 includes the amount remaining in the organogels, total amount released, the initial drug loading and the percentage of

recovery for both concentrations 0.3% and 0.5% w/w gemcitabine C14 concentrations.

In summary, organogels injected as a solid reflected the greater ability of 5% w/w 12-HSA/MCT organogel as a depot system by showing the slowest release and the lowest percentage of release which is 26.62% and 18.95% of 0.3% and 0.5% w/w gemcitabine C14 from 5% w/w 12-HSA/MCT in comparison with the release of 0.15 mg gemcitabine from polyurethane/ poloxamer 407 film which released 35% from the total loading dose within 3 days of the *in vitro* release study [206]. Also, the 35% of the released gemcitabine from polyurethane/ poloxamer 407 film still higher compared with the liquefied 5% w/w 12-HSA/MCT organogels by NMP which released around 35% from both 0.3% and 0.5% w/w gemcitabine C14 after 30 days.

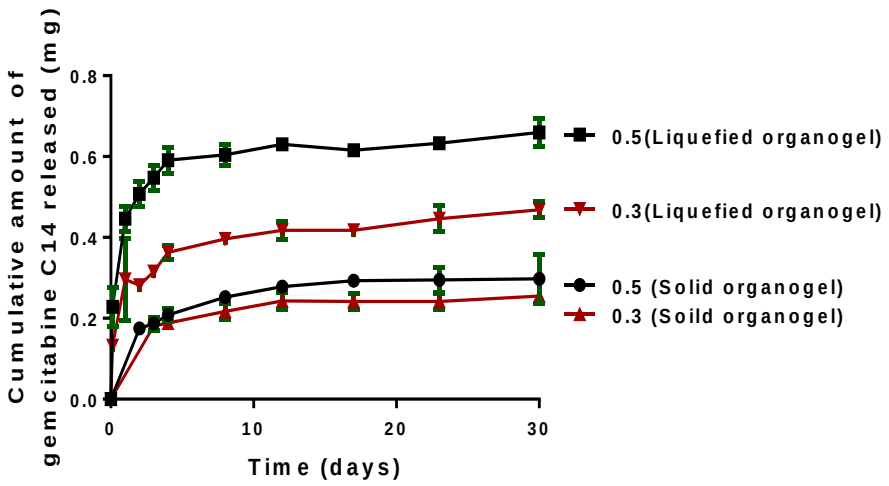

Figure 4-9: Cumulative drug release from 0.5% and 0.3% w/w gemcitabine C14 in 5% w/w 12-HSA/MCT organogels using solid and NMP liquefied gels; release medium is 0.01M of Na phosphate buffer pH 6.8 with 0.1% w/v SDS where each value represents the mean ± SD (n=3).

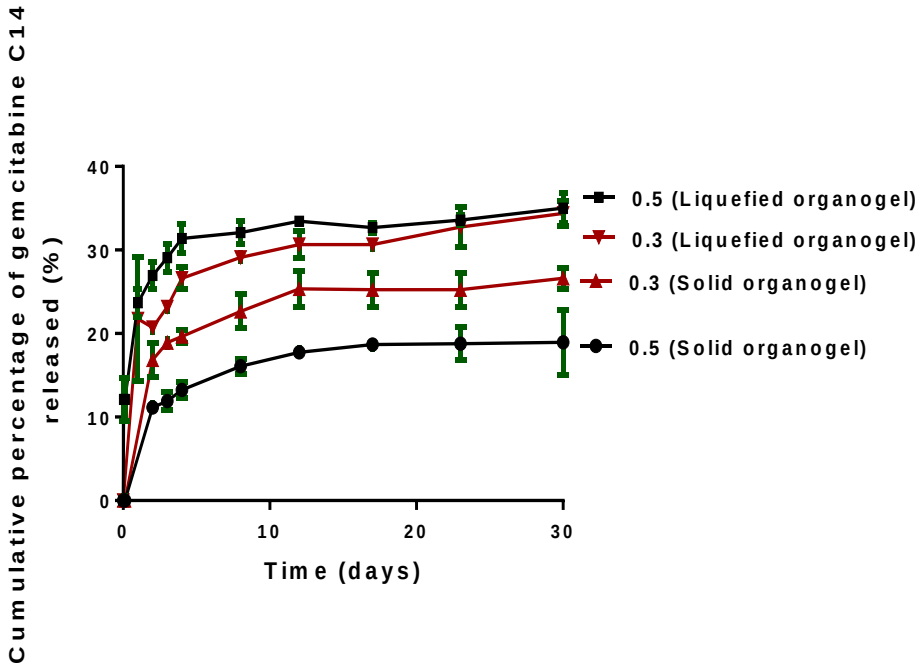

Figure 4-10: Cumulative percentage released from 0.5% and 0.3% gemcitabine C14 in 5 % w/w 12-HSA/MCT organogels using solid and NMP liquefied gels; release medium is 0.01M of Na phosphate buffer pH 6.8 with 0.1% w/v SDS where each value represents the mean ± SD (n=3).

Table 4-3: Amount remaining in the organogel, total amount released, initial loading and percentage recovery for the 0.5% and 0.3% w/w gemcitabine C14 in 5% w/w 12-HSA/MCT for both delivery methods (solid and NMP liquefied gels).

Delivery method	Concentration gemcitabine C14 (% w/w)	Amount of gemcitabine C14 remaining in organogel (mg)	Total amount released from organogel (mg)	Initial loading of gemcitabine C14 (mg)	% recovery
Solid organogel	0.5	1.08±0.12	0.29±0.06	1.57±0.11	87.26
	0.3	0.62±0.07	0.25±0.01	1.04±0.05	83.65
Liquefied organogel	0.5	1.32±0.07	0.65±0.03	1.88±0.005	104.78
	0.3	0.85±0.17	0.46±0.02	1.36±0.15	96.32

Since we are working with a very insoluble drug, there is always a concern that low solubility in the release medium cannot adequately mimic the sink conditions *in vivo* and partitioning into tissue. Hence an alternative sample and separate method (method 2) was also used to study the drug release where each day the release buffer was removed and fresh buffer placed on top of the organogel. Other groups have used similar methods such as Wu *et al* studied the *in vitro* release of doxorubicin from the organogel of phospholipid, MCT and ethanol where a 5 ml volume of the release medium was removed totally and replaced with fresh buffer for 20 days [64]. Also, Kreye used the sample and separate method to study the release from compressed oily implants of theophylline and propranolol for 30 days [207]. Figure 4-11A shows the daily amount of gemcitabine C14 released where there was a slight difference in the amount released of gemcitabine C14 between the two concentrations 0.5% and 0.3% w/w. We think this kind of release pattern from different concentrations of gemcitabine C14 was due to the same the underlying structure of the 12-HSA/MCT organogel controlling the release.

Moreover, the same data was presented in Figure 4-11B which showed the cumulative percentage amount released from 0.3% and 0.5% w/w gemcitabine C14 from the selected organogel was 70.07% ± 2.61 and 56.18% ± 1.25 respectively. This method gave excellent percentage recoveries as presented in Table 4-4 which also includes details of the amount remaining, the total amount released, initial drug loading for both 0.3% w/w and 0.5% w/w concentrations.

When comparing methods 1 and 2, there is a higher percentage released for method 2 which is not unexpected as the release medium was wholly removed and then replaced with the same amount of medium.

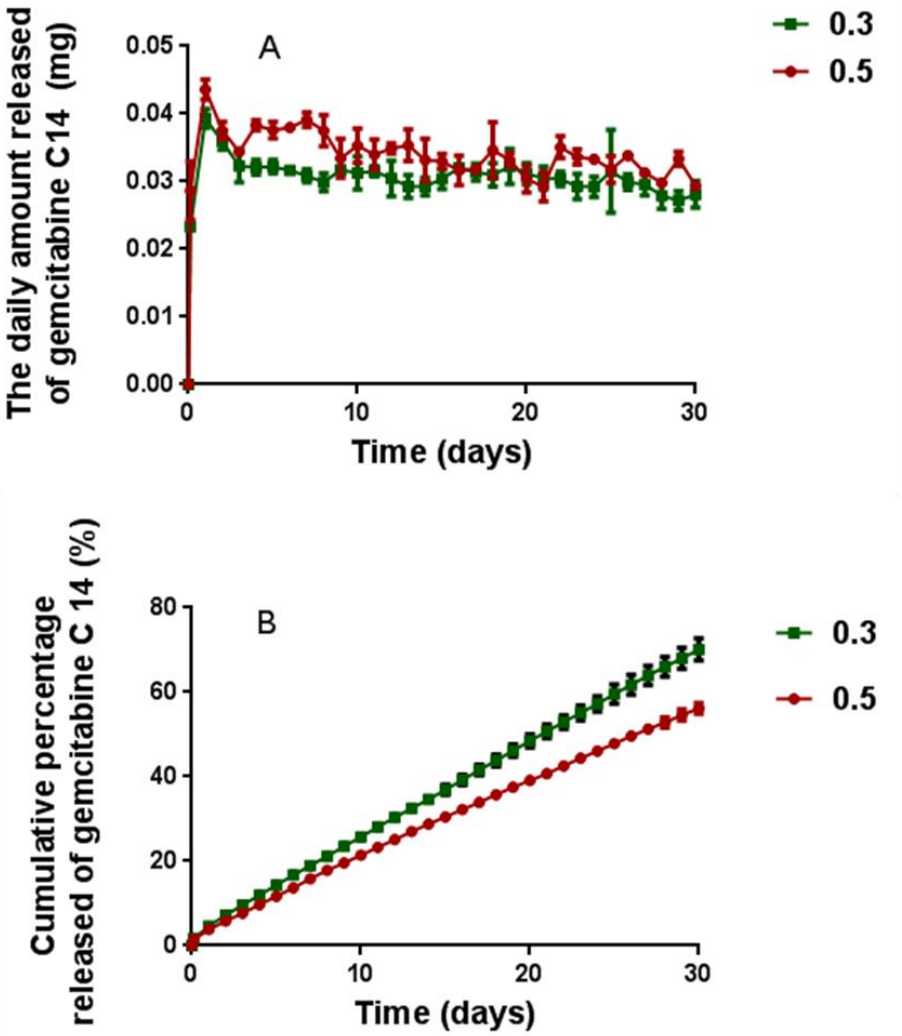

Figure 4-11: A -Daily amounts released form 0.5% and 0.3% w/w of gemcitabine C14 in 5% w/w 12-HSA/ MCT orgnogels using method 2. B - Percentage of cumulative amount released of 0.5% and 0.3%w/w of gemcitabine C14 in 5% w/w 12-HSA/MCT organogels using method 2 (sample and separate) where release medium is 0.01M of Na phosphate buffer pH 6.8 with 0.1% w/v SDS where each value represents the mean ± SD (n=3).

Table 4-4: Amount remaining, total amount released, initial drug loading and percentage recovery drug release from 0.5% w/w and 0.3% w/w of gemcitabine C14 in 5% w/w 12-HSA/MCT of method 2 (sample and separate).

Concentration gemcitabine C14 (w/w%)	Remaining amount gemcitabine C14 in organogel (mg)	Amount of gemcitabine C14 released (mg)	Initial drug loading of gemcitabine C14 (mg)	% recovery
0.5	1.01±0.23	1.060±0.02	1.880 ±0.005	106.3%
0.3	0.41±0.24	0.953±0.03	1.362 ±0.15	100%

4.1.1.3.7 Analysis of *in vitro* release kinetics

The drug release data of the selected organogel were fitted to Korsemeyer-peppas model as shown in Table 4-5 where all the release data were highly correlated to the Korsemeyer-peppas equation. The least R^2 was 0.84 and the highest was 0.979. The n exponent values of both delivery methods i.e. solid and liquefied organogels for method 1 were less than 0.45 which indicates Fickian diffusion. This was similar to the antipyrene release from an olive oil organogel with 1% w/w behenamide and 1% w/w erucamide which showed Fickian diffusion after fitting the release data to the Korsemeyer-peppas equation [201]. Method 2 (sample and separate) showed for both concentrations anomalous diffusion where n values were 0.725 and 0.715. This is similar to the release of progesterone from poly q-caprolactone matrices which showed anomalous diffusion by applying Korsemeyer-peppas formula where the method that executed to study the release was also sample and separate method [208]. The anomalous diffusion was explained by Tarvainen *et al* as a result of diffusion and erosion and this supports the interpretation of the difference of the n between method 1 and 2 in our work [209]. The main cause of erosion in our work is the SDS which was important to solubilise the gemcitabine C14 where at the same time, SDS was solubilising the organogel. The organogel solubility in method 1 by SDS might reach a saturation condition and hence the mechanism of the release was predominantly just diffusion. Whilst method 2 showed the diffusion and the erosion because the principle of the sample and separate method was changing the volume completely and daily which helps to not reach the saturated solubility of the organogel and hence aids erosion.

Table 4-5: Korsemeyer-peppas model parameters of the release of gemcitabine C14 from the 5% w/w 12-HSA/MCT organogel.

Gemcitabine C14 % w/w	Method of drug release	Korsemeyer-peppas R^2	n exponent
0.5	Method 1- solid organogel	0.954	0.198
0.3	Method 1- solid organogel	0.840	0.166
0.5	Method 1- liquefied organogel	0.921	0.197
0.3	Method liquefied organogel	0.963	0.229
0.5	Method 2- (sample and separate) liquefied organogel	0.977	0.725
0.3	Method 2- (sample and separate) liquefied organogel	0.979	0.715

4.1.1.3.8 *In vitro* simulation

As a preliminary study to the *in vivo* work, an *in vitro* simulation of injection into the tumour was investigated using chicken breast as shown in Table 4-6 where all images were taken after sectioning the tissues. The 5% w/w 12-HSA/MCT organogel with Nile red and sheared through a syringe showed an existence of an intact organogel after cutting the tissue near the hole that the organogel was injected into. This reflected the strength of the selected organogel. Also, this organogel had enough elasticity to be injected through a syringe and a 25 gauge needle as shown for the organogel with DiD incorporated (blue colour). As presented in Table 4-6, the 5% w/w 12-HSA/MCT was a solid depot and stayed in the same place and it did not show any breaking in the physical structure. An important note should be mentioned when the organogel was injected using the needle of 25

gauge, there was a need to hold the syringe and needle strongly through the process of injection due to the slight resistance upon injection

DiD was also incorporated into the liquefied organogel and completely vanished after adding the NMP. Thus another lipophilic dye (Nile red) was incorporated into the liquefied organogel. After cutting the tissue, solid red aggregates were observed which confirmed the diffusion of NMP out of the organogel aided by buffer which was added after the injection of the liquefied organogel to the hole in the tissue.

Similar to our work, chicken tissue was used by Rungseevijitprapa *et al* where they injected their microparticles into chicken to inform them prior to injection into rats. They tried to inject microparticles into chicken meat using different sizes of needles. They found the force of injection was directly proportional to the viscosity of the system and to the type of tissue where the injection into muscle tissue was different than the injection into subcutaneous tissue [210].

In summary, using chicken tissue to simulate the injection of our selected organogel as a solid and liquefied an intact solid organogel depot and aggregates of the organogel were observed respectively.

Table 4-6: Simulation *in vitro* of delivery methods (solid or liquefied) using chicken breast.

Solid organogel		Liquefied organogel
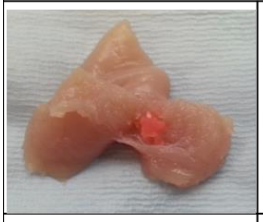	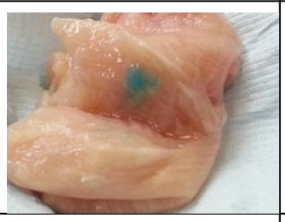	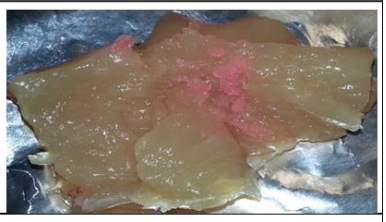
Tissue with a hole.	Tissue without hole.	Tissue with a hole.

4.1.1.4 Conclusions

The 5% w/w 12-HSA/MCT achieved the aim of our work which was a depot organogel to be injected into the tumour. After addition of gemcitabine C14, the organogel did not exhibit any significant changes in both the thermal stability and the mechanical strength. Also it was shown to control and give slow the release of gemcitabine C14. The cumulative percentage released was 26.62% and 18.95% for 0.3% and 0.5% w/w gemcitabine C14 in 5% w/w 12-HSA/MCT (solid organogel) respectively as measured using method 1 (constant volume of release medium). Whilst for the liquefied organogel, the cumulative percentage released was 34.37% and 35.02% for 0.3% and 0.5% w/w gemcitabine C14 in 5% w/w 12-HSA/MCT respectively. Data for both delivery methods fitted to Korsemeyer-peppas model and showed Fickian diffusion. The cumulative percentage released as measured using method 2 (sample and separate) of 0.3% and 0.5% w/w gemcitabine C14 in 5% w/w 12-HSA/MCT was 70.7% and 56.18% respectively and the drug release was a combination of diffusion and erosion (anomalous diffusion) after fitting to the Korsemeyer-peppas model. Moreover, the 5% w/w 12-HSA/MCT was sheared and injected into the chicken breast and then reformed into a solid depot showing promise for future *in vivo* studies.

4.1.2 Section B (gemcitabine C14 in 14% w/w 12-HSA/PG)

4.1.2.1 Materials

Rhodamine B 98% (CAS number 81-88-9 and Lot number A0359862) was purchased from Fischer scientific UK LTD.

4.1.2.2 Experimental work

4.1.2.2.1 Organogel formation

To the selected organogels 14% w/w 12-HSA in PG, 0.5%, 0.3% and 0.1% w/w of gemcitabine C14 was added to 20 ml scintillation vials separately and placed in a water bath at 90 °C. This method of organogel preparation was used in all the studies below.

4.1.2.2.2 DSC

This experiment was carried out as described in **3.3.3**.

4.1.2.2.3 Polarised light microscope

The slides were observed as described in section **3.3.4**.

4.1.2.2.4 Optical light microscopy

This study was carried out as described in section **3.3.6**.

4.1.2.2.5 Amplitude sweep

This experiment was executed as described in section **3.3.7.1**.

4.1.2.2.6 Drug release study

The drug release study was carried out as described in section **4.1.1.2.5.2**. The volume of the release medium was reduced to 20 ml after day 17 and then another reduction to 15 ml after day 22. These reductions were due to the decrease in the amount of the gemcitabine C14 released to ensure concentration was above the limit of detection.

4.1.2.2.7 Release of propylene glycol

The propylene glycol release was studied by ATR-FTIR. The calibration curve was constructed from the characteristic groups of PG molecule using the ratio of intensities of the stretching of two peaks in the spectra at 1040 cm^{-1} (C-O stretching) and 3258 cm^{-1} (O-H stretching) for 0.0009375, 0.01875, 0.0375, 0.075, 0.15 and 0.3 mg/ml of PG in buffer. Then the release of PG was investigated for 1 g of both 14% w/w 12-HSA/PG and 0.5% w/w gemcitabine C14 in 14% w/w 12-HSA/PG organogels. These organogels were placed in 10 ml of sodium phosphate buffer pH 6.8, 0.01 M at 37 °C. One millilitre was taken and replaced after the following time periods: 5 minutes, 30 minutes, 60 minutes and after 2 hours. This was done in triplicate.

4.1.2.2.8 *In vitro* simulation

A hole was made in a piece of fresh chicken breast then this tissue was incubated in water at 37 °C for 3 hours. The selected organogel with rhodamine B was pushed with syringe into the hole of the tissue. After 15 minutes post injection, the tissue was sectioned to check the status of organogel.

4.1.2.3 Results

4.1.2.3.1 Organogel formation

Vial inversion i.e. no flow of the vial contents upon inversion was used to test the addition of gemcitabine C14 to the selected organogel 14% w/w 12-HSA/PG. The following concentrations of 0.1%, 0.3% and 0.5% w/w were added to the 14% w/w 12-HSA/PG and it was found that the addition did not alter the gelation as shown in Figure 4-12. The first step in organogel preparation was to solubilise the gemcitabine C14 in PG. Within 15 minutes in the water bath at 90 °C, all concentrations of gemcitabine C14 were completely soluble. This quick dissolution of gemcitabine C14 in PG is very attractive in terms of a practical manufacturing process as compared to the 5 hours it took to dissolve in MCT.

Figure 4-12: Vial inversion of organogels where 1, 2, and 3 represents 0.1%, 0.3% and 0.5% w/w gemcitabine C14 in 14% w/w 12-HSA/PG as labeled where these organogels were prepared by heating to 90 °C for 30 minutes and then cooled down to room temperature. The inverted vials represent solid organogels at room temperature.

4.1.2.3.2 DSC

Also, the organogels containing gemcitabine C14 were analysed using DSC to study the effect of adding gemcitabine C14 on both the transitions temperatures (solidifying and melting) and their enthalpies as shown in Table 4-7. Statistically, the peak and the onset of melting and solidifying temperatures of organogels containing gemcitabine C14 showed no significant change ($p>0.5$) compared to the onset and the peak of melting/solidifying transition temperatures of the organogel without drug. Accordingly, the small added amounts of gemcitabine C14 did not disturb the spherulites arrangements of the main gelator (12-HSA). This result was in agreement with the 0.7 % w/w of 12-HSA in 1, 2-dichlorobenzene which showed that the transition temperature from gel to liquid did not change after the addition of 0.1% w/w carbon nanotubes [211].

Further to the main peaks, the addition of gemcitabine C14 to the selected organogel showed the appearance of additional peaks in the solidifying and melting thermograms as shown in Figure 4-13 and Figure 4-14. Moreover, these additional peaks at 70.28 °C ± 1.3 and 79.83 °C ± 0.32 appeared at similar temperatures in solidifying and melting thermograms to the additional peaks in 14% w/w 12-HSA/PG of 70.5 °C ± 0.78 and 79.7 °C ± 0.42 respectively. These additional peaks in **3.4.3** 12-HSA were identified as crystals. Also, many thermograms of the organogels with the gemcitabine C14 did not show these additional peaks clearly, and this may be explained that the time for these crystals to form was not enough or that gemcitabine C14 is inhibiting nucleation.

Table 4-7: Thermal properties (solidifying and melting) of gemcitabine C14 in 14% w/w 12-HSA/PG organogels. Each value is an average of 3 replicates and ± standard deviation (SD). The rate of heating and solidifying was 10 °C/minutes and the samples were held at 100 °C and 0 °C for 30 minutes and 2 minutes respectively.

Gemcitabine C14 w/w %	Solidifying temperature onset (°C)	Peak of Solidifying temperature (°C)	Solidifying enthalpy (J/g)	Melting Temperature onset (°C)	Melting temperature (°C)	Melting entahlpy (J/g)
0	28.10 ±2.24	19.31 ±3.06	20.78 ±2.98	38.75 ±0.15	48.11 ±0.13	14.31 ±2.61
0.1	31.21 ±3.03	24.21 ±2.20	23.14 ±2.60	38.54 ±0.44	47.88 ±0.50	17.23 ±1.40*
0.3	31.27 ±1.50	19.58 ±2.40	17.56 ±3.20	38.06 ±0.24	47.74 ±0.15	11.92 ±01.60
0.5	30.39 ±1.10	24.95 ±1.10	18.33 ±0.94	38.73 ±0.09	47.74 ±0.15	11.75 ±0.86

*** indicates higher significant value of the enthalpy of melting temperature of 0.1% w/w gemcitabine C14 14% w/w 12-HSA/PG compared to 0.3% and 0.5% w/w gemcitabine C14 14% w/w 12-HSA/PG.**

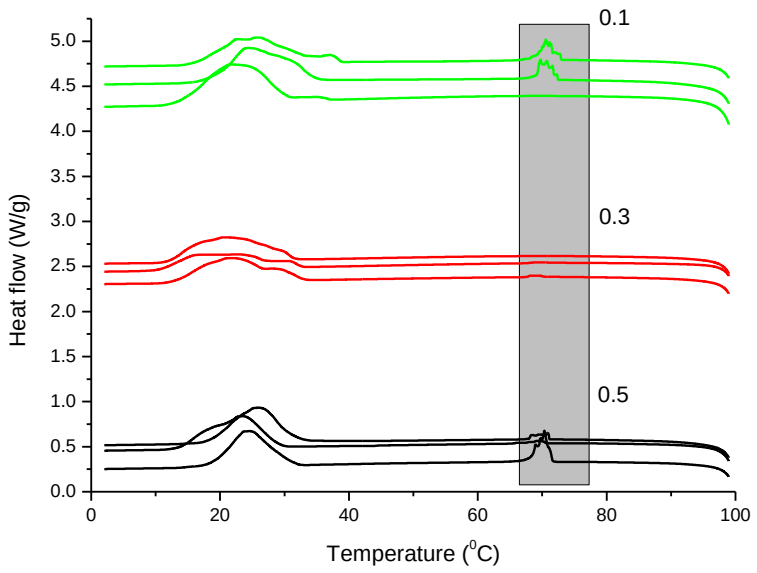

Figure 4-13: Solidifying thermograms of DSC of different concentrations % w/w of gemcitabine C14 in 14% w/w 12-HSA/PG organogels and the label points out the additional peaks at 70.28 °C ± 1.3 where rate of cooling was 10 °C/minutes.

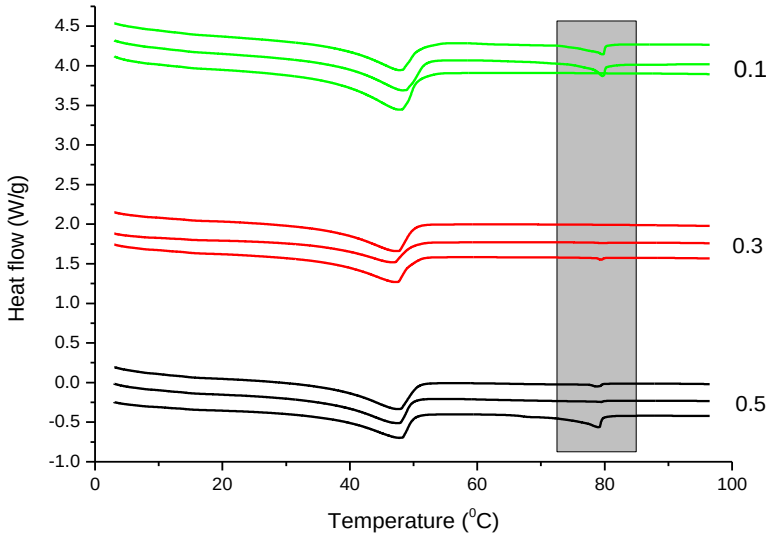

Figure 4-14: Melting thermograms of DSC of different concentrations % w/w of gemcitabine C14 in 14% w/w 12-HSA/PG organogels and the label points out the additional peaks at 79.83 °C ± 0.32 where the melting rate was 10 °C/minutes.

4.1.2.3.3 Polarised microscope

The organogels with gemcitabine C14 were observed by polarised light microscopy and between day 1 and day 6 no significant changes were seen. Thus only the images at day 1 and day 6 are shown. The images of the organogel with 0.1% w/w gemcitabine C14 in 14% w/w 12-HSA/PG in Figure 4-15 showed the same trend as the same organogel without drug where clear crystals were observed. Whereas the organogels of 0.3% and 0.5% w/w gemcitabine C14 in 14% w/w 12-HSA/PG did not show any crystals.

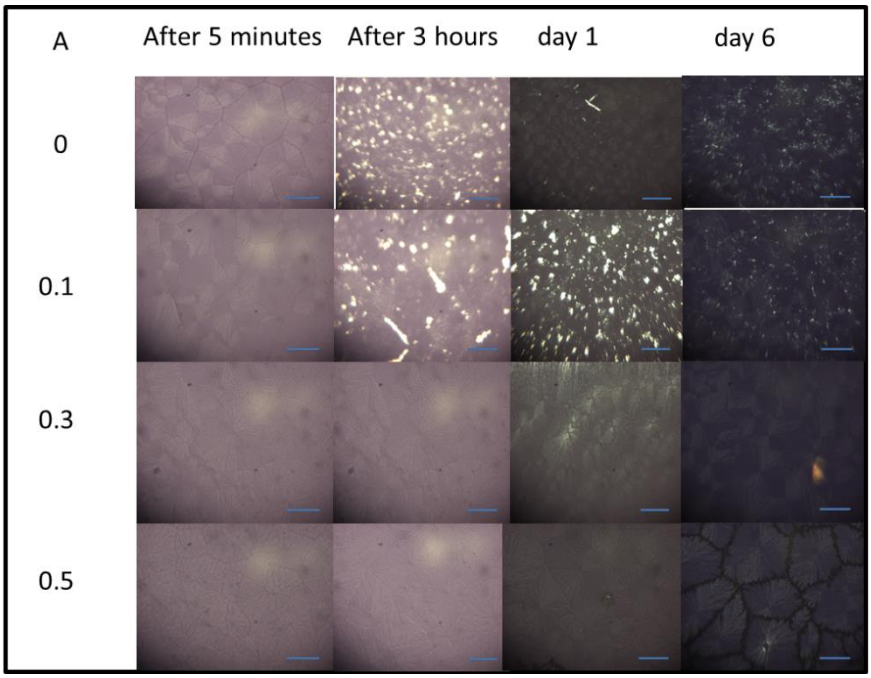

Figure 4-15: Polarised images of organogels. Column A represents the % w/w of gemcitabine C14 in 14% w/w 12-HSA/PG organogels where the other columns represent the time periods. The objective was X10 and the magnification bar is 200 µm.

4.1.2.3.4 Optical light microscope

4.1.2.3.4.1 Organogels with 12-HSA and gemcitabine C14

Furthermore, the morphology of the scaffold of organogels containing different concentrations of gemcitabine C14 was examined by optical light microscope. The images in Figure 4-16 showed that after 5 minutes of preparation, the 3 organogels with drug incorporated had spherulities and these were similar to the spherulities of 14% w/w of 12-HSA/PG organogel without drug.

After 3 hours, the images of 0.1% w/w of gemcitabine C14 in 14% w/w 12-HSA/PG organogel showed fibres between the margins of the spherulities whilst 0.3% and 0.5% w/w gemcitabine C14 in 14% w/w 12-HSA/PG did not show this change. However, the organogels were then followed from day 1 to day 6 and gaps were at day 1 then observed between adjacent spherulites connected by fibres. Additionally, all organogels showed more growth at day 2.

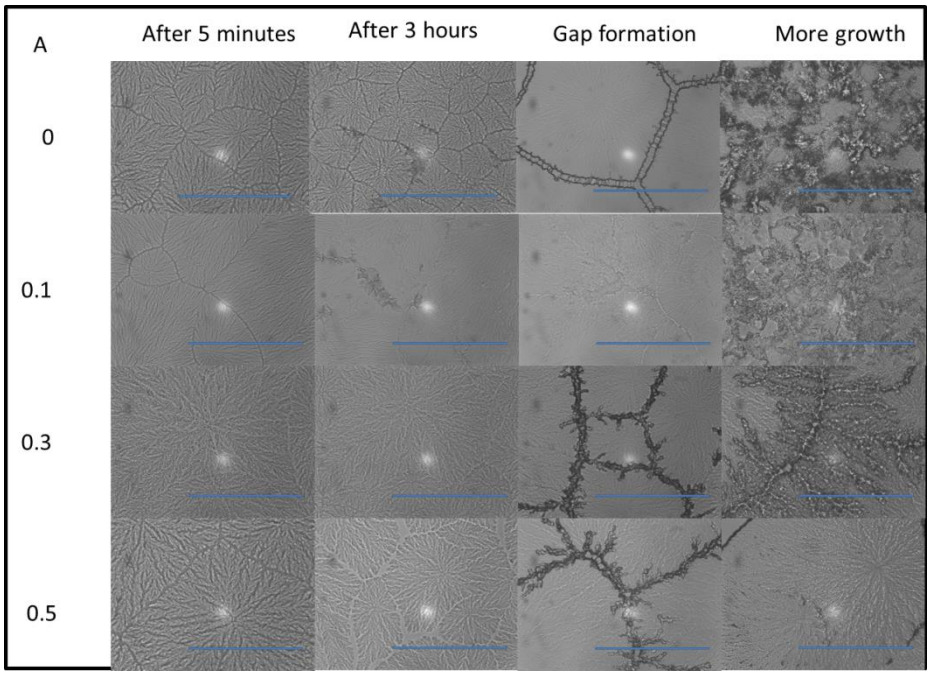

Figure 4-16: Optical light microscopy images of gemcitabine C14 0.1%, 0.3% and 0.5% w/w in 14% w/w 12-HSA/PG organogels, where column A represents the percentage of solid content of gemcitabine. The column of "gap formation" presents the gap between neighbour spherulites and started at day 1 while column of "more growth" presents the dark areas and this starts at day 2. The objective was X40 and the scale: 200 µm. The light reflection of the microscope appears as a white dot in most images.

4.1.2.3.4.2 Gemcitabine C14 in PG (no 12-HSA)

Gemcitabine C14 was solubilised quickly in PG. A precipitate then appeared in 0.3% and 0.5% w/w gemcitabine C14/PG after 2 days and 24 hours respectively. These precipitates were studied by light microscope as shown in columns B, C and D in Figure 4-17. The images of 0.3% w/w gemcitabine C14 in PG showed fine fibres at day 1 and then these fibres turn denser to form a scaffold as shown in column C and also voids were observed within the scaffold as shown in column B. The growth of the fibre scaffold of 0.5% w/w gemcitabine C14 in PG also increased with time as shown in column D. These scaffolds that were formed by 0.5% w/w and 0.3% w/w of gemcitabine C14 in PG weren't able to support PG upon vial inversion, however, they did form an organogel in plastic containers such as a syringe after 6 days as shown in Figure 4-18.

In summary, 0.3% and 0.5% w/w gemcitabine C14 in PG formed fibre scaffolds which gave an organogel in plastic syringe but a precipitate / weak gel in glass vials.

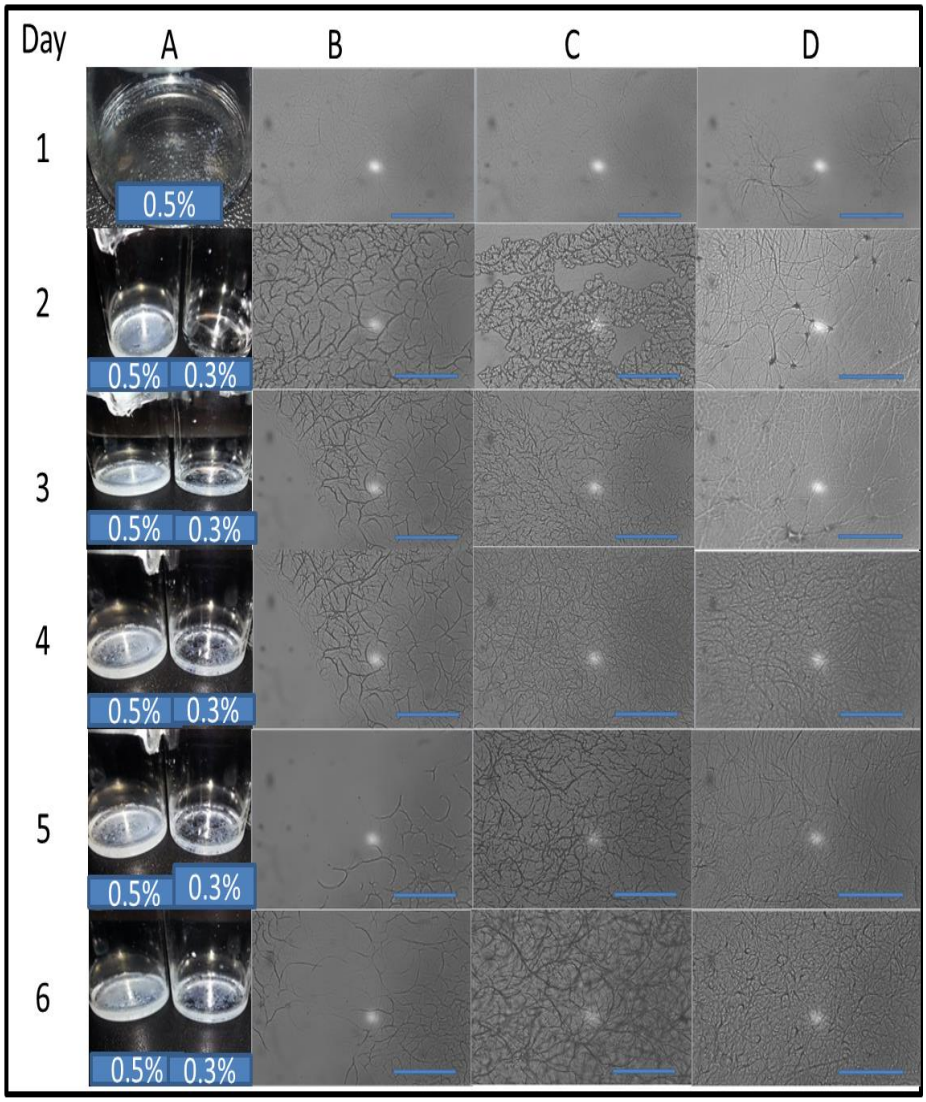

Figure 4-17: Growth of the scaffold of 0.5% w/w and 0.3% w/w gemcitabine C14 in PG with time and their optical images where column A represent the organogels in 20 ml scintillation vials with time. Column B shows the voids in 0.3% w/w gemcitabine C14 scaffold. Column C shows the fibre growth of 0.3% w/w gemcitabine C14/PG and column D presents fibre growth of 0.5% w/w gemcitabine C14/PG. The light reflection of the microscope appears as a white dot in most images where all scaffold photos were scaled against 100µm.

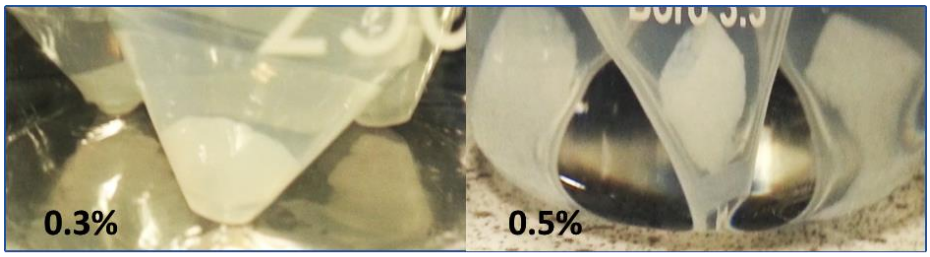

Figure 4-18: Organogels of 0.3% and 0.5% w/w of gemcitabine C14 in PG in buffer (no 12-HSA).

4.1.2.3.5 Amplitude sweep

By vial inversion, the addition of gemcitabine C14 did not alter the organogels. However, further testing was necessary by oscillatory rheology (amplitude sweep) as shown in Figure 4-19 and Table 4-8 to examine the mechanical strength of the gels. The storage modulus of organogels without drug showed the highest value compared to the other organogels containing different amounts of gemcitabine C14 and followed this order: 0% > 0.1% > 0.3% > 0.5% w/w. LVER values also showed a similar trend. Statistically, the G′ of the organogel without drug was significantly higher ($p< 0.05$) and ($p< 0.01$) in comparison to the organogels loaded with 0.5% and 0.3% w/w respectively. Moreover, the LVER of this organogel was also significantly higher than the organogel containing 0.5% w/w gemcitabine C14. Additionally, there was no significant difference ($p> 0.05$) in the flow points of the organogels with different concentrations of gemcitabine C14. The decrease in G′ of the selected organogel upon addition of gemcitabine C14 was similar to Moschakis *et al* study which revealed a decrease in G′ when the proportions of the 2 gelators of 20% w/w was (30: 70) Ɣ-oryzanol and phytosterols in sunflower oil changed to (60: 40) Ɣ-oryzanol and phytosterols and this was attributed to the changes between aggregates [212].

This decrease in the G′ and LVER could be due to two gelators in the same fibre scaffold or may be the gemcitabine C14 fibre network affects the interactions in the 12-HSA scaffold and led to a weaker scaffold as depicted in Figure 4-20.

This hypothesis of 2 gelators in the same scaffold was explained by Raeburn and Adams where either the 2 gelators self- sort and form separate scaffolds in the same volume or the 2 gelators form fibres and being parts of the same fibre [213].

To conclude, the addition of gemcitabine C14 showed a decrease in G′ and LVER values as the concentration of gemcitabine C14 increased in the 14% w/w 12-HSA/PG organogel.

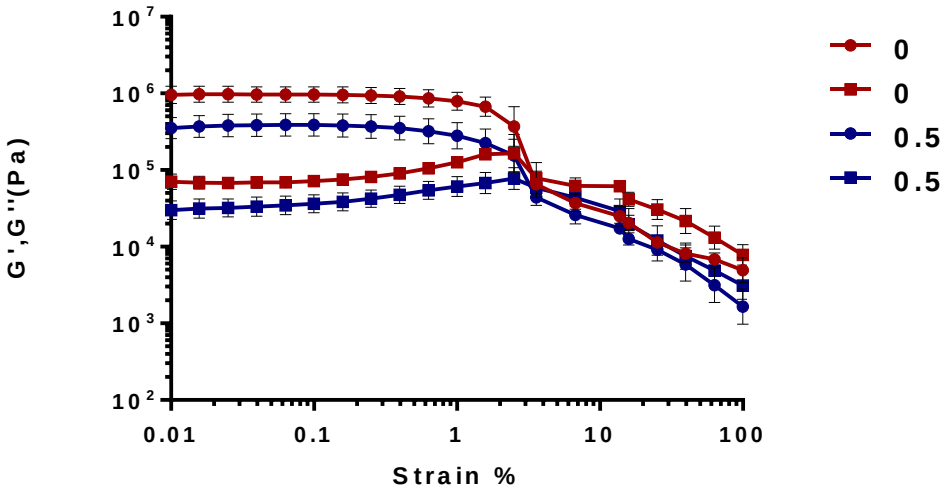

Figure 4-19: Amplitude sweeps of gemcitabine C14 %w/w in 14% w/w 12-HSA/PG organogels and the applied strain was from 0% to 100% and the angular frequency was 10 rad s^{-1}. Each plot is a mean of 4 replicates where the black bars represent the standard deviation, where ⟶● represents G′ and ⟶■ represents G″. The amplitude sweep parameters of all oragnogels are shown in Table 4-8.

Table 4-8: Amplitude sweep parameters of gemcitabine C14 %w/w of 14% w/w 12-HSA/PG organogels. Each value represents the mean ± SD (n=4). Statistical analysis was done using one way ANOVA with Tukey's post hoc test since the significant value is (p< 0.05).

Gemcitabine C14 %w/w	G′ x 10^4 (Pa)	G″ x 10^3 (Pa)	LVER (%)	Flow point (%)
0	95.8500±27.7206 •*	70.625±18.136	0.43±0.09	3.27±1.14
0.1	61.1750±19.0242	44.575 ±8.389	0.25±0.13	2.82 ±0.82
0.3	54.9750±13.4336	42.550±8.893	0.25±0.05	4.63±1.12
0.5	35.2250±13.3809	29.850 ±9.567	0.18±0.09 Δ	3.44 ±0.31

• and * indicates a significant higher G′ of organogel without drug ($p < 0.05$) and ($p < 0.01$) in comparison to 0.5% w/w and 0.3% w/w of gemcitabine C14 in14% w/w 12-HSA/PG respectively.

Δ represents a significant higher LVER of organogel without drug ($p > 0.05$) in comparison to 0.5% w/w gemcitabine C14 in 14% w/w 12-HSA/PG.

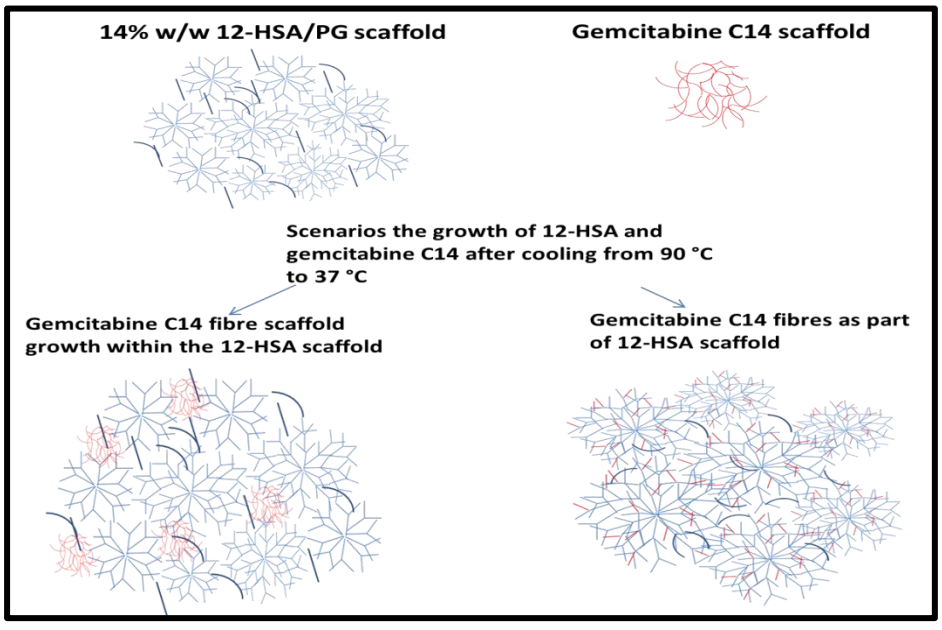

Figure 4-20: Cartoon schematic shows the scenarios of the growth of 12-HSA and gemcitabine C14 scaffolds after cooling from 90 °C to 37 °C.

4.1.2.3.6 Release study

The release study was executed to examine the ability of the selected organogel (14% w/w 12-HSA/PG) to meet our goal of formulating an organogel that can be localised in the tumour and control the release of gemcitabine C14. 14% w/w 12-HSA/PG organogel showed the ability to be sheared through a syringe and 21 gauge needle and reform as shown in Figure 4-21 A and B.

Sample and separate methodology was used for the drug release study to investigate the *in vitro* release gemcitabine C14 from 14% w/w 12-HSA/PG organogel. The description and use of this method is described previously in this chapter (see section **4.1.1.3.6**).

This study was carried out with 0.5% and 0.3% w/w gemcitabine C14 in the organogel. The release study was conducted 6 days after the preparation of the organogels containing 0.5% and 0.3% w/w of gemcitabine C14 to allow for the changes in the scaffold structure to occur. The controls i.e. organogels with only 0.5% and 0.3% w/w gemcitabine C14 in PG were also evaluated as shown in Figure 4-22 in buffer.

Figure 4-22 showed that the 14% w/w 12-HSA/PG was controlling the gemcitabine C14 release, where the cumulative percentage released from the organogel containing 0.3% w/w of gemcitabine C14 was 1.34%, 2.64% and 4.13% after 3 hours, day 1 and day 2 respectively and where the cumulative percentage released from the organogels containing 0.5% w/w of gemcitabine C14 was: 0.81%, 1.6% and 2.5% after 3 hours, day 1 and day 2 respectively. Whilst the organogels with no 12-HSA, the cumulative percentage released from 0.3% w/w gemcitabine C14 in PG was 5.27%, 45.42% and 73.47% and the cumulative percentage released from 0.5% w/w gemcitabine C14 in PG was 4.15%, 12.18% and 73.9% after 3 hours, day 1 and day 2

respectively. These data revealed that the 14% w/w 12-HSA/PG controlled the release of gemcitabineC14 and gave an almost constant release per day in comparison to the fast release from the control organogels (no 12-HSA). Clearly shown in Figure 4-23A is the daily release of gemcitabine C14 for 30 days which was almost a constant value and the same for both concentrations of drug and this could be attributed to the internal structure of 14% w/w 12-HSA/PG scaffold which led to a constant release.

Moreover, Figure 4-23B shows the cumulative percentage gemcitabine C14 released. The release of gemcitabine C14 represents 40% and 26% of the initial loaded in the organogel containing 0.3% and 0.5% w/w respectively. The remaining organogel was analysed and the mass balance was calculated as shown in Table 4-9.

In conclusion, the selected organogel slowed the release of gemcitabine C14 when it was followed for 30 days and where the control organogel (without 12-HSA) released the drug within 2 days.

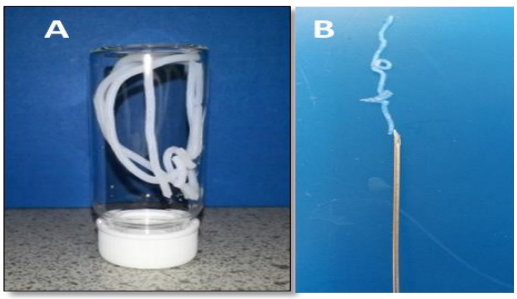

Figure 4-21: A: 14% w/w 12-HSA/PG organogel shared by syringe. B: 14% w/w 12-HSA/PG organogel sheared by 21 gauge needle and syringe.

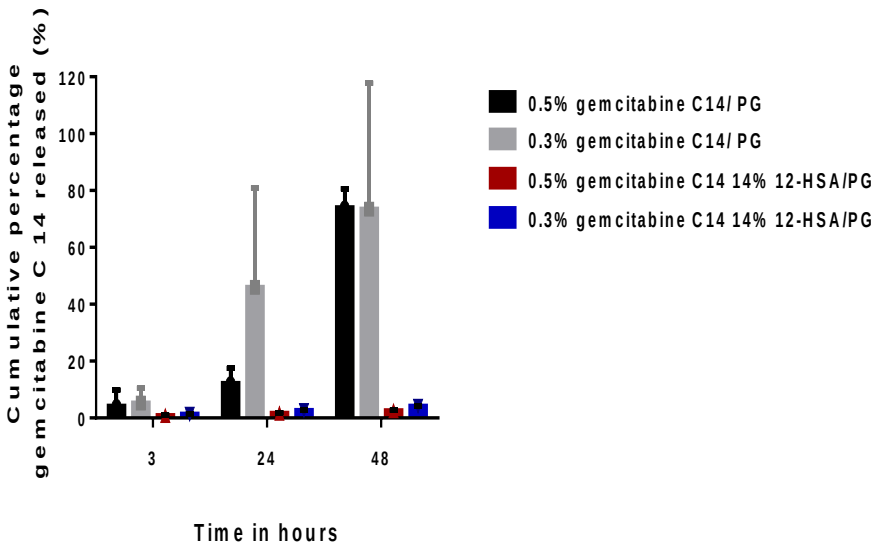

Figure 4-22: The drug release of 0.3% and 0.5% w/w gemcitabine C14 in 14% w/w 12-HSA/PG organogels and the control gels (without 12-HSA) 0.3 and 0.5% w/w gemcitabine C14 in PG where the release medium is 0.01M of Na phosphate buffer pH 6.8 with 0.1% w/v SDS where each value represents the mean ± SD (n=3).

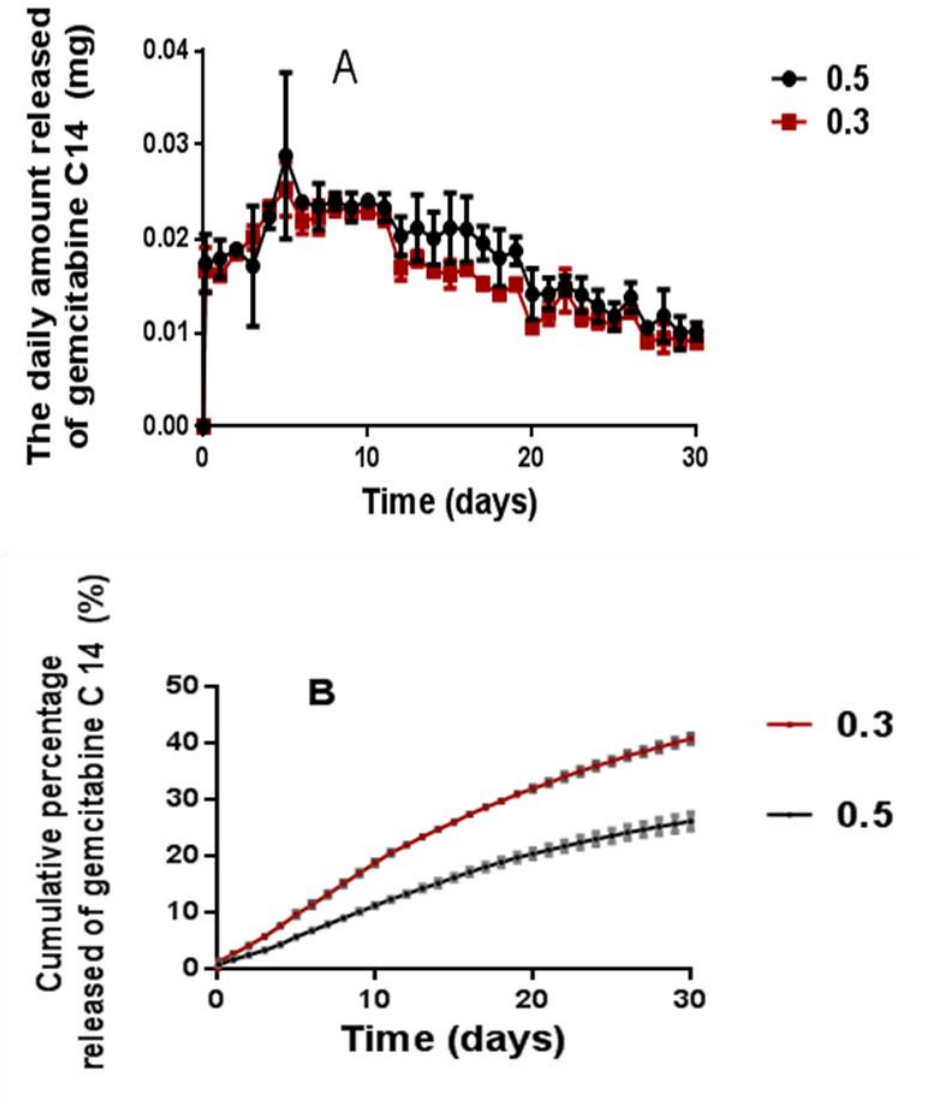

Figure 4-23: A- The daily amount released from different concentrations % w/w of gemcitabine C14 in 14% w/w 12-HSA/PG organogels. B- The cumulative percentage gemcitabine C14 released from different concentrations % w/w of gemcitabine C14 in14% w/w 12-HSA/PG organogel where release medium is 0.01M of Na phosphate buffer pH 6.8 with 0.1% w/v SDS where each value represents the mean ± SD (n=3).

Table 4-9: Details of the total amount released, initial drug loading, amount remaining in the organogels and the percentage recovery of 0.3% and 0.5 % w/w gemcitabine C14 in 14% w/w 12-HSA/PG organogels.

Gemcitabine C14 concentration % w/w	Total amount of gemcitabine C14 release (mg)	Initial drug loading of gemcitabine C14 (mg)	Amount remaining of gemcitabine C14 (mg)	Percentage recovery (%)
0.3	0.50 ± 0.01	1.24 ±0.08	0.78 ± 0.15	103%
0.5	0.56 ± 0.03	2.14 ± 0.11	1.51 ± 0.06	96.7%

4.1.2.3.7 Analysis of *in vitro* release kinetics

The release data of 0.5% and 0.3% gemcitabine C14 from 14% w/w 12-HSA/PG were fitted to Korsemeyer-peppas model and were highly correlated to the Korsemeyer-peppas equation as shown in Table 4-10. The n exponent values for both concentrations were 0.741 and 0.723 which indicates an anomalous diffusion. These release kinetics are similar to that of gemcitabine C14 release from 5% w/w 12-HSA/MCT organogels as also determined using the sample and separate method. The drug release is a combination of diffusion and erosion as discussed in **4.1.1.3.7** and was due to the changing of the total volume of release medium daily that aided the solubilisation of 12-HSA by SDS in the release medium. Also, this led to more solubilised gemcitabine C14 in the release medium.

Table 4-10: Korsemeyer-peppas model parameters for the release of gemcitabine C14 from the 14% 12-HSA/PG organogel.

Gemcitabine C14 % w/w	Korsemeyer-peppas R^2	n exponent
0.5	0.965	0.741
0.3	0.968	0.723

4.1.2.3.8 Release of propylene glycol

Since PG is highly miscible with aqueous environments. PG could be predicted to leave the organogel and leave behind a 12-HSA scaffold when the organogel is placed in buffer for *in vitro* release studies and most importantly when injected *in vivo*. Hence the release of PG was studied by FTIR 6 days after organogel preparation. This release was quantified by using a calibration curve where the ratios of intensities of two peaks in the spectra at 1040 cm^{-1} and 3258 cm^{-1} were plotted against PG concentration in buffer. This plot gave a straight line with a high correlation value (R^2) 0.9994 as shown in Figure 4-24A. The organogels of 14% w/w 12-HSA/PG and the loaded organogel with 0.5% w/w gemcitabine C14 were selected for the release study. As shown in Figure 4-24B, most of PG was released after 30 minutes from 14% w/w 12-HSA/PG and the organogel contained 0.5% w/w gemcitabine C14 showed most of PG release within 2 hours. This longer time (2 hours) of PG released might be due to the presence of a gemcitabine C14 scaffold or a combined scaffold of 12-HSA and gemcitabine C14.

In summary, regardless of the PG leaving in 30 minutes and 2 hours from the 14% w/w 12-HSA/PG without drug and with drug respectively, the 14% w/w 12-HSA in PG organogel controlled release of gemcitabine C14.

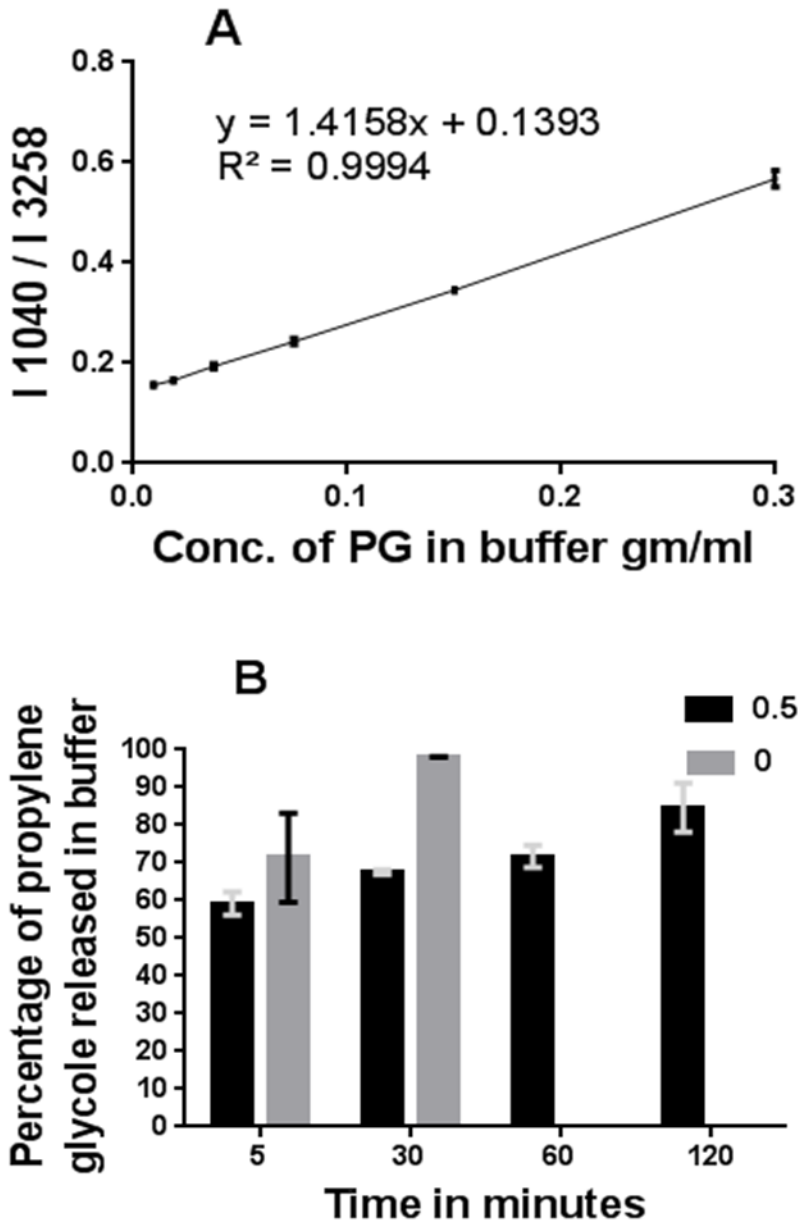

Figure 4-24: A-Calibration curve of different concentrations of PG in buffer (n=3). B- represents release of PG from 14% w/w 12-HSA with and without 0.5% w/w gemcitabine C14 6 days after organogel preparation (n=3 ± SD) where release medium is 0.01M of Na phosphate buffer pH 6.8.

4.1.2.3.9 *In vitro* simulation

An *in vitro* study was needed to simulate injection *in vivo* i.e. the ability of the selected organogel to stay solid after injection into the tumour. The organogel with rhodamin B incorporated was pushed into a hole in a piece of chicken breast. After sectioning of the tissue, the organogel showed as an intact gel as shown in Figure 4-25. This organogel could be sheared and reformed once the stress was removed. This reforming to the initial structure of the scaffold was observed for N4-octanoyl-2′-deoxycytidine hydrogel after applying a high strain value of 500% in time dependant recovery test [214].

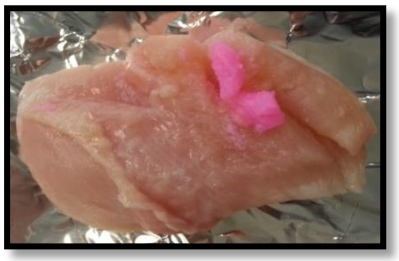

Figure 4-25: Sectioned chicken breast tissue containing the 14% w/w 12-HSA/PG organogel with rhodamine B.

4.1.2.4 Conclusions

The 14% w/w 12-HSA/PG organogel achieved the aim of our work which was a depot to be injected into the tumour and control the release of gemcitabine C14 for 30 days. In addition, this organogel was thermally stable after addition of different concentrations of gemcitabine C14 but showed a decrease in G′ and LVER values after addition of different concentrations of gemcitabine C14. The decrease in mechanical strength and controlled release of gemcitabine C14 suggests a combined gemcitabine C14 and 12-HSA scaffold or that the gemcitabine C14 fibre scaffold affects the interactions in the 12-HSA scaffold.

Chapter five

Conclusion and future work

5. Conclusion and future work

5.1 General conclusion

The importance of localised delivery of chemotherapeutic drugs for cancer treatment and specifically solid tumours has been widely reported. This approach increases the bioavailability of the anticancer drugs in the tumour and decreases the systemic side effects associated with i.v dosing. In this study, the anticancer drug *N*4-myristoyl gemccitabine (a lipophilic derivative of gemcitabine) was formulated as organogel to achieve localised delivery. Thus, the aim of these studies was to examine and assess the best organogels for delivering the anticancer drug, where this study was motivated by two main research questions. Firstly, if the prepared oragnogels were suitable for the intra-tumoural injection and the second question was whether the selected organogels slowed down the release of the anticancer drug. These two characteristics were to ensure the direct contact of the organogel containing the *N*4-myristoyl gemcitabine with the cancerous cells achieving better efficacy. The studies focused on 12-hydroxystearic acid (12-HSA) as the gelator and using 2 types of solvents as the liquid part of the organogel. The first type of solvent was a series of oils (soybean oil (SO), medium chain triglyceride (MCT), glyceryl tributyrate (TGB) and glyceryl triacetate (GTA)) whilst, the second type of solvent was propylene glycol (PG). To date, no research has studied 12-HSA as the gelator part of the organogel with the SO, MCT, TGB, GTA and PG as the liquid part of organogels for intratumoural delivery.

We conducted many studies on the selected range of 0.5% to 5% w/w 12-HSA in different oils such as table top rheology and DSC to screen thermal stability. Also, the morphology was evaluated by optical

microscopy and the interactions of gelator and solvent at the molecular level were studied by ATR-FTIR. To test the mechanical strength of the organogels, amplitude sweep, frequency sweep, time dependant recovery and creep and recovery tests were executed to differentiate between the organogels. The best organogels were the 5% w/w 12-HSA in SO and MCT due to their highest thermal stability, denser scaffolds, thixotropic behaviour and were the least compliant compared to the other concentrations. The same experiments were utilised to evaluate the selected range of 0.5% to 14% w/w 12-HSA in PG. 14% w/w 12-HSA in PG was selected again due to its higher thermal stability, thixotropic behaviour and was less compliant compared to other concentrations of 12-HSA in PG.

The following paragraphs will present a comparison between the selected organogels of 5% w/w 12-HSA in SO and MCT (Chapter 2) and 14% w/w 12-HSA in PG (Chapter 3) according to the goals mentioned above.

Table top rheology and DSC were carried out to investigate the first goal, the thermal stability by monitoring solution to gel and gel to solution transitions temperatures of the organogels. Herein Focusing on solidifying temperatures in DSC, the solution to gel transition temperatures for 5% w/w 12-HSA in MCT or SO were 46.4 °C ± 0.5 and 57.6 °C ± 1 respectively and the transition temperature for 14% w/w in PG was 19.31 °C ± 3.06. This in fact means that the 5% w/w of 12-HSA was enough to gel MCT and SO at high temperatures whilst PG needed larger amounts of 14% w/w of 12-HSA and at a lower temperature to be solidified. To conclude, 5% w/w 12-HSA in oils are more thermally stable than 14% w/w 12-HSA/PG.

The second goal in this work was the strength or the elasticity of the organogel and this was evaluated by amplitude sweep, frequency sweep

and creep and recovery test but only time dependent recovery test could be used to discriminate between the organogels in oils and the organogels in PG. This test showed higher instantaneous recoveries of 89.44% and 85.06% for 5% w/w of 12-HSA in MCT and SO respectively as compared to the 66% for 14% w/w 12-HSA/PG. This indicates that the transient junctions are reconnected quicker in 5% 12-HSA in oils than in 14% w/w 12-HSA in PG.

In summary, the outcome of this comparison according to the thermal aspect and the mechanical strength would lead us to choose 5% w/w 12-HSA in oils as the superior organogel. We will now describe and compare the drug release from the selected organogels as described in in detail in Chapter 4.

*N*4-myristoyl gemcitabine was added to the selected organogels and the effect of the addition evaluated for 3 different concentrations (0.1%, 0.3% and 0.5% w/w). DSC was used to investigate any changes in the thermal stability and the morphology of the scaffold was explored by optical microscopy. Additionally, amplitude sweep testing was carried out to evaluate any changes in the strength of the organogels.

The *N*4-myristoyl gemcitabine did not alter the 5% w/w 12-HSA/MCT in term of its thermal or mechanical strength; whilst it did not modify the 14% w/w 12-HSA in PG thermally, and showed a decrease in the storage modulus. Additionally, 5% w/w 12-HSA/MCT and 14% w/w 12-HSA in PG organogels were capable of being injected through a 25 gauge needle and forming an in-situ depot.

Drug release from the organogels was then carried out. The cumulative percentage released from 0.5% and 0.3% w/w *N*4-myristoyl gemcitabine in 5% w/w 12-HSA/MCT organogels as a solid organogel was 18.95% and 26.62% after 30 days whilst for the organogel

liquefied with N-methyl pyrrolidone (NMP), the cumulative percentage released was 35.02% and 34.37% within the same frame time. Further to this, a sample and separate release method was used to study the liquefied form of the 5% w/w 12-HSA/MCT. Also, this method revealed that the 5% w/w 12-HSA/MCT organogels gave a slow release of *N*4-myristoyl gemcitabine and 56.18% and 70.07% was released from the 0.5% and 0.3% w/w selected organogels respectively within 30 days.

For the 14% w/w 12-HSA in PG evaluated using the sample and separate method, the cumulative percentage released for 0.5% and 0.3% w/w *N*4-myristoyl gemcitabine in 14% w/w 12-HSA/PG organogels was 26% and 40% respectively after 30 days.

The last step in this work was the simulation in vitro of injection into the solid tumour or tumour resection site using chicken breast. After injection into the chicken breast, all selected organogel appeared to be elastic solids.

To conclude, our selected organogels (5% w/w 12-HSA/MCT and 14% w/w 12-HSA/PG) met the goal of our work firstly, by showing the strength and the elasticity to be injected. Secondly, they were able to slow down the release of *N*4-myristoyl gemcitabine.

5.2 Future work

The results of chapter 2 and 4 were a platform for an *in vivo* study for 5% w/w 12-HSA/MCT organogel. The preparative work for *in vivo* should be studied in advance such as preparing calibration curve of the selected dye DiD in the buffer where DiD is the suitable dye to incorporated in the organogel. DiD (1,1-dioctadecyl-3,3,3`,3`-tetramethylindodicarbocyanine perchlorate) has been selected due to its lipophilicity which helps incorporation and ability to be solubilised in the oils [215]. Indeed Hirsjärvi *et al* have used DiD to investigate lipid nanocapsules and lipid nanoemulsion performance in mice by fluorescent imaging [216]. Calibration curve of DiD in the buffer will help to study the release of the dye in buffer to check if this dye immigrates outside the oganogel. Where part of the future work is to inject the 5% w/w 12-HSA/MCT organogel incorporated with DiD into a subcutaneous xenograft model. This experiment will give an idea about the performance of the selected organogel into the tumour and whether it will stay intact or not. The plan for these experiments is firstly to grow the tumours from HCT116 cells and by implanting them subcutaneously into the left flank of each mouse. The mice will then be divided into 2 groups where the first group of mice includes cored tumours to be injected by syringe with the selected organogel. For the second group of mice tumours will be injected directly with the selected organogel with a 25 gauge needle and syringe. These organogels in the tumours will be monitored by imaging via a fluorescent signal using IVIS spectrum for: 3 hours, 24 hours 72 hours then weekly for 30 days. Also, tumours will be subjected to histological analysis to study the effect of the selected organogel on the tumour tissue. The liquefied form of the organogel by NMP as a way of delivery of the 5% w/w 12-HSA/MCT was excluded from this study due to the photobleaching of DiD dye by NMP.

The organogel should be sterilised before injection in the tumour. Indeed, the organogel was already heated to 90 °C as mentioned in the preparation method as explained in **4.1.1.2.1.** This should be tested whether 90 °C is enough to sterilise the organogel or not, otherwise a suitable sterilisation method should follow the oragnogel preparation or before the preparation to investigate the free of organogel from living microorganism.

Also, stability study should be applied by following the selected oragnogel with time by ATR-TIR to study the changes in the hydrogen bonding between carbonyl and hydroxyl groups. Stability could be set by DSC via studying the changes in transition temperatures that could be happened.

Many experiments could have been carried out in chapter 4 for the selected organogel 14% w/w 12-HSA/PG but were restricted due to time limitation; for example a release study using a lower concentrations of 12-HSA.

An efficacy study could be carried out for the selected organogels in oil and in PG by injecting intratumourally the selected organogel with and without gemcitabine C14 to study the tumour size and the time frame that lead to reduction in tumour size. Parallel to this, a group of tumours that contained organogels could be subjected to the histology analysis to examine the effect of the selected organogel on the tumour tissue.

Appendix

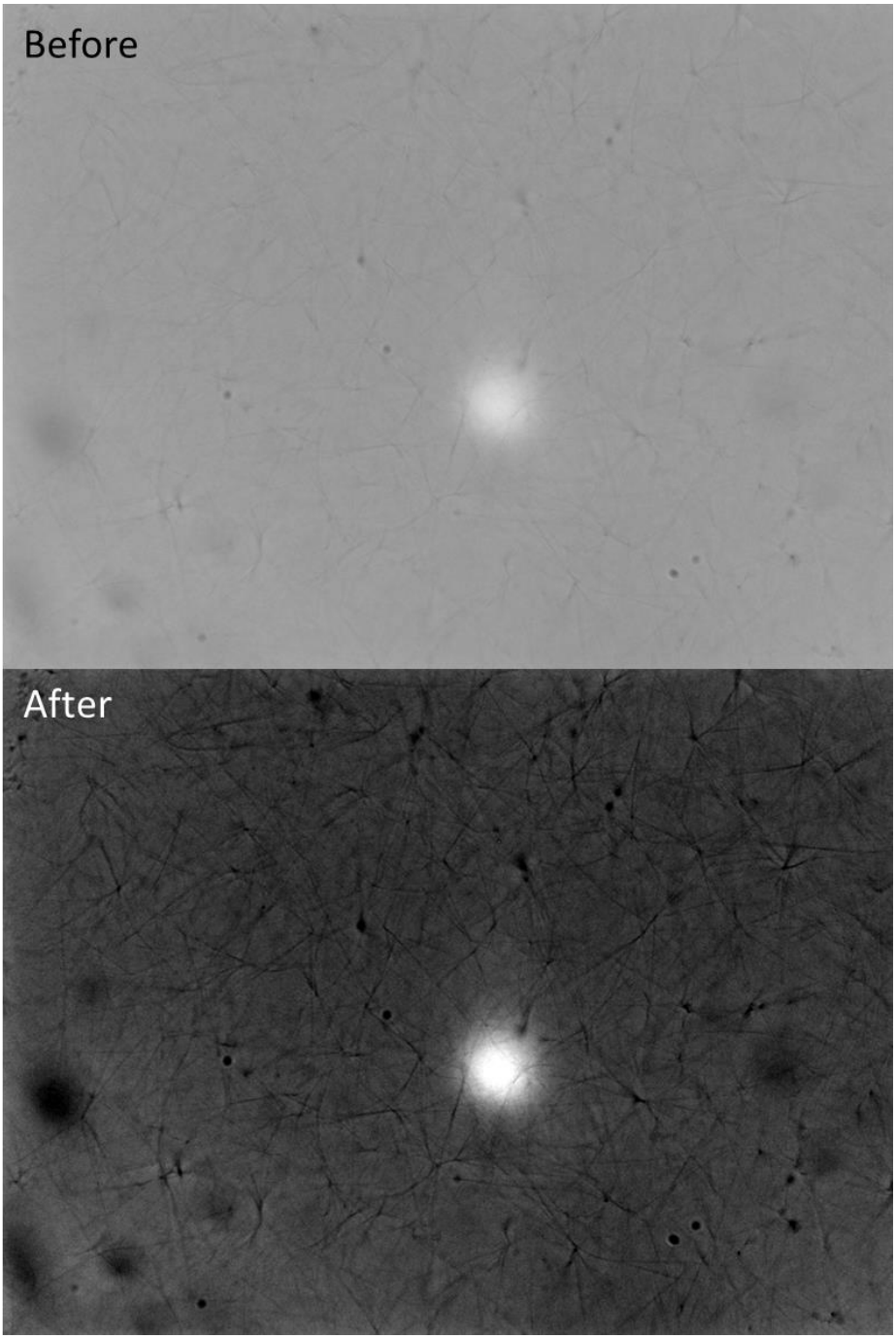

Figure A- 1: The image (G) 3% w/w 12-HSA/MCT was processed with PhotoShop 3 to obtain better contrast by selecting image option then auto contrast option.

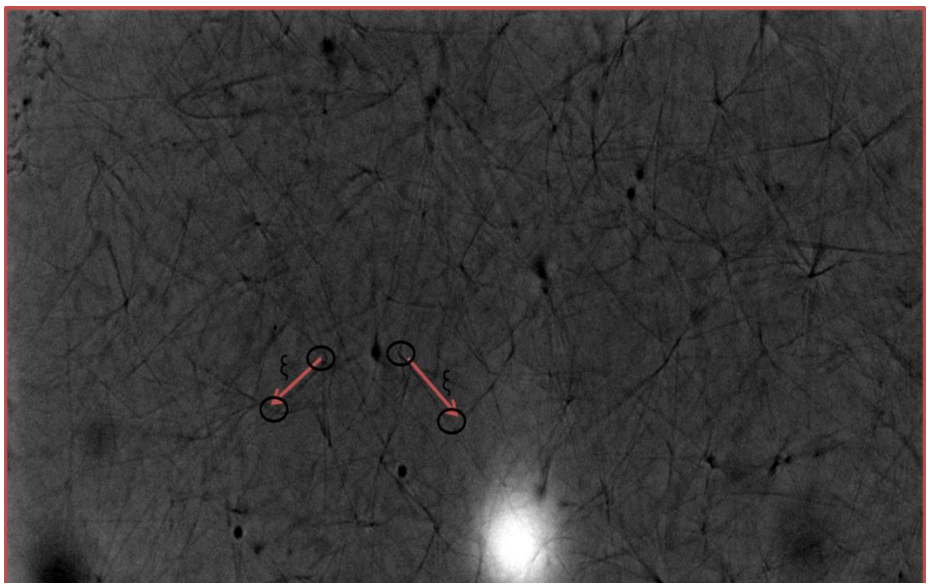

Figure A- 2: The black circles show the points of fiber branching and the arrows that connect between 2 circles to measure the correlation length ξ in the image of 3% w/w 12-HSA/MCT.

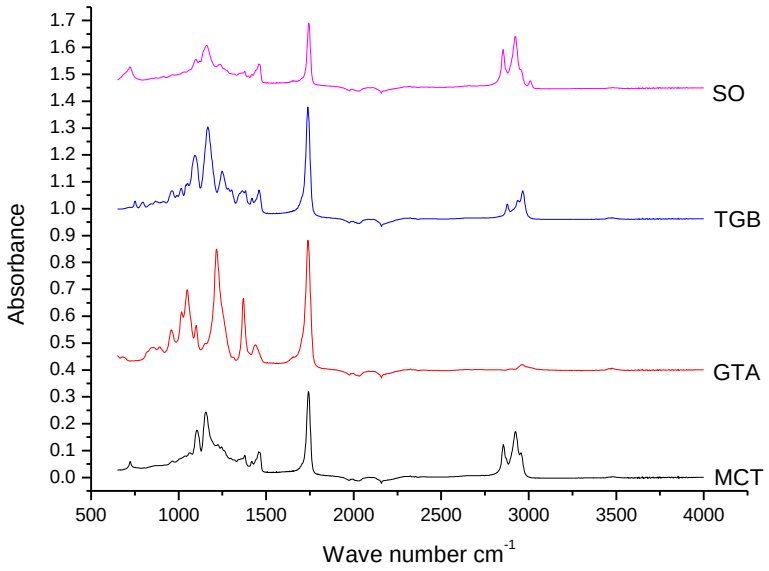

Figure A- 3: The FTIR spectra of oils SO, TGB, GTA and MCT.

References

1. Jemal, A., F. Bray, M.M. Center, J. Ferlay, E. Ward, and D. Forman, *Global cancer statistics.* CA: a cancer journal for clinicians, 2011. **61**(2): p. 69-90.
2. Gavhane, Y., A. Shete, A. Bhagat, V. Shinde, K. Bhong, G. Khairnar, and A. Yadav, *Solid tumors: facts, challenges and solutions.* International Journal of Pharma Sciences and Research, 2011. **2**(1): p. 1-12.
3. Giacchetti, S., M. Itzhaki, G. Gruia, R. Adam, R. Zidani, F. Kunstlinger, S. Brienza, E. Alafaci, F. Bertheault-Cvitkovic, and C. Jasmin, *Long-term survival of patients with unresectable colorectal cancer liver metastases following infusional chemotherapy with 5-fluorouracil, leucovorin, oxaliplatin and surgery.* Annals of Oncology, 1999. **10**(6): p. 663-669.
4. Jain, R.K., *Normalization of tumor vasculature: an emerging concept in antiangiogenic therapy.* Science, 2005. **307**(5706): p. 58-62.
5. Yasuda, H., *Solid tumor physiology and hypoxia-induced chemo/radio-resistance: novel strategy for cancer therapy: nitric oxide donor as a therapeutic enhancer.* Nitric Oxide, 2008. **19**(2): p. 205-216.
6. Minchinton, A.I. and I.F. Tannock, *Drug penetration in solid tumours.* Nature Reviews Cancer, 2006. **6**(8): p. 583-592.
7. Wolinsky, J.B., Y.L. Colson, and M.W. Grinstaff, *Local drug delivery strategies for cancer treatment: gels, nanoparticles, polymeric films, rods, and wafers.* Journal of controlled release, 2012. **159**(1): p. 14-26.
8. Hertel, L.W., G.B. Boder, J.S. Kroin, S.M. Rinzel, G.A. Poore, G.C. Todd, and G.B. Grindey, *Evaluation of the antitumor activity of gemcitabine (2', 2'-difluoro-2'-deoxycytidine).* Cancer research, 1990. **50**(14): p. 4417-4422.
9. S Gesto, D., N. MFSA Cerqueira, P. A Fernandes, and M. J Ramos, *Gemcitabine: a critical nucleoside for cancer therapy.* Current medicinal chemistry, 2012. **19**(7): p. 1076-1087.
10. Spratlin, J., R. Sangha, D. Glubrecht, L. Dabbagh, J.D. Young, C. Dumontet, C. Cass, R. Lai, and J.R. Mackey, *The absence of human equilibrative nucleoside transporter 1 is associated with reduced survival in patients with gemcitabine-treated pancreas adenocarcinoma.* Clinical Cancer Research, 2004. **10**(20): p. 6956-6961.
11. Mini, E., S. Nobili, B. Caciagli, I. Landini, and T. Mazzei, *Cellular pharmacology of gemcitabine.* Annals of Oncology, 2006. **17**(suppl 5): p. v7-v12.

12. Judith A. Gilbert, O.E.S., Yuan Ji,Linda L. Pelleymounter,Bruce W.Eckloff, Eric D. Wieben,MatthewM. Ames,and RichardM. Weinshilboum, *Gemcitabine Pharmacogenomics: Cytidine Deaminase and Deoxycytidylate Deaminase Gene Resequencing and Functional Genomics.* Clin Cancer Res, 2006. **12**(6): p. 1794-1803.
13. Immordino, M.L., P. Brusa, F. Rocco, S. Arpicco, M. Ceruti, and L. Cattel, *Preparation, characterization, cytotoxicity and pharmacokinetics of liposomes containing lipophilic gemcitabine prodrugs.* Journal of Controlled Release, 2004. **100**(3): p. 331-346.
14. Michelle A.Clark, R.F., Jose A. Rey, Karen Whalen, *Lippincott's Illustrated reviews:pharmacology*, ed. R.A. Harvey. 2012.
15. Bouffard, D.Y., J. Laliberté, and R.L. Momparler, *Kinetic studies on 2', 2'-difluorodeoxycytidine (Gemcitabine) with purified human deoxycytidine kinase and cytidine deaminase.* Biochemical pharmacology, 1993. **45**(9): p. 1857-1861.
16. Paulson, A.S., H.S. Tran Cao, M.A. Tempero, and A.M. Lowy, *Therapeutic advances in pancreatic cancer.* Gastroenterology, 2013. **144**(6): p. 1316-1326.
17. Hilbig, A. and H. Oettle, *Gemcitabine in the treatment of metastatic pancreatic cancer.* Expert review of anticancer therapy, 2008. **8**(4): p. 511-523.
18. El Maalouf, G., C. Le Tourneau, G.N. Batty, S. Faivre, and E. Raymond, *Markers involved in resistance to cytotoxics and targeted therapeutics in pancreatic cancer.* Cancer Treat Rev, 2009. **35**(2): p. 167-74.
19. Soonmo Peter Kang1, M.W.S., *Three-Drug Combination Regimen in Pancreatic Cancer Treatment: Are We There Yet?* Journal of the Pancreas, 2011. **12**(2): p. 78-82.
20. Faivre, S., E. Raymond, J.M. Woynarowski, and E. Cvitkovic, *Supraadditive effect of 2', 2'-difluorodeoxycytidine (gemcitabine) in combination with oxaliplatin in human cancer cell lines.* Cancer chemotherapy and pharmacology, 1999. **44**(2): p. 117-123.
21. Kawakami, H., I. Okamoto, W. Okamoto, M. Takeda, S. Ueda, T. Kudo, S.-i. Nishina, Y. Fujisaka, M. Miyazaki, and J. Tsurutani, *Practical Use of Gemcitabine and Cisplatin Combination Therapy as First-Line Treatment for Japanese Patients with Advanced Biliary Tract Cancer.* Journal of Cancer Therapy, 2013. **4**(06): p. 1068-1073.
22. Narunsky, L., R. Oren, F. Bochner, and M. Neeman, *Imaging aspects of the tumor stroma with therapeutic implications.* Pharmacol Ther, 2014. **141**(2): p. 192-208.
23. Wang, Z., Y. Li, D. Kong, S. Banerjee, A. Ahmad, A.S. Azmi, S. Ali, J.L. Abbruzzese, G.E. Gallick, and F.H. Sarkar, *Acquisition of epithelial-mesenchymal transition phenotype of gemcitabine-resistant pancreatic cancer cells is linked with activation of the notch signaling pathway.* Cancer Res, 2009. **69**(6): p. 2400-2407.

24. Hung, S.W., H.R. Mody, and R. Govindarajan, *Overcoming nucleoside analog chemoresistance of pancreatic cancer: a therapeutic challenge.* Cancer letters, 2012. **320**(2): p. 138-149.
25. Tsume, Y., T. Incecayir, X. Song, J.M. Hilfinger, and G.L. Amidon, *The development of orally administrable gemcitabine prodrugs with D-enantiomer amino acids: Enhanced membrane permeability and enzymatic stability.* European Journal of Pharmaceutics and Biopharmaceutics, 2014. **86**(3): p. 514-523.
26. Stella, B., S. Arpicco, F. Rocco, V. Marsaud, J.M. Renoir, L. Cattel, and P. Couvreur, *Encapsulation of gemcitabine lipophilic derivatives into polycyanoacrylate nanospheres and nanocapsules.* Int J Pharm, 2007. **344**(1-2): p. 71-77.
27. Castelli, F., M.G. Sarpietro, F. Rocco, M. Ceruti, and L. Cattel, *Interaction of lipophilic gemcitabine prodrugs with biomembrane models studied by Langmuir-Blodgett technique.* J Colloid Interface Sci, 2007. **313**(1): p. 363-368.
28. Moysan, E., Y. González-Fernández, N. Lautram, J. Béjaud, G. Bastiat, and J.-P. Benoit, *An innovative hydrogel of gemcitabine-loaded lipid nanocapsules: when the drug is a key player of the nanomedicine structure.* Soft Matter, 2014. **10**(11): p. 1767-1777.
29. Pili, B., C. Bourgaux, H. Amenitsch, G. Keller, S. Lepetre-Mouelhi, D. Desmaele, P. Couvreur, and M. Ollivon, *Interaction of a new anticancer prodrug, gemcitabine-squalene, with a model membrane: coupled DSC and XRD study.* Biochim Biophys Acta, 2010. **1798**(8): p. 1522-32.
30. Wickremsinhe, E.R., L.B. Lee, C.A. Schmalz, J. Torchia, and K.J. Ruterbories, *High sensitive assay employing column switching chromatography to enable simultaneous quantification of an amide prodrug of gemcitabine (LY2334737), gemcitabine, and its metabolite dFdU in human plasma by LC–MS/MS.* Journal of Chromatography B, 2013. **932**: p. 117-122.
31. Wickremsinhe, E., J. Bao, R. Smith, R. Burton, S. Dow, and E. Perkins, *Preclinical absorption, distribution, metabolism, and excretion of an oral amide prodrug of gemcitabine designed to deliver prolonged systemic exposure.* Pharmaceutics, 2013. **5**(2): p. 261-276.
32. Scharovsky, O.G., L.E. Mainetti, and V.R. Rozados, *Metronomic chemotherapy: changing the paradigm that more is better.* Current oncology, 2009. **16**(2): p. 7-15.
33. Gianfranco Pasut , F.C., Lisa Dalla Via , Silvia Arpicco ,Francesco M. Veronese , Oddone Schiavon *Antitumoral activity of PEG–gemcitabine prodrugs targeted by folic acid.* Journal of Controlled Release, 2008. **127** p. 239–248.
34. Choi, H.S., W. Liu, F. Liu, K. Nasr, P. Misra, M.G. Bawendi, and J.V. Frangioni, *Design considerations for tumour-targeted nanoparticles.* Nature nanotechnology, 2010. **5**(1): p. 42-47.

35. Ohara, Y., T. Oda, K. Yamada, S. Hashimoto, Y. Akashi, R. Miyamoto, A. Kobayashi, K. Fukunaga, R. Sasaki, and N. Ohkohchi, *Effective delivery of chemotherapeutic nanoparticles by depleting host Kupffer cells.* International journal of cancer, 2012. **131**(10): p. 2402-2410.
36. Gullotti, E. and Y. Yeo, *Extracellularly activated nanocarriers: a new paradigm of tumor targeted drug delivery.* Molecular pharmaceutics, 2009. **6**(4): p. 1041-1051.
37. Kaminskas, L.M., V.M. McLeod, C.J. Porter, and B.J. Boyd, *Association of chemotherapeutic drugs with dendrimer nanocarriers: an assessment of the merits of covalent conjugation compared to noncovalent encapsulation.* Molecular pharmaceutics, 2012. **9**(3): p. 355-373.
38. Zwicke, G.L., G.A. Mansoori, and C.J. Jeffery, *Utilizing the folate receptor for active targeting of cancer nanotherapeutics.* Nano Reviews & Experiments, 2012. **3**: p. 1-11.
39. Kamaly, N., Z. Xiao, P.M. Valencia, A.F. Radovic-Moreno, and O.C. Farokhzad, *Targeted polymeric therapeutic nanoparticles: design, development and clinical translation.* Chemical Society Reviews, 2012. **41**(7): p. 2971-3010.
40. Kumar, R., I. Roy, T.Y. Ohulchanskky, L.A. Vathy, E.J. Bergey, M. Sajjad, and P.N. Prasad, *In vivo biodistribution and clearance studies using multimodal ORMOSIL nanoparticles.* ACS nano, 2010. **4**(2): p. 699-708.
41. Hwang, H.-Y., I.-S. Kim, I.C. Kwon, and Y.-H. Kim, *Tumor targetability and antitumor effect of docetaxel-loaded hydrophobically modified glycol chitosan nanoparticles.* Journal of Controlled Release, 2008. **128**(1): p. 23-31.
42. Qin, X., Z. Guo, Z. Liu, W. Zhang, M. Wan, and B. Yang, *Folic acid-conjugated graphene oxide for cancer targeted chemo-photothermal therapy.* Journal of photochemistry and photobiology B: Biology, 2013. **120**: p. 156-162.
43. Bao, A., W.T. Phillips, B. Goins, X. Zheng, S. Sabour, M. Natarajan, F.R. Woolley, C. Zavaleta, and R.A. Otto, *Potential use of drug carried-liposomes for cancer therapy via direct intratumoral injection.* International journal of pharmaceutics, 2006. **316**(1): p. 162-169.
44. Slingerland, M., H.-J. Guchelaar, and H. Gelderblom, *Liposomal drug formulations in cancer therapy: 15 years along the road.* Drug discovery today, 2012. **17**(3): p. 160-166.
45. Khan, D.R., M.N. Webb, T.H. Cadotte, and M.N. Gavette, *Use of Targeted Liposome-based Chemotherapeutics to Treat Breast Cancer.* Breast cancer: basic and clinical research, 2015. **9**(Suppl 2): p. 1-5.
46. Koning, G.A., A.M. Eggermont, L.H. Lindner, and T.L. ten Hagen, *Hyperthermia and thermosensitive liposomes for improved delivery of chemotherapeutic drugs to solid tumors.* Pharmaceutical research, 2010. **27**(8): p. 1750-1754.

47. Bae, Y.H. and K. Park, *Targeted drug delivery to tumors: myths, reality and possibility.* Journal of Controlled Release, 2011. **153**(3): p. 198-205.
48. Jesse B. Wolinsky , Y.L.C., Mark W. Grinstaff, *Local drug delivery strategies for cancer treatment: Gels, nanoparticles, polymeric films, rods, and wafers.* Journal of Controlled Release, 2012. **159**: p. 14–26.
49. Solano, A.G.R., A. de Fátima Pereira, F.C.H. Pinto, L.G.R. Ferreira, L.A. de Oliveira Barbosa, S.L. Fialho, P.S. de Oliveira Patricio, A. da Silva Cunha Jr, G.R. da Silva, and G.A. Pianetti, *Development and Evaluation of Sustained-Release Etoposide-Loaded Poly (ε-Caprolactone) Implants.* AAPS PharmSciTech, 2013. **14**(2): p. 890-900.
50. Dang, W., T. Daviau, P. Ying, Y. Zhao, D. Nowotnik, C.S. Clow, B. Tyler, and H. Brem, *Effects of GLIADEL® wafer initial molecular weight on the erosion of wafer and release of BCNU.* Journal of Controlled Release, 1996. **42**(1): p. 83-92.
51. Liu, R., J.B. Wolinsky, J. Walpole, E. Southard, L.R. Chirieac, M.W. Grinstaff, and Y.L. Colson, *Prevention of local tumor recurrence following surgery using low-dose chemotherapeutic polymer films.* Annals of surgical oncology, 2010. **17**(4): p. 1203-1213.
52. Kim, S., Y. Liu, M.W. Gaber, J.D. Bumgardner, W.O. Haggard, and Y. Yang, *Development of chitosan–ellagic acid films as a local drug delivery system to induce apoptotic death of human melanoma cells.* Journal of Biomedical Materials Research Part B: Applied Biomaterials, 2009. **90**(1): p. 145-155.
53. Deurloo, M.J., S. Bohlken, W. Kop, C.F. Lerk, W. Hennink, H. Bartelink, and A.C. Begg, *Intratumoural administration of cisplatin in slow-release devices.* Cancer chemotherapy and pharmacology, 1990. **27**(2): p. 135-140.
54. Doiron, A., D.T. Yapp, M. Olivares, J.X. Zhu, and S. Lehnert, *Tumor radiosensitization by sustained intratumoral release of bromodeoxyuridine.* Cancer research, 1999. **59**(15): p. 3677-3681.
55. Ahmed, T.A., H.M. Ibrahim, A.M. Samy, A. Kaseem, M.T. Nutan, and M.D. Hussain, *Biodegradable injectable in situ implants and microparticles for sustained release of montelukast: in vitro release, pharmacokinetics, and stability.* AAPS PharmSciTech, 2014. **15**(3): p. 772-780.
56. Han, H.D., C.K. Song, Y.S. Park, K.H. Noh, J.H. Kim, T. Hwang, T.W. Kim, and B.C. Shin, *A chitosan hydrogel-based cancer drug delivery system exhibits synergistic antitumor effects by combining with a vaccinia viral vaccine.* International journal of pharmaceutics, 2008. **350**(1): p. 27-34.
57. Ruel-Gariépy, E., M. Shive, A. Bichara, M. Berrada, D. Le Garrec, A. Chenite, and J.-C. Leroux, *A thermosensitive chitosan-based hydrogel for the local delivery of paclitaxel.* European Journal of Pharmaceutics and Biopharmaceutics, 2004. **57**(1): p. 53-63.

58. Al-Abd, A.M., K.-Y. Hong, S.-C. Song, and H.-J. Kuh, *Pharmacokinetics of doxorubicin after intratumoral injection using a thermosensitive hydrogel in tumor-bearing mice.* Journal of Controlled Release, 2010. **142**(1): p. 101-107.
59. Konishi, M., Y. Tabata, M. Kariya, H. Hosseinkhani, A. Suzuki, K. Fukuhara, M. Mandai, K. Takakura, and S. Fujii, *In vivo anti-tumor effect of dual release of cisplatin and adriamycin from biodegradable gelatin hydrogel.* Journal of Controlled Release, 2005. **103**(1): p. 7-19.
60. Kim, J.H., J.H. Lee, K.S. Kim, K. Na, S.C. Song, J. Lee, and H.J. Kuh, *Intratumoral delivery of paclitaxel using a thermosensitive hydrogel in human tumor xenografts.* Arch Pharm Res, 2013. **36**(1): p. 94-101.
61. Ta, H.T., C.R. Dass, and D.E. Dunstan, *Injectable chitosan hydrogels for localised cancer therapy.* Journal of Controlled Release, 2008. **126**(3): p. 205-216.
62. Francois Plourde , A.M., Anne-Claude Couffin-Hoarau , Didier Hoarau , Huy Ong , Jean-Christophe Leroux, *First report on the efficacy of l-alanine-based in situ-forming implants for the long-term parenteral delivery of drugs.* Journal of Controlled Release, 2005. **108**: p. 433-441.
63. Bastiat, G., F. Plourde, A. Motulsky, A. Furtos, Y. Dumont, R. Quirion, G. Fuhrmann, and J.-C. Leroux, *Tyrosine-based rivastigmine-loaded organogels in the treatment of Alzheimer's disease.* Biomaterials, 2010. **31**(23): p. 6031-6038.
64. Wu, W., H. Chen, F. Shan, J. Zhou, X. Sun, L. Zhang, and T. Gong, *A novel doxorubicin-loaded in situ forming gel based high concentration of phospholipid for intratumoral drug delivery.* Molecular pharmaceutics, 2014. **11**(10): p. 3378-3385.
65. Gao, W., Y. Liang, X. Peng, Y. Hu, L. Zhang, H. Wu, and B. He, *In situ injection of phenylboronic acid based low molecular weight gels for efficient chemotherapy.* Biomaterials, 2016. **105**: p. 1-11.
66. Attenello, F.J., D. Mukherjee, G. Datoo, M.J. McGirt, E. Bohan, J.D. Weingart, A. Olivi, A. Quinones-Hinojosa, and H. Brem, *Use of Gliadel (BCNU) wafer in the surgical treatment of malignant glioma: a 10-year institutional experience.* Annals of Surgical Oncology, 2008. **15**(10): p. 2887-2893.
67. Kim, J.H., J.-H. Lee, K.-S. Kim, K. Na, S.-C. Song, J. Lee, and H.-J. Kuh, *Intratumoral delivery of paclitaxel using a thermosensitive hydrogel in human tumor xenografts.* Archives of pharmacal research, 2013. **36**(1): p. 94-101.
68. Aude Motulskya, M.L., Anne-Claude Couffin-Hoaraua, Didier Hoarauc, Frank Bouryd, Jean-Pierre Benoitd, Jean-Christophe Lerouxa,, *Characterization and biocompatibility of organogels based on L-alanine for parenteral drug delivery implants.* Biomaterials, 2005. **26**: p. 6242-6253.
69. Singh, V.K., K. Pal, D.K. Pradhan, and K. Pramanik, *Castor oil and sorbitan monopalmitate based organogel as a probable matrix for*

controlled drug delivery. Journal of Applied Polymer Science, 2013. **130**(3): p. 1503-1515.
70. Vintiloiu, A. and J.-C. Leroux, *Organogels and their use in drug delivery—a review.* Journal of Controlled Release, 2008. **125**(3): p. 179-192.
71. Garg, T., A. Bilandi, B. Kapoor, S. Kumar, and R. Joshi, *Organogels: advanced and novel drug delivery system.* International Research Journal of Pharmacy, 2011. **2**(12): p. 15-21.
72. Jadhav, N., K. Patil, J. Patil, P. Patil, and S. Pawar, *A REVIEW ON ORGANOGELS: LIPID BASED CARRIER SYSTEMS.* Pharma Science Monitor, 2012. **3**(4): p. 3132-3143.
73. Micheal A Rogers, A.J.W., Alejandro G. Marangoni, *crystalline stability of self-assembled fibrillar networks of 12- hydroxystearic acid in edible oils.* food research international, 2008. **41**: p. 1026-1034.
74. Hughes, N.E., A.G. Marangoni, A.J. Wright, M.A. Rogers, and J.W.E. Rush, *Potential food applications of edible oil organogels.* Trends in Food Science & Technology, 2009. **20**(10): p. 470-480.
75. Basak, S., J. Nanda, and A. Banerjee, *A new aromatic amino acid based organogel for oil spill recovery.* Journal of Materials Chemistry, 2012. **22**(23): p. 11658-11664.
76. Stortz, T.A., A.K. Zetzl, S. Barbut, A. Cattaruzza, and A.G. Marangoni, *Edible oleogels in food products to help maximize health benefits and improve nutritional profiles.* Lipid Technology, 2012. **24**(7): p. 151-154.
77. Dassanayake, L.S.K., D.R. Kodali, and S. Ueno, *Formation of oleogels based on edible lipid materials.* Current Opinion in Colloid & Interface Science, 2011. **16**(5): p. 432-439.
78. Morales, M., V. Gallardo, B. Clarés, M. García, and M. Ruiz, *Study and description of hydrogels and organogels as vehicles for cosmetic active ingredients.* Journal of cosmetic science, 2009. **60**(6): p. 627-636.
79. Raut, S., S.S. Bhadoriya, V. Uplanchiwar, V. Mishra, A. Gahane, and S.K. Jain, *Lecithin organogel: a unique micellar system for the delivery of bioactive agents in the treatment of skin aging.* Acta Pharmaceutica Sinica B, 2012. **2**(1): p. 8-15.
80. Aggeli, A., M. Bell, L.M. Carrick, C.W. Fishwick, R. Harding, P.J. Mawer, S.E. Radford, A.E. Strong, and N. Boden, *pH as a trigger of peptide β-sheet self-assembly and reversible switching between nematic and isotropic phases.* Journal of the American Chemical Society, 2003. **125**(32): p. 9619-9628.
81. Maitra, N.M.S.a.U., *Supramolecular gels: Functions and uses.* Chemical Society Reviews, 2005. **34**: p. 821-836.
82. Murdan, S., *Organogels in drug delivery.* Expert opinion on drug delivery, 2005. **2**(3): p. 489-505.

83. Wang, C., Z. Li, X. Wang, W. Wei, S. Chen, and Z. Sui, *Gelation mechanism and microstructure of organogels formed with L-Valine dihydrazide derivatives.* Colloids and Surfaces A: Physicochemical and Engineering Aspects, 2011. **384**(1): p. 490-495.
84. Liu, X.Y. and P.D. Sawant, *Mechanism of the formation of self-organized microstructures in soft functional materials.* Advanced Materials, 2002. **14**(6): p. 421-426.
85. Li, J.L. and X.Y. Liu, *Architecture of Supramolecular Soft Functional Materials: From Understanding to Micro-/Nanoscale Engineering.* Advanced functional materials, 2010. **20**(19): p. 3196-3216.
86. Xiong, J.-Y., X.-Y. Liu, J.-L. Li, and M.W. Vallon, *Architecture of macromolecular network of soft functional materials: from structure to function.* The Journal of Physical Chemistry B, 2007. **111**(20): p. 5558-5563.
87. Rogers, M.A. and A.G. Marangoni, *Non-isothermal nucleation and crystallization of 12-hydroxystearic acid in vegetable oils.* Crystal Growth and Design, 2008. **8**(12): p. 4596-4601.
88. Li, J.L., X.Y. Liu, C.S. Strom, and J.Y. Xiong, *Engineering of small molecule organogels by design of the nanometer structure of fiber networks.* Advanced materials, 2006. **18**(19): p. 2574-2578.
89. Liu, X.Y., P.D. Sawant, W.B. Tan, I. Noor, C. Pramesti, and B. Chen, *Creating new supramolecular materials by architecture of three-dimensional nanocrystal fiber networks.* Journal of the American Chemical Society, 2002. **124**(50): p. 15055-15063.
90. Yan, N., Z. Xu, K.K. Diehn, S.R. Raghavan, Y. Fang, and R.G. Weiss, *How do liquid mixtures solubilize insoluble gelators? Self-assembly properties of pyrenyl-linker-glucono gelators in tetrahydrofuran–water mixtures.* Journal of the American Chemical Society, 2013. **135**(24): p. 8989-8999.
91. Murdan, S., G. Gregoriadis, and A.T. Florence, *Novel sorbitan monostearate organogels.* Journal of pharmaceutical sciences, 1999. **88**(6): p. 608-614.
92. Singh, V.K., K. Pramanik, S.S. Ray, and K. Pal, *Development and characterization of sorbitan monostearate and sesame oil-based organogels for topical delivery of antimicrobials.* Aaps Pharmscitech, 2015. **16**(2): p. 293-305.
93. Pernetti, M., K. van Malssen, D. Kalnin, and E. Flöter, *Structuring edible oil with lecithin and sorbitan tri-stearate.* Food Hydrocolloids, 2007. **21**(5): p. 855-861.
94. Abdallah, D.J. and R.G. Weiss, *n-Alkanes gel n-alkanes (and many other organic liquids).* Langmuir, 2000. **16**(2): p. 352-355.
95. Abdallah, D.J., L. Lu, and R.G. Weiss, *Thermoreversible organogels from alkane gelators with one heteroatom.* Chemistry of materials, 1999. **11**(10): p. 2907-2911.
96. Terech, P. and S. Friol, *Rheometry of an androstanol steroid derivative paramagnetic organogel. Methodology for a comparison*

with a fatty acid organogel. Tetrahedron, 2007. **63**(31): p. 7366-7374.
97. Jung, J.H., Y. Ono, K. Sakurai, M. Sano, and S. Shinkai, *Novel vesicular aggregates of crown-appended cholesterol derivatives which act as gelators of organic solvents and as templates for silica transcription.* Journal of the American Chemical Society, 2000. **122**(36): p. 8648-8653.
98. Roijers, A.B.Æ.R.d.A.Æ.E.C., *Fibrils of c-Oryzanol + b-Sitosterol in Edible Oil Organogels.* J Am Oil Chem Soc, (2008) **85**: p. 1127–1134.
99. Li, Y., K. Liu, J. Liu, J. Peng, X. Feng, and Y. Fang, *Amino acid derivatives of cholesterol as "latent" organogelators with hydrogen chloride as a protonation reagent.* Langmuir, 2006. **22**(16): p. 7016-7020.
100. Suzuki, M. and K. Hanabusa, *L-Lysine-based low-molecular-weight gelators.* Chemical Society Reviews, 2009. **38**(4): p. 967-975.
101. Maji, S.K., S. Malik, M.G. Drew, A.K. Nandi, and A. Banerjee, *A synthetic tripeptide as a novel organo-gelator: a structural investigation.* Tetrahedron letters, 2003. **44**(21): p. 4103-4107.
102. Banerjee, A., G. Palui, and A. Banerjee, *Pentapeptide based organogels: the role of adjacently located phenylalanine residues in gel formation.* Soft Matter, 2008. **4**(7): p. 1430-1437.
103. Brinksma, J., B.L. Feringa, R.M. Kellogg, R. Vreeker, and J. van Esch, *Rheology and thermotropic properties of bis-urea-based organogels in various primary alcohols.* Langmuir, 2000. **16**(24): p. 9249-9255.
104. Jeong, Y., K. Hanabusa, H. Masunaga, I. Akiba, K. Miyoshi, S. Sakurai, and K. Sakurai, *Solvent/gelator interactions and supramolecular structure of gel fibers in cyclic bis-urea/primary alcohol organogels.* Langmuir, 2005. **21**(2): p. 586-594.
105. Anda Vintiloiu, J.-C.L., *Organogels and their use in drug delivery-A review.* journal of controlled release, 2008. **125**: p. 179-192.
106. Abdallah, D.J., S.A. Sirchio, and R.G. Weiss, *Hexatriacontane organogels. The first determination of the conformation and molecular packing of a low-molecular-mass organogelator in its gelled state.* Langmuir, 2000. **16**(20): p. 7558-7561.
107. Marangoni, A.G., *The formation of a 12-hydroxystearic acid/vegetable oil organogel under shear and thermal fields.* Journal of the American Oil Chemists' Society, 2013. **90**(4): p. 529-544.
108. Burkhardt, M., L. Noirez, and M. Gradzielski, *Organogels based on 12-hydroxy stearic acid as a leitmotif: Dependence of gelation properties on chemical modifications.* Journal of colloid and interface science, 2016. **466**: p. 369-376.
109. Mallia, V.A. and R.G. Weiss, *Self-assembled fibrillar networks and molecular gels employing 12-hydroxystearic acid and its isomers and derivatives.* Journal of Physical Organic Chemistry, 2014. **27**(4): p. 310-315.

110. Burkhardt, M., S. Kinzel, and M. Gradzielski, *Macroscopic properties and microstructure of HSA based organogels: sensitivity to polar additives.* Journal of colloid and interface science, 2009. **331**(2): p. 514-521.
111. Abraham, S., Y. Lan, R.S. Lam, D.A. Grahame, J.J.H. Kim, R.G. Weiss, and M.A. Rogers, *Influence of positional isomers on the macroscale and nanoscale architectures of aggregates of racemic hydroxyoctadecanoic acids in their molecular gel, dispersion, and solid states.* Langmuir, 2012. **28**(11): p. 4955-4964.
112. Songwei Wu, J.G., Thomas J. Emge, Michael A. Rogers, *Solvent-Induced Polymorphic Nanoscale Transitions for 12-Hydroxyoctadecanoic Acid Molecular Gels.* crystal growth design, 2013. **13**: p. 1360-1366.
113. Rogers, M.A., T. Pedersen, and L. Quaroni, *Hydrogen-bonding density of supramolecular self-assembled fibrillar networks probed using synchrotron infrared spectromicroscopy.* Crystal Growth and Design, 2009. **9**(8): p. 3621-3625.
114. Youbo Di, W.H., and Jinming Dai, *Investigation of Self-Assembly of Two-Component Organogel System Based on Trigonal Acids and Aminobenzothiazole Derivatives.* Journal of Nanomaterials, 2013. **2013**: p. 1-15.
115. Adhikari, B., J. Nanda, and A. Banerjee, *Pyrene-Containing Peptide-Based Fluorescent Organogels: Inclusion of Graphene into the Organogel.* Chemistry–A European Journal, 2011. **17**(41): p. 11488-11496.
116. Escuder, B. and J.F. Miravet, *Functional molecular gels*. Vol. 1. 2013: Royal Society of Chemistry.
117. Liu, S., W. Yu, and C. Zhou, *Solvents effects in the formation and viscoelasticity of DBS organogels.* Soft Matter, 2013. **9**(3): p. 864-874.
118. Bhatia, A., B. Singh, K. Raza, S. Wadhwa, and O.P. Katare, *Tamoxifen-loaded lecithin organogel (LO) for topical application: development, optimization and characterization.* International journal of pharmaceutics, 2013. **444**(1): p. 47-59.
119. Fouad, S.A., E.B. Basalious, M.A. El-Nabarawi, and S.A. Tayel, *Microemulsion and poloxamer microemulsion-based gel for sustained transdermal delivery of diclofenac epolamine using in-skin drug depot: in vitro/in vivo evaluation.* International journal of pharmaceutics, 2013. **453**(2): p. 569-578.
120. Singh, V.K., I. Banerjee, T. Agarwal, K. Pramanik, M.K. Bhattacharya, and K. Pal, *Guar gum and sesame oil based novel bigels for controlled drug delivery.* Colloids and Surfaces B: Biointerfaces, 2014. **123**: p. 582-592.
121. Park, E.J., S. Amatya, M.S. Kim, J.H. Park, E. Seol, H. Lee, Y.-H. Shin, and D.H. Na, *Long-acting injectable formulations of antipsychotic drugs for the treatment of schizophrenia.* Archives of pharmacal research, 2013. **36**(6): p. 651-659.

122. Li, F., M. Hanson, and R. Larock, *Soybean oil–divinylbenzene thermosetting polymers: synthesis, structure, properties and their relationships.* Polymer, 2001. **42**(4): p. 1567-1579.
123. Nomura, T., N. Koreeda, F. Yamashita, Y. Takakura, and M. Hashida, *Effect of particle size and charge on the disposition of lipid carriers after intratumoral injection into tissue-isolated tumors.* Pharmaceutical research, 1998. **15**(1): p. 128-132.
124. Yeşim Karasulu, H., B. Karabulut, G. Kantarci, I. Özgüney, C. Sezgin, U.A. Sanli, and E. Göker, *Preparation of arsenic trioxide-loaded microemulsion and its enhanced cytotoxicity on MCF-7 breast carcinoma cell line.* Drug delivery, 2004. **11**(6): p. 345-350.
125. Iwanaga, K., T. Sumizawa, M. Miyazaki, and M. Kakemi, *Characterization of organogel as a novel oral controlled release formulation for lipophilic compounds.* International journal of pharmaceutics, 2010. **388**(1): p. 123-128.
126. Long, D., T. Gong, Z. Zhang, R. Ding, and Y. Fu, *Preparation and evaluation of a phospholipid-based injectable gel for the long term delivery of leuprolide acetaterrh.* Acta Pharmaceutica Sinica B, 2016. **6**(4): p. 329-335.
127. Strickley, R.G., *Solubilizing excipients in oral and injectable formulations.* Pharmaceutical research, 2004. **21**(2): p. 201-230.
128. Kan, P., Z.-B. Chen, C.-J. Lee, and I.-M. Chu, *Development of nonionic surfactant/phospholipid o/w emulsion as a paclitaxel delivery system.* Journal of Controlled Release, 1999. **58**(3): p. 271-278.
129. Surapaneni, M.S., S.K. Das, and N.G. Das, *Designing paclitaxel drug delivery systems aimed at improved patient outcomes: current status and challenges.* ISRN pharmacology, 2012. **2012**: p. 1-15.
130. Giermasz, A., D. Nowis, A. Jalili, G. Basak, M. Marczak, M. Makowski, A. Czajka, I. Młynarczuk, G. Hoser, and S. Lewandowski, *Antitumor activity of tributyrin in murine melanoma model.* Cancer letters, 2001. **164**(2): p. 143-148.
131. McHugh, A., *The role of polymer membrane formation in sustained release drug delivery systems.* Journal of controlled release, 2005. **109**(1): p. 211-221.
132. Madan, M., A. Bajaj, S. Lewis, N. Udupa, and J. Baig, *In situ forming polymeric drug delivery systems.* Indian journal of pharmaceutical sciences, 2009. **71**(3): p. 242-251.
133. Singh, K. and S. HariKumar, *Injectable In-Situ Gelling Controlled Release Drug Delivery System.* International Journal of Drug Development and Research, 2012. **4**(2): p. 56-69.
134. Lin Chen, a.J.R., a Sam Sutton,a David G. Spiller,b James Williams,a James S. Sharp,c Peter C. Griffiths,d Richard K. Heenan,e Stephen M. King,e Alison Paul,d Steve Furzeland,f Derek Atkinsf and Dave J. Adams, *Tuneable mechanical properties in low molecular weight gels.* Soft Matter, 2011. **7**: p. 9721-9727.

135. Toro-Vazquez, J.F., J. Morales-Rueda, V.A. Mallia, and R.G. Weiss, *Relationship between molecular structure and thermo-mechanical properties of candelilla wax and amides derived from (R)-12-hydroxystearic acid as gelators of safflower oil.* Food Biophysics, 2010. **5**(3): p. 193-202.
136. YILMAZ, M.T., *Comparison Of Effectiveness Of Adaptive Neuro-Fuzzy Inference System And Artificial Neural Networks For Estimation Of Linear Creep And Recovery Properties Of Model Meat Emulsions.* Journal of Texture Studies, 2012. **43**: p. 384–399.
137. Patel, A.R., M. Babaahmadi, A. Lesaffer, and K. Dewettinck, *Rheological profiling of organogels prepared at critical gelling concentrations of natural waxes in a triacylglycerol solvent.* Journal of agricultural and food chemistry, 2015. **63**(19): p. 4862-4869.
138. Anne-Claude Couffin-Hoarau, A.M., Pascal Delmas, and Jean-Christophe Leroux, *In situ–Forming Pharmaceutical Organogels Based on the Self-Assembly of L-Alanine Derivatives.* Pharmaceutical Research,, 2004. **21**(3): p. 454-457.
139. Gao, J., S. Wu, and M. Rogers, *Harnessing Hansen solubility parameters to predict organogel formation.* Journal of Materials Chemistry, 2012. **22**(25): p. 12651-12658.
140. Schweighauser, L., M.A. Strauss, S. Bellotto, and H.A. Wegner, *Attraction or Repulsion? London Dispersion Forces Control Azobenzene Switches.* Angewandte Chemie International Edition, 2015. **54**(45): p. 13436-13439.
141. Rogers, M.A., A.J. Wright, and A.G. Marangoni, *Crystalline stability of self-assembled fibrillar networks of 12-hydroxystearic acid in edible oils.* Food research international, 2008. **41**(10): p. 1026-1034.
142. Martins, A.J., M.A. Cerqueira, L.H. Fasolin, R.L. Cunha, and A.A. Vicente, *Beeswax organogels: Influence of gelator concentration and oil type in the gelation process.* Food Research International, 2016. **84**: p. 170-179.
143. Tu, T., W. Assenmacher, H. Peterlik, R. Weisbarth, M. Nieger, and K.H. Dötz, *An Air-Stable Organometallic Low-Molecular-Mass Gelator: Synthesis, Aggregation, and Catalytic Application of a Palladium Pincer Complex.* Angewandte Chemie International Edition, 2007. **46**(33): p. 6368-6371.
144. Rogers, M.A. and V. Kontogiorgos, *Temperature Dependence of Relaxation Spectra for Self-Assembled Fibrillar Networks of 12-Hydroxystearic Acid in Canola Oil Organogels.* Food biophysics, 2012. **7**(2): p. 132-137.
145. Cai, X., Y. Wu, L. Wang, N. Yan, J. Liu, X. Fang, and Y. Fang, *Mechano-responsive calix [4] arene-based molecular gels: agitation induced gelation and hardening.* Soft Matter, 2013. **9**(24): p. 5807-5814.
146. Ni Yan, Z.X., Kevin K. Diehn, Srinivasa R. Raghavan, Yu Fang, and Richard G. Weiss, *How Do Liquid Mixtures Solubilize Insoluble Gelators? Self-Assembly Properties of Pyrenyl-Linker-Glucono*

Gelators in Tetrahydrofuran−Water Mixtures. journal of the American Chemical Society, 2013. **135**: p. 8989-8999.
147. Wright, A.J. and A.G. Marangoni, *Formation, structure, and rheological properties of ricinelaidic acid-vegetable oil organogels.* Journal of the American Oil Chemists' Society, 2006. **83**(6): p. 497-503.
148. Davies, G. and J. Stokes, *Thin film and high shear rheology of multiphase complex fluids.* Journal of Non-newtonian fluid mechanics, 2008. **148**(1): p. 73-87.
149. Jaclyn Raeburn, C.M.-C., Beatrice N. Cattoz, Marc A. Little, Ann E. Terry, Andre Zamith Cardoso,a Peter C. Griffiths and Dave J. Adams, *The effect of solvent choice on the gelation and final hydrogel properties of Fmoc–diphenylalanine.* Soft Matter, 2014. **11**: p. 927-935.
150. Marangoni, A.G. and S.S. Narine, *Physical properties of lipids*. 2002: CRC Press.
151. Chakrabarty, A. and U. Maitra, *Organogels from dimeric bile acid esters: in situ formation of gold nanoparticles.* The Journal of Physical Chemistry B, 2013. **117**(26): p. 8039-8046.
152. Tang, D. and A.G. Marangoni, *Quantitative study on the microstructure of colloidal fat crystal networks and fractal dimensions.* Advances in colloid and interface science, 2006. **128**: p. 257-265.
153. Rogers, M.A., A.J. Wright, and A.G. Marangoni, *Nanostructuring fiber morphology and solvent inclusions in 12-hydroxystearic acid/canola oil organogels.* Current opinion in colloid & interface science, 2009. **14**(1): p. 33-42.
154. Lam, R., M.A. Rogers, and A.G. Marangoni, *Thermo-mechanical method for the determination of the fractal dimension of fat crystal networks.* Journal of thermal analysis and calorimetry, 2009. **98**(1): p. 7-12.
155. Moniruzzaman, M. and P.R. Sundararajan, *Low molecular weight organogels based on long-chain carbamates.* Langmuir, 2005. **21**(9): p. 3802-3807.
156. Babu, S.S., V.K. Praveen, S. Prasanthkumar, and A. Ajayaghosh, *Self-Assembly of Oligo (para-phenylenevinylene) s through Arene—Perfluoroarene Interactions: π Gels with Longitudinally Controlled Fiber Growth and Supramolecular Exciplex-Mediated Enhanced Emission.* Chemistry–A European Journal, 2008. **14**(31): p. 9577-9584.
157. Lam, R., L. Quaroni, T. Pedersen, and M.A. Rogers, *A molecular insight into the nature of crystallographic mismatches in self-assembled fibrillar networks under non-isothermal crystallization conditions.* Soft Matter, 2010. **6**(2): p. 404-408.

158. Jing-Liang Li, Rong-Yao Wang,, Xiang-Yang Liu, and Hai-Hua Pan, *Nanoengineering of a Biocompatible Organogel by Thermal Processing.* J. Phys. Chem. B, 2009. **113**: p. 5011-5015.
159. Gao, J., S. Wu, T. Emge, and M. Rogers, *Nanoscale and microscale structural changes alter the critical gelator concentration of self-assembled fibrillar networks.* CrystEngComm, 2013. **15**(22): p. 4507-4515.
160. Ferenc Abraham, S.W., Richard G.Rogers, Michael A., *Influence of chirality on the modes of self-assembly of 12-hydroxystearic acid in molecular gels of mineral oil.* Soft Matter, 2011. **7**: p. 7359.
161. Wu, S., J. Gao, T. Emge, and M. Rogers, *Influence of solvent on the supramolecular architectures in molecular gels.* Soft Matter, 2013. **9**(25): p. 5942-5950.
162. Behera, B., V. Patil, S. Sagiri, K. Pal, and S. Ray, *Span-60-based organogels as probable matrices for transdermal/topical delivery systems.* Journal of applied polymer science, 2012. **125**(2): p. 852-863.
163. Pénzes, T., I. Csóka, and I. Erős, *Rheological analysis of the structural properties effecting the percutaneous absorption and stability in pharmaceutical organogels.* Rheologica acta, 2004. **43**(5): p. 457-463.
164. P. Terech, D.P., V. Bordas, and C. Rossat, *Rheological Properties and Structural Correlations in Molecular Organogels.* Langmuir, 2000. **16**: p. 4485-4494.
165. Ström, A., E. Schuster, and S.M. Goh, *Rheological characterization of acid pectin samples in the absence and presence of monovalent ions.* Carbohydrate polymers, 2014. **113**: p. 336-343.
166. Bonacucina, G., M. Cespi, and G.F. Palmieri, *Characterization and stability of emulsion gels based on acrylamide/sodium acryloyldimethyl taurate copolymer.* Aaps Pharmscitech, 2009. **10**(2): p. 368-375.
167. Laupheimer, M., N. Preisig, and C. Stubenrauch, *The molecular organogel n-decane/12-hydroxyoctadecanoic acid: Sol–gel transition, rheology, and microstructure.* Colloids and Surfaces A: Physicochemical and Engineering Aspects, 2015. **469**: p. 315-325.
168. Collin, D., R. Covis, F. Allix, B. Jamart-Grégoire, and P. Martinoty, *Jamming transition in solutions containing organogelator molecules of amino-acid type: rheological and calorimetry experiments.* Soft Matter, 2013. **9**(10): p. 2947-2958.
169. Guenet, J.-M., *Organogels: Thermodynamics, Structure, Solvent Role, and Properties*. 2016: Springer.
170. Chen, L., J. Raeburn, S. Sutton, D.G. Spiller, J. Williams, J.S. Sharp, P.C. Griffiths, R.K. Heenan, S.M. King, and A. Paul, *Tuneable mechanical properties in low molecular weight gels.* Soft Matter, 2011. **7**(20): p. 9721-9727.
171. Mallia, V.A.G., M. Blair, D. L. Weiss, R. G., *Robust organogels from nitrogen-containing derivatives of (R)-12-hydroxystearic acid as*

gelators: comparisons with gels from stearic acid derivatives. Langmuir, 2009. **25**(15): p. 8615-8625.

172. Helen, W., P. de Leonardis, R.V. Ulijn, J. Gough, and N. Tirelli, *Mechanosensitive peptide gelation: mode of agitation controls mechanical properties and nano-scale morphology.* Soft Matter, 2011. **7**(5): p. 1732-1740.
173. Jones, D.S., B.C. Muldoon, A.D. Woolfson, and F.D. Sanderson, *An examination of the rheological and mucoadhesive properties of poly (acrylic acid) organogels designed as platforms for local drug delivery to the oral cavity.* Journal of pharmaceutical sciences, 2007. **96**(10): p. 2632-2646.
174. Lim, P.F.C., X.Y. Liu, L. Kang, P.C.L. Ho, Y.W. Chan, and S.Y. Chan, *Limonene GP1/PG organogel as a vehicle in transdermal delivery of haloperidol.* International journal of pharmaceutics, 2006. **311**(1): p. 157-164.
175. Wenqi Liu, P.X., Feifei Xin, Yuehui Hou, Tao Sun, Jingcheng Hao, and Aiyou Hao, *Novel Double Phase Transforming Organogel Based on β-Cyclodextrin in 1,2-Propylene Glycol.* J. Phys. Chem. B, 2012. **116**(43): p. 13106–13113.
176. Wang, H., J. Zhang, W. Zhang, and Y. Yang, *Host–guest interactions of 5-fluorouracil in supramolecular organogels.* European Journal of Pharmaceutics and Biopharmaceutics, 2009. **73**(3): p. 357-360.
177. Krakoff, J., C.A. Koch, K.A. Calis, R. Alexander, and L.K. Nieman, *Use of a parenteral propylene glycol-containing etomidate preparation for the long-term management of ectopic Cushing's syndrome.* The Journal of Clinical Endocrinology & Metabolism, 2001. **86**(9): p. 4104-4108.
178. Seedher, N. and S. Bhatia, *Solubility enhancement of Cox-2 inhibitors using various solvent systems.* Aaps Pharmscitech, 2003. **4**(3): p. 36-44.
179. Date, A.A. and M. Nagarsenker, *Parenteral microemulsions: an overview.* International journal of pharmaceutics, 2008. **355**(1): p. 19-30.
180. Akers, M.J., *Excipient–drug interactions in parenteral formulations.* Journal of Pharmaceutical Sciences, 2002. **91**(11): p. 2283-2300.
181. Edelsztein, V.C., A.S. Mac Cormack, M. Ciarlantini, and P.H. Di Chenna, *Self-assembly of 2, 3-dihydroxycholestane steroids into supramolecular organogels as a soft template for the in-situ generation of silicate nanomaterials.* Beilstein journal of organic chemistry, 2013. **9**(1): p. 1826-1836.
182. Watase, M., Y. Nakatani, and H. Itagaki, *On the origin of the formation and stability of physical gels of di-O-benzylidene-D-sorbitol.* The Journal of Physical Chemistry B, 1999. **103**(13): p. 2366-2373.

183. Blake, A.I. and A.G. Marangoni, *The use of cooling rate to engineer the microstructure and oil binding capacity of wax crystal networks.* Food Biophysics, 2015. **10**(4): p. 456-465.
184. van Herpt, J.T., M.C. Stuart, W.R. Browne, and B.L. Feringa, *Mechanically induced gel formation.* Langmuir, 2013. **29**(28): p. 8763-8767.
185. Takeno, H. and T. Mochizuki, *A structural development of an organogel explored by synchrotron time-resolved small-angle X-ray scattering.* Colloid and Polymer Science, 2013. **291**(12): p. 2783-2789.
186. Wright, A.J. and A.G. Marangoni, *Time, temperature, and concentration dependence of ricinelaidic acid–canola oil organogelation.* Journal of the American Oil Chemists' Society, 2007. **84**(1): p. 3-9.
187. Zhang, M. and C.F. Zukoski, *Binary diamondoid building blocks for molecular gels.* Langmuir, 2014. **30**(25): p. 7540-7546.
188. Lai, W.C. and C.H. Wu, *Studies on the self-assembly of neat DBS and DBS/PPG organogels.* Journal of applied polymer science, 2010. **115**(2): p. 1113-1119.
189. Michael A. Rogers, a.A.G.M., *Non-Isothermal Nucleation and Crystallization of 12-Hydroxystearic Acid in Vegetable Oils.* CRYSTAL GROWTH & DESIGN, 2008. **8**(12): p. 4596–4601.
190. Leunig, M., A.E. Goetz, M. Dellian, G. Zetterer, F. Gamarra, R.K. Jain, and K. Messmer, *Interstitial fluid pressure in solid tumors following hyperthermia: possible correlation with therapeutic response.* Cancer research, 1992. **52**(2): p. 487-490.
191. Kirilov, P., F. Gauffre, S. Franceschi-Messant, E. Perez, and I. Rico-Lattes, *Rheological characterization of a new type of colloidal dispersion based on nanoparticles of gelled oil.* The Journal of Physical Chemistry B, 2009. **113**(32): p. 11101-11108.
192. Baral, A., S. Roy, A. Dehsorkhi, I.W. Hamley, S. Mohapatra, S. Ghosh, and A. Banerjee, *Assembly of an injectable noncytotoxic peptide-based hydrogelator for sustained release of drugs.* Langmuir, 2014. **30**(3): p. 929-936.
193. Schön, E.M., E. Marqués-López, R.P. Herrera, C. Alemán, and D.D. Díaz, *Exploiting Molecular Self-Assembly: From Urea-Based Organocatalysts to Multifunctional Supramolecular Gels.* Chemistry–A European Journal, 2014. **20**(34): p. 10720-10731.
194. Chopin-Doroteo, M., J.A. Morales-Rueda, E. Dibildox-Alvarado, M.A. Charó-Alonso, A. de la Peña-Gil, and J.F. Toro-Vazquez, *The effect of shearing in the thermo-mechanical properties of candelilla wax and candelilla wax–tripalmitin organogels.* Food Biophysics, 2011. **6**(3): p. 359-376.
195. Debnath, S., G. Vanitha, H.P. Bindu, and N.M. Babu, *Applications of organogels in drug delivery.* Indian Journal of Research in Pharmacy and Biotechnology, 2014. **2**(1): p. 976-981.

196. Sagiri, S., B. Behera, R. Rafanan, C. Bhattacharya, K. Pal, I. Banerjee, and D. Rousseau, *Organogels as matrices for controlled drug delivery: a review on the current state.* Soft Materials, 2014. **12**(1): p. 47-72.
197. Bonacucina, G., M. Cespi, M. Misici-Falzi, and G.F. Palmieri, *Colloidal soft matter as drug delivery system.* Journal of pharmaceutical sciences, 2009. **98**(1): p. 1-42.
198. Pisal, S., V. Shelke, K. Mahadik, and S. Kadam, *Effect of organogel components on in vitro nasal delivery of propranolol hydrochloride.* AAPS PharmSciTech, 2004. **5**(4): p. 92-100.
199. Ibrahim, M.M., S.A. Hafez, and M.M. Mahdy, *Organogels, hydrogels and bigels as transdermal delivery systems for diltiazem hydrochloride.* Asian Journal of Pharmaceutical Sciences, 2013. **8**(1): p. 48-57.
200. Wang, W., C. Li, J. Zhang, A. Dong, and D. Kong, *Tailor-made gemcitabine prodrug nanoparticles from well-defined drug–polymer amphiphiles prepared by controlled living radical polymerization for cancer chemotherapy.* J. Mater. Chem. B, 2014. **2**(13): p. 1891-1901.
201. Ohsedo, Y., M. Taniguchi, M. Oono, K. Saruhashi, and H. Watanabe, *Long-chain alkylamide-derived oil gels: mixing induced onset of thixotropy and application in sustained drug release.* New Journal of Chemistry, 2015. **39**(8): p. 6482-6490.
202. Skilling, K.J., A. Ndungu, B. Kellam, M. Ashford, T.D. Bradshaw, and M. Marlow, *Gelation properties of self-assembling N-acyl modified cytidine derivatives.* Journal of Materials Chemistry B, 2014. **2**(47): p. 8412-8417.
203. Sintang, B., M. Dona, T. Rimaux, D. Van de Walle, K. Dewettinck, and A.R. Patel, *Oil structuring properties of monoglycerides and phytosterols mixtures.* European Journal of Lipid Science and Technology, 2016: p. 1-14.
204. Bastiat, G. and J.-C. Leroux, *Pharmaceutical organogels prepared from aromatic amino acid derivatives.* Journal of materials chemistry, 2009. **19**(23): p. 3867-3877.
205. Wang, D., J. Zhao, X. Liu, F. Sun, Y. Zhou, L. Teng, and Y. Li, *Parenteral thermo-sensitive organogel for schizophrenia therapy, in vitro and in vivo evaluation.* European Journal of Pharmaceutical Sciences, 2014. **60**: p. 40-48.
206. Lee, J.W., S.-G. Yang, and K. Na, *Gemcitabine-releasing polymeric films for covered self-expandable metallic stent in treatment of gastrointestinal cancer.* International journal of pharmaceutics, 2012. **427**(2): p. 276-283.
207. Kreye, F., F. Siepmann, and J. Siepmann, *Drug release mechanisms of compressed lipid implants.* International journal of pharmaceutics, 2011. **404**(1): p. 27-35.
208. Chang, H.-I., M.R. Williamson, Y. Perrie, and A.G. Coombes, *Precipitation casting of drug-loaded microporous PCL matrices:*

Incorporation of progesterone by co-dissolution. Journal of controlled release, 2005. **106**(3): p. 263-272.
209. Tarvainen, T., M. Malin, T. Suutari, M. Pöllänen, J. Tuominen, J. Seppälä, and K. Järvinen, *Pancreatin enhanced erosion of and macromolecule release from 2, 2-bis (2-oxazoline)-linked poly (ϵ-caprolactone).* Journal of controlled release, 2003. **86**(2): p. 213-222.
210. Rungseevijitprapa, W. and R. Bodmeier, *Injectability of biodegradable in situ forming microparticle systems (ISM).* european journal of pharmaceutical sciences, 2009. **36**(4): p. 524-531.
211. Moniruzzaman, M., A. Sahin, and K.I. Winey, *Improved mechanical strength and electrical conductivity of organogels containing carbon nanotubes.* Carbon, 2009. **47**(3): p. 645-650.
212. Moschakis, T., E. Panagiotopoulou, and E. Katsanidis, *Sunflower oil organogels and organogel-in-water emulsions (part I): Microstructure and mechanical properties.* LWT-Food Science and Technology, 2016. **73**: p. 153-161.
213. Raeburn, J. and D.J. Adams, *Multicomponent low molecular weight gelators.* Chemical Communications, 2015. **51**(25): p. 5170-5180.
214. Skilling, K.J., B. Kellam, M. Ashford, T.D. Bradshaw, and M. Marlow, *Developing a self-healing supramolecular nucleoside hydrogel.* Soft Matter, 2016. **12**(43): p. 8950-8957.
215. Fritzsch, B., K. Muirhead, F. Feng, B. Gray, and B. Ohlsson-Wilhelm, *Diffusion and imaging properties of three new lipophilic tracers, NeuroVue™ Maroon, NeuroVue™ Red and NeuroVue™ Green and their use for double and triple labeling of neuronal profile.* Brain research bulletin, 2005. **66**(3): p. 249-258.
216. Hirsjärvi, S., S. Dufort, J. Gravier, I. Texier, Q. Yan, J. Bibette, L. Sancey, V. Josserand, C. Passirani, and J.-P. Benoit, *Influence of size, surface coating and fine chemical composition on the in vitro reactivity and in vivo biodistribution of lipid nanocapsules versus lipid nanoemulsions in cancer models.* Nanomedicine: Nanotechnology, biology and medicine, 2013. **9**(3): p. 375-387.